Role of myosin IIA in the small intestine immunosurveillance by dendritic cells

Violaine Randrian

UNIVERSITE PARIS DESCARTES
Spécialité Biologie
Ecole doctorale Frontières du Vivant

THESE DE DOCTORAT

Soutenue le 13 Octobre 2017 par
Violaine RANDRIAN

Pour obtenir le titre de

DOCTEUR EN SCIENCES

DE L'UNIVERSITE PARIS DESCARTES

Role of Myosin IIA in the Small Intestine Immunosurveillance by Dendritic Cells

---

Thèse dirigée par **Ana-Maria LENNON DUMENIL**

Jury :

Dr. Danijela Matic VIGNJEVIC	Rapporteur
Dr. Pierre GUERMONPREZ	Rapporteur
Dr. Eduardo VILLABLANCA	Examinateur
Dr. Emmanuel DONNADIEU	Examinateur
Dr. Ana-Maria LENNON DUMENIL	Directeur de thèse

LA LIGUE CONTRE LE CANCER

Frontières du Vivant

UNIVERSITÉ PARIS DESCARTES

institut Curie
Ensemble, prenons le cancer de vitesse.

à mes Parents,

Acknowledgements-Remerciements

To the Jury members:

I thank all the jury members to have kindly accepted to read and assess my thesis manuscript. I particularly thank Danijela Vignjevic and Pierre Guermonprez for their advice and constructive remarks as reviewers. I also thank Emmanuel Donnadieu and Eduardo Vilablanca to have accepted to be examiners. I especially thank Pierre Guermonprez and Eduardo Villablanca to have traveled to Paris to attend my defense.

A ma Directrice de Thèse:

Chère Ana, cette soutenance parachève les dix ans de notre rencontre. Il est difficile d'évaluer à quel point je me suis identifiée à toi, personnalité solaire, trilingue hypermnésique à l'enthousiasme inépuisable qui a assumé de miser sur moi dès mon premier stage de Master 1 dans ton laboratoire. Un immense merci pour cette confiance que tu m'as accordée, qui m'a permis de m'accomplir en tant que scientifique.

A mes collègues :

Martina, un grand merci pour ton accueil à Stockholm, ton énergie. Paulo et Martina, merci pour votre compétence et vos capacités à la transmettre qui ont été un tournant dans ma thèse.

Denis, je sais combien ton expérience en imagerie, ta grande capacité de mise au point, ton calme olympien et ta bonne volonté ont été un accélérateur indispensable de ma thèse : un immense merci pour cela.

Sasha, Alexandra Serguevnia, merci pour tout, ta rigueur et ta maturité scientifique, cette très impressionnante capacité de travail, ta gentillesse, nos échanges sur la science, les chefs, les hommes, la vie. Confiance, ton avenir est radieux.

Christel, un immense merci pour ta rigueur scientifique, ta compétence, ta fiabilité, qui ont été d'un grand secours.

Mathieu, ta dégaine brute de décoffrage masque ton perfectionnisme et ton exigence scientifique qui ont été très bénéfiques pour mon travail. Tout ça en me faisant rire et j'en avais bien besoin, merci.

Un grand merci à l'équipe Lennon :

Paolo, Judith, Graciela, Doriane, Zarhaa, Odile, Hélène, Mathieu, Anita pour cette atmosphère attentive et positive qui a été très bénéfique pour mon travail.

Merci aux anciens : Maria-Isabel, Anne, Pablo V., Pablo S., Dorian, Marine, Camille qui ont également beaucoup contribué à l'évolution de ma démarche scientifique.

Marine, voisine de bureau, confidente bienveillante, un grand merci pour ton soutien d'aînée.

Camille, ta personnalité positive et confiante m'a beaucoup aidée dans cette deuxième partie de thèse. Merci.
Dorian, merci d'avoir dépassé ton aversion pour les médecins pour m'aider à me construire en tant que doctorante, à former mon esprit scientifique et mon approche technique (la mise au point, toujours la mise au point !!).
Pablo S., merci beaucoup de ton indulgence pour mon niveau d'espagnol, nos échanges enrichissants et ton aide à la construction de mon manuscrit.
Anita, chère co-doctorante, je te remercie sincèrement de ta bienveillance, ton indétrônable sourire rayonnant qui m'a permis de traverser quelques moments de panique.
Hélène, tu es maintenant le pilier de ce laboratoire sur lequel nous nous appuyons tous. Merci pour ton implication dans le laboratoire, tes talents de médiatrice/négociatrice, ton aide très précieuse et spontanée pendant la rédaction de mon manuscrit et l'élaboration de la présentation.

A l'U932 et à l'Institut Curie :
Je tiens à remercier ici toutes les personnes qui ont facilité l'accomplissement de ce travail par leurs conseils, leur esprit collaboratif : une pensée pour Florence et son soutien constructif ; Aymeric pour ta confiance en la vie, une vraie leçon ; Silvia pour m'avoir évité l'angoisse de la page blanche ; François-Xavier, que je croise mine de rien depuis mes débuts ici, pour ta bienveillance et ton esprit Géo-trouve-tout (du L2 à la stérilisation d'huile d'olive !), Ahmed pour ta bonne humeur, Nilushi pour ton aide souriante et sans accroc, Ruby pour le temps et l'énergie que tu as pris pour m'aider à débuter en cytométrie, Elodie et Cassandra pour m'aider à démêler les fils de l'administration et des financements y compris pendant les vacances de Noël.
Merci Marie pour ton énergie, ton enthousiasme et ton efficacité qui m'ont permis d'améliorer la partie imagerie de ce travail.
Je remercie également Virginie, Isabelle, Céline, Aude, Océane, Cédrick, et avant lui Pierrick, qui m'ont été d'une grande aide pendant ces trois ans à travailler avec des souris.

A mes camarades et amis:
Ralitza, merci pour ton sourire et ton aide en toute simplicité tout au long de cette thèse, jusqu'à organiser mon séjour en Bulgarie !
Pierre-Antoine, merci d'avoir partagé ton érudition de la faune, la flore, l'astronomie, de m'avoir fait découvrir le tango. Vous avez en commun avec Joël, autre cavalier, une impressionnante capacité d'organisation multi-tâches, merci beaucoup à vous !
Paul-Gydéon brillant jeune docteur de biologie, merci pour ces discussions entre co-moniteurs.
Mikaël, ton flegme britannique cache une admirable énergie, merci pour nos échanges autour de la santé de demain et un grand bravo pour tes réalisations.

Merci aux membres du Bureau de l'AMPS et particulièrement à Ariel. Des réalisations sans conflit, sans querelle d'ego avec des moments festifs et une réelle attention aux autres: l'associatif constructif et sans douleur ça existe !!!
Jev, merci pour tes ondes positives et tes talents diplomatiques que j'ai découvert à YRLS et qui m'impressionnent toujours autant, je comprends maintenant ce qu'est l'intelligence sociale.

Aux amis de toujours :
Marie-Tiphaine, notre amitié traverse les années malgré tous les obstacles. Merci pour ta force intérieure, tes conseils pragmatiques et avisés.
Xavier, à travers nos déjeuners hebdomadaires entre voisins tu sais tout du double-cursus médecine-science : le Master 2, l'externat, le stress du concours, le stress de la thèse… Merci pour nos échanges de point de vue, ton soutien permanent et félicitations pour ton beau parcours.
Clémence, la palme de l'ancienneté à qui je peux demander de relire un manuscrit entre deux astreintes… euh…pour tout de suite ? Avec un retour détaillé. Avec toi je partage la vision du service public, d'exigence scientifique et ce malgré les centaines de kilomètres qui nous séparent. Ton parcours admirable et ton dévouement sont un exemples pour moi.

A ma famille :
Merci à ceux, oncles, tantes, cousins, qui remettent leurs fiches à jours en permanence et ne se lassent pas de suivre les péripéties de mon parcours estudiantin, prochaine étape Clermont-Ferrand !

Merci à ma marraine et à mon parrain qui ont jalonné ma vie intellectuelle des œuvres de Stefan Zweig, Michel Pastoureau et Marcel Proust. Vos parcours universitaires dans vos Humanités respectives ont sans nul doute contribué à mon « envie d'aller plus loin ».

Merci à mes parents qui me soutiennent avec une énergie sans faille depuis toujours. Je tiens à vous exprimer ici toute ma gratitude et mon affection qui ne sont pas des mots assez forts pour refléter mes sentiments. J'espère être capable de transmettre ces valeurs fortes et tout cet amour.

Abstract

Several routes for antigen capture have been described in the small intestine, mainly upon pathogenic infection: direct sampling by Dendritic Cells (DCs), sampling by macrophages that deliver antigens to DCs in the stroma, antigenic passage through goblet cells. Previous *in vitro* work in the lab showed that myosin IIA is essential to coordinate antigen uptake and processing with DC migration. The objective of my thesis was to combine several imaging methods including intravital microscopy, *ex vivo* confocal microscopy and immunofluorescence on gut tissue to flow cytometry in order to unravel the impact of myosin IIA on DC physiology *in vivo*.

My work shows that $CD103^+CD11b^+$ DCs, which are unique to the gut, constantly patrol the epithelium of the small intestine at steady state: they are recruited from the lamina propria (LP) and penetrate into the epithelium by transmigrating through the basal membrane that separates these two compartments. DC transmigration requires myosin IIA *in vivo*. Remarkably, we found that DC transmigration into the epithelium occurs mainly in the upper parts of the small intestine, the duodenum and the jejunum, but is not observed in the ileum. DC transmigration does not require the gut microbiota but relies on retinal, a vitamin A metabolite of that they convert into its active form all-*trans* retinoic acid (AtRA). Strikingly, single cell RNA-seq showed that intra-epithelial $CD103^+CD11b^+$ DCs constitute a homogenous cell population with a distinct transcriptomic signature from their LP counterpart. They are enriched with RNA related to antigen presentation, autophagy and lysosome pathways. Our results further suggest that these cells have a different function from LP $CD103^+CD11b^+$ DCs, as they do not significantly impact proliferation or differentiation of T helper lymphocytes but control the $CD8^+\alpha\beta$ intraepithelial lymphocytes (IELs) pool.

These findings highlight the importance of the epithelial tissue as a first line of defense against pathogens in the upper parts of the small intestine. They also raise new questions about the regulation of the immune response in the epithelium and the mutual influences between lumen, epithelium and intestinal lamina propria.

Résumé

Plusieurs méthodes de capture antigénique ont été décrites dans l'intestin grêle, surtout en cas d'infection: échantillonnage direct par les cellules dendritiques (DC), capture par les macrophages qui délivrent ensuite l'antigène aux DC du stroma, passage des antigènes à travers les cellules caliciformes. Des travaux antérieurs *in vitro* dans le laboratoire ont montré l'importance de la myosine IIA dans la coordination de la migration des DC avec la capture et de l'apprêtement antigénique. L'objectif de ma thèse était de combiner plusieurs méthodes d'imagerie telle que la microscopie intravitale, la microscopie confocale *ex vivo* et l'immunofluorescence sur tissus à la cytométrie en flux pour déterminer l'impact de la myosine IIA sur la capture antigénique *in vivo*.

Cette étude montre que les DC patrouillent en permanence dans l'épithélium de l'intestin grêle, y compris hors conditions infectieuses. Elles sont recrutées dans la lamina propria (LP) et pénètrent dans l'épithélium par transmigration à travers la membrane basale qui sépare ces deux compartiments. La myosine IIA est indispensable à la transmigration de $CD103^+CD11b^+$DC. Ces événements de transmigration surviennent plus fréquemment dans les parties proximales de l'intestin grêle, duodénum and jéjunum, que dans l'iléon. Chez les souris adultes, ces DC ne sont pas recrutées sous l'influence du microbiote mais sont sensibles au rétinal, un métabolite de la vitamine A qu'elles transforment en une molécule active l'acide trans-rétinoïque (AtRA). D'après notre analyse transcriptomique, les DC intra-épithéliales constituent une population homogène dont le profil est distinct de celui de leurs homologues de la LP. Elles sont enrichies en ARN des voies liées à l'apprêtement antigénique, l'autophagie et les lysosomes. Ces résultats suggèrent qu'elles ont une fonction différente des $CD103^+CD11b^+$DC de la LP: elles n'agissent pas sur la prolifération ni la différenciation des lymphocytes T mais contrôlent spécifiquement l'effectif des lymphocytes intra-épithéliaux $CD8^+\alpha\beta$.

Ces découvertes reflètent l'importance de l'épithélium comme première ligne de défense contre les pathogènes. Elles soulèvent également de nouvelles questions concernant la régulation de la réponse immune dans l'épithélium et les interactions mutuelles entre la lumière intestinale, l'épithélium et le stroma des villosités.

List of Abbreviations

2/3D	two/three dimensions
ALDH	aldehyde dehydrogenase
AMP	antimicrobial protein
APC	antigen presenting cell
AtRA	all-trans retinoic acid
BATF3	basic leucine zipper transcriptional factor ATF-like 3
BCZ	B cell zone
CCL19/21/25	chemokine (C-C motif) ligand 19/21/25
CCR2/7/9	chemokine (C-C motif) receptor 2/7/9
CD4/8/11/64/68/103	cluster of differentiation 4/8/11/64/68/103
c/pDC	classical/plasmacytoid dendritic cell
CDP	common dendritic cell precursor
CiAN	confinement induced actin network
CLIP	classII-associated Invariant chain peptide
cMOP	common monocyte progenitor
CRABP1/2	cellular retinoic acid binding proteins 1/2
CSF1/M-CSF	colony-stimulating factor 1
CSF2/GM-CSF	colony-stimulating factor 2
CX3CR1	chemokine (C-X3-C motif) receptor 1
CXCL1/8	chemokine (C-X-C motif) ligand 1/8
CYP26	cytochrome P 26
DSS	dextran sulfate salt
ECM	extra-cellular matrix
ELC	essential light chains
ER	endoplasmic reticulum
F-actin	fibrillar-actin
FAE	follicle-associated epithelium
GALT	gut associated lymphoid tissue
GAP	Goblet cell Associated Antigen Passage
HMM	Heavy meromyosin
HSC	haematopoietic stem cell
id2	inhibitor of DNA protein 2
IEC	intestinal epithelial cell
IEL	Intra-epithelial lymphocytes
IFNγ	Interferon γ
IgA	immunoglobulin A
Ii	invariant chain
IL-1/2/4/5/10/12/13/17/34	interleukin 1/2/4/5/10/12/13/17/34
ILC1/2/3	innate lymphoid cell 1/2/3
IRF4	interferon-regulatory factor 4
IRF8	interferon regulatory protein 8
KO	knock out

List of Abbreviations

LC3	1A/1B-light chain 3
LMPP	lymphoid-primed multipotent progenitor
LP	lamina propria
LPS	lipopolysaccharide
MadCam1	mucosal addressing cell adhesion molecule-1
MHC	major histocompatibility complex
MHCI	MHC class I
MHCII	MHC class II
MLC	myosin light chain
MLCK	myosin light chain kinase
MLN	mesenteric lymph nodes
MMP	matrix metallo-proteases
NF-κb	nuclear factor kappa-b
NM II	non-muscle myosin II
PAMP	pathogens associated microbial peptide
PC1/2/3	principal component 1/2/3
PCA	principal component analysis
PRR	pattern recognition receptors
RALDH	retinaldehyde dehydrogenases
RAR	retinoic acid receptor
RARE	retinoic acid response elements
RELMα	resistin-like molecule-α
RLC	regulatory light chains
RXR	retinoid X receptors
SED	subepithelial-dome
SFB	Segmented Filamentous Bacteria
SI	small intestine
SIgA	secretory immunoglobulin A
SILT	Solitary Isolated lymphoid tissue
SPF	Specific Pathogen Free
STRA 6	stimulated by retinoic acid 6 receptor
TCZ	T cell zone
TED	trans-epithelial dendrite
TGFβ	Tumor Growth Factor beta
Th1/2/17	helper T cell 1/2/17
TIMP	tissue inhibitor of matrix proteases
TLR	toll-like receptor
TNFα	tumor necrosis factor α
Treg	regulatore T cell
TSLP	thymic stromal lymphoprotein
t-SNE	t-distributed stochastic neighbor embedding
WT	wild type

Introduction

Results

Discussion

Table of Content

Table of Content

INTRODUCTION

A-Linking innate and adaptative immunity

Defenses against pathogens occur through two types of responses innate and adaptative immunity as illustrated in Figure 1. Innate immunity gathers all cell types able to recognize a broad class of pathogenic micro-organisms through Pattern Recognition Receptors (PRR) and ready to react against an invader without further stimulation. In contrast, the adaptative immune system identifies accurate response to a given peptide extracted from the pathogen, called an antigen, by B and T lymphocytes.

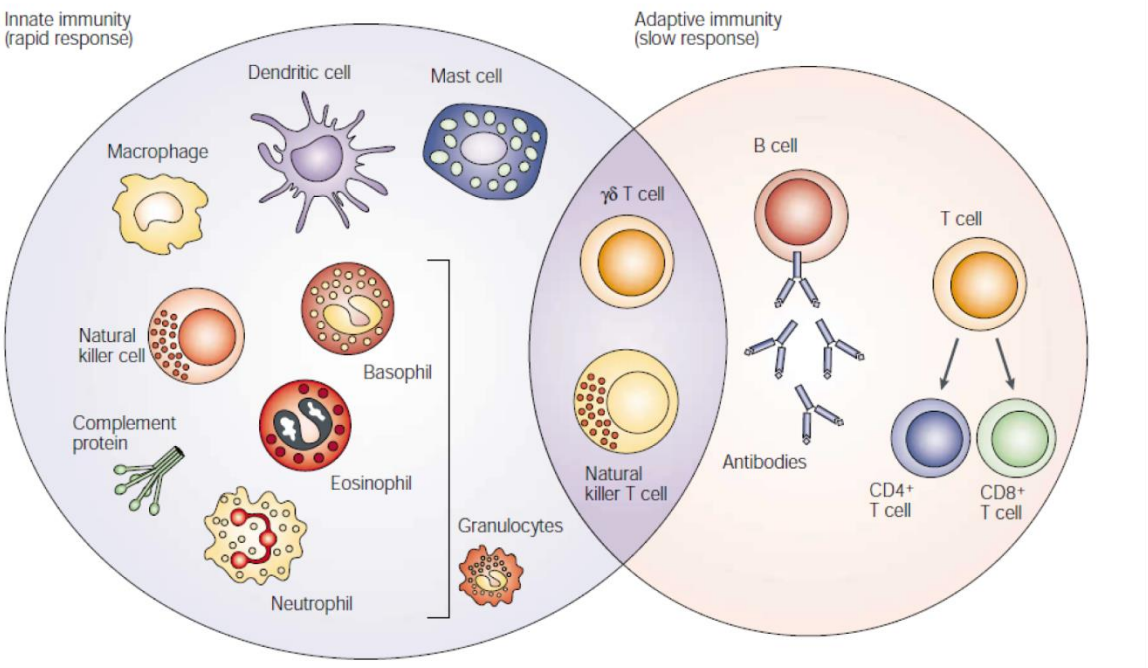

Figure 1. The different players of the immune system. The innate immune response functions as the first line of defense against infection. It consists of soluble factors, such as complement proteins, and diverse cellular components including granulocytes (basophils, eosinophils and neutrophils), mast cells, macrophages, dendritic cells and natural killer cells. The adaptive immune response is slower to develop, but manifests as increased antigenic specificity and memory. It consists of antibodies, B cells, and $CD4^+$ and $CD8^+$ T lymphocytes. Natural killer T cells and T cells are cytotoxic lymphocytes that straddle the interface of innate and adaptive immunity. Dranoff G, Nat. Rev. Cancer, 2004

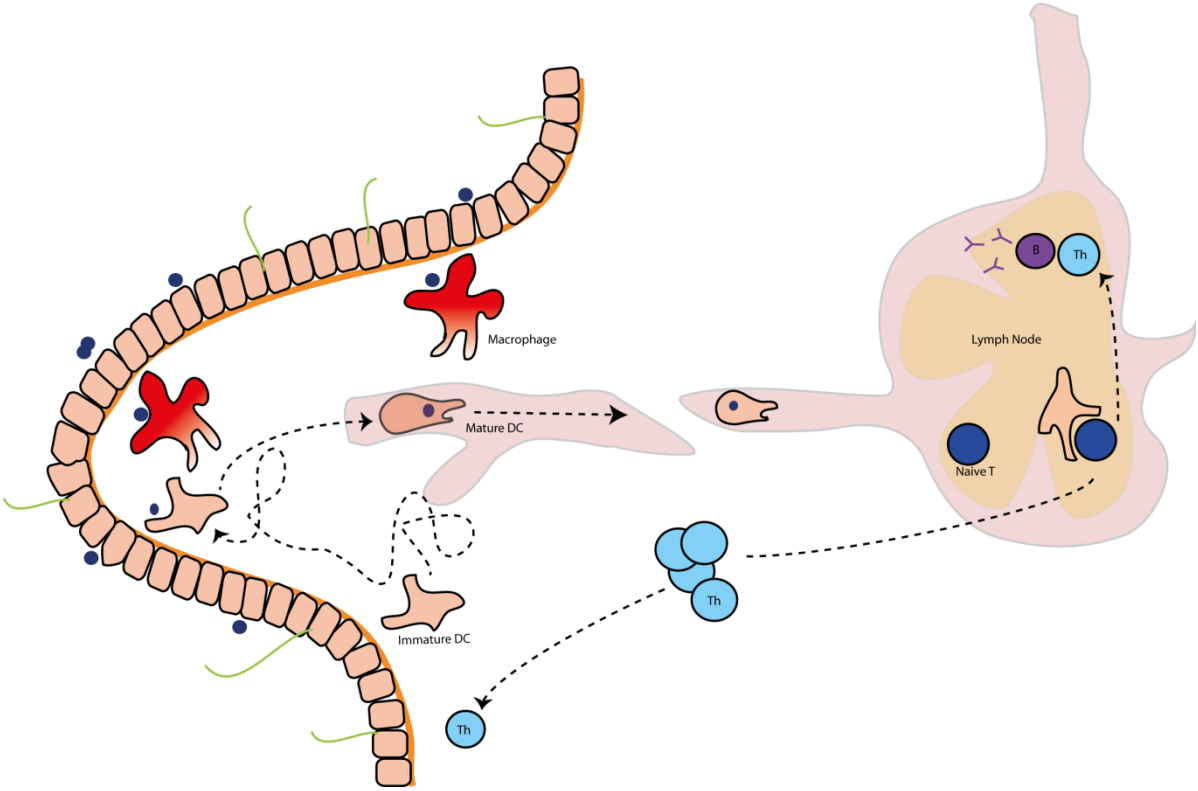

Figure 2. Initiating a response to a new antigen. Antigen encountered in peripheral tissue, here the lamina propria of the small intestine, is either cleared by macrophages or efficiently taken up by immature DCs that turn into a mature state and migrate fast to the draining lymph node. Then, antigen presentation induces T cell proliferation and differentiation into helper T cells (Th). Th are homed to the tissue where the antigen has to be cleared. Th are also involved in B cell maturation that leads to antibody production.

A-1- DCs play a crucial role connecting innate and adaptative system

A specific stimulation is required to trigger the adaptative response. Dendritic cells (DCs) ensure the key connection between the innate immune system and proper stimulation of the lymphocyte response. Peripheral tissue surveillance is under the control of two types of tissue resident mononuclear phagocytes that surveil tissues differently: DCs and Macrophages. Both can detect danger signals and internalize antigens but while tissue-resident macrophages remain sessile, DCs are rather migratory cells. Both macrophages and DCs internalize antigens through different processes called phagocytosis and macropinocytosis, respectively. Phagocytosis was first described in 1880 by Elie Metchnikoff who was awarded with the Nobel prize for this key contribution. Macrophages get attached to their target through recognition receptors to perform phagocytosis. Macrophages specifically endocyte the particles following their contours, so that there is almost no non-specific fluid uptake. Once linkage is strengthen by a set of integrins getting attached to their ligand on the particle surface, macrophages engulf the particle through pseudopod extensions. This step relies on local activation of the cytoskeleton, especially actin polymerization for extension and actomyosin ring contraction for the phagocytic cup. The newly formed vesicle called phagosome is fused with endolysosomes where the particle gets processed and degraded. Ralph M. Steinman (J Exp Med., 1973) was awarded with the Nobel Prize in 2011 for the first description of DCs he provided. He reported their various shapes: elongated or stellate due to their numerous pseudopods.

RM. Steinman did not observe as efficient phagocytosis by DCs as compared to macrophages even in conditions of cell culture that were highly favoring phagocytosis. DCs mainly perform macropinocytosis which, in contrast with phagocytosis, does not rely on the necessarily limited availability of specific receptors. Macropinocytosis is a non saturable phenomenon that relies on surface membrane recycling and involves the whole actin cytoskeleton. As a consequence DCs constantly engulf a large volume of fluid. Afterwards, they use receptors to retain and accumulate molecules in macropinosomes that are characteristic of foreigners referred to as antigens. Of note, DCs can also be infected and cytosolic antigens are processed through autophagy into autophagosomes that fuse with lysosomes. Misinterpretation of the signal brought by a self-antigen or an exogenous non-pathogenic antigen can lead to a non-adapted inflammatory response to the signal and pathologic situations of auto-immunity with extensive tissue damage.

The active suppression of pro-inflammatory signals and effectors in case of non-pathogenic situation is called tolerance. On the contrary, tolerating a pathogenic antigen leads to invasive infection. Upon antigen capture, Toll-like receptors (TLRs), a sub-family of PRRs activates a cascade of reactions leading to the activation of the nuclear factor NF-κb. On the one hand it promotes an innate immune response by anti-microbial peptides production that will have an immediate toxic action towards the pathogen. On the other hand, activated DCs secrete cytokines. Moreover, they migrate to draining lymph nodes where they present antigens to T cells. Both DCs and T lymphocytes interact with B cells resulting in their proliferation leading to their activation and the formation of germinal centers and in their maturation to high-affinity antibody producers.

A-2- DCs present exogenous antigens to T cells

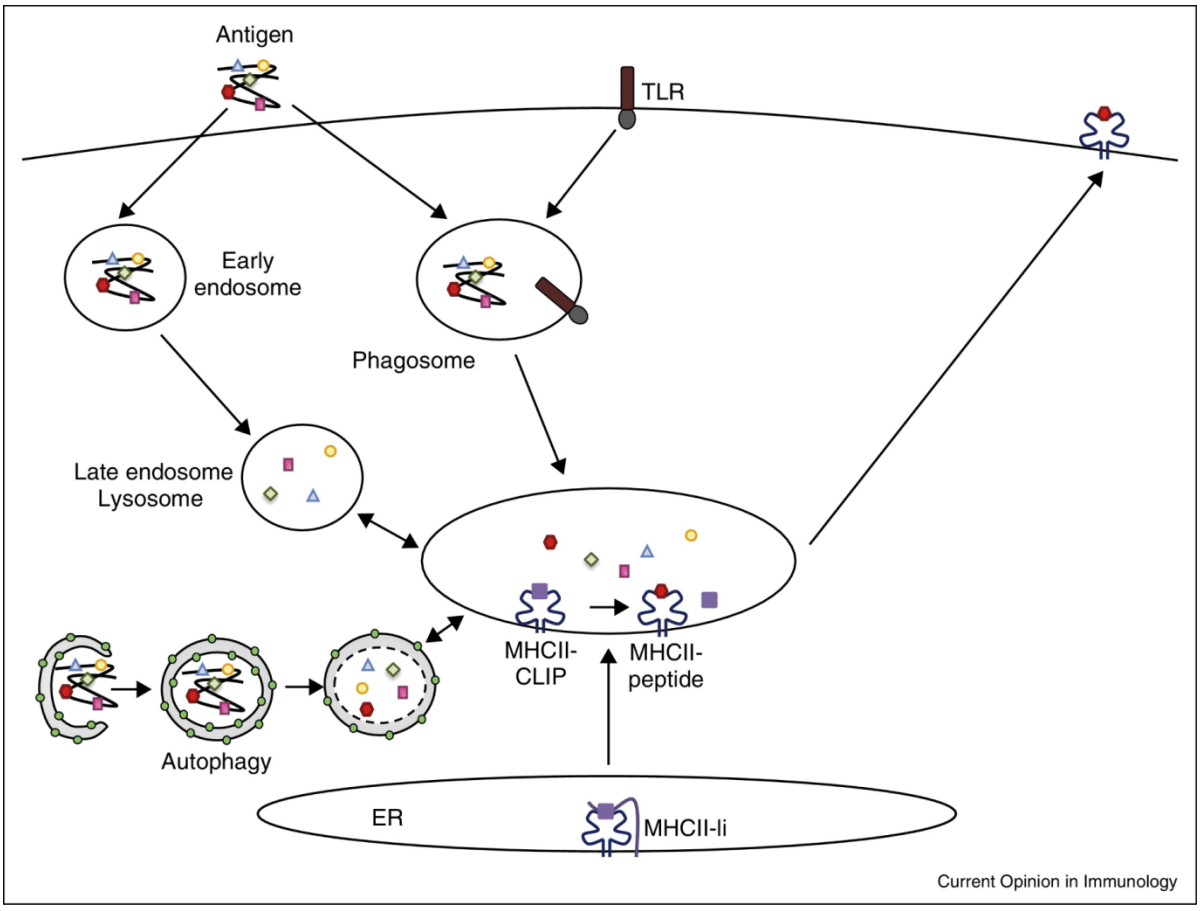

Figure 3. Intracellular trafficking of antigens during MHC II presentation. MHC II presentation involves trafficking of antigens into early endosomes and egress to late endosomes where antigen degradation elicits MHC II epitopes. Phagocytosed antigens are degraded in phagolysosomes, with this process enhanced by recruitment of TLR to phagosomes. MHC II-Ii complexes are cleaved into MHC II-CLIP before the fusion of ER vesicles with lysosomes. Green dots represent 1A/1B-light chain 3 (LC3), the main autophagy associated protein. Adapted from Mintern JD, Curr Op Immunol., 2015

To prime naïve T cells, DCs present them antigenic peptides from exogenous antigens loaded onto Major Histocompatibility Complexes (MHC) molecules. Antigen processing takes place in endolysosomes, which are endocytic compartments to which macropinosomes deliver their content. These vesicles also acquire selectively proteins needed for antigen processing such as cathepsin S and are enriched in MHC molecules. After controlled proteolysis, antigenic peptides are loaded onto MHC molecules. DCs can perform cross-presentation *i.e.* present antigenic peptides from endogenous antigens. They generated in the cytosol by the proteasome and delivered to lysosomes where they are loaded on a MHC I molecule. When loaded on MHC class I (MHC I), the presented antigen can prime CD8+ T cells. Thanks to cross-presentation, DCs can trigger a cytotoxic response to a pathogen without being infected. When loaded on MHC class II (MHC II) the presented antigen, usually exogenous antigen endocytosed by the presenting cell, can prime CD4+ T cells. MHC II proteins are produced in the endoplasmic reticulum (ER) as complexes of nine molecules with a ratio of two molecules of MHC class II for one molecule of Invariant chain (Ii). Ii helps MHC II folding and occupies the peptide binding site, preventing early binding of endogenous peptides. This complex of molecules is transferred to endo-lysosomes. Thanks to a dileucine motif in the cytosolic tail of Ii in this acidic environment enriched in proteases such as cathepsin S, Ii is degraded into a Class II-associated Invariant chain peptide (CLIP). Ultimately, CLIP is exchanged with an antigenic peptide onto MHC II molecules and complexes are exposed to the DC surface membrane for CD4+ T lymphocyte activation. Depending on the associated signals secreted by DCs and by the microenvironment, CD4+ T cells, also called helper T cells (Th), proliferate and differentiate into different types of subsets, the most known being Th1, Th2, Th17 that are mostly pro-inflammatory, or Treg that are essential for tolerance induction. Our group has shown that, in B cells, the cytosolic tail of Ii binds to the actin motor-protein Myosin II. These complexes are required for macropinocytosis and proper antigen processing, thereby coordinating these processes with DC migration. the MHC II (Vascotto F, JCB., 2007). A key role of Myosin II has also been shown in coordinating antigen processing with cell migration in DCs (Chabaud M, Nat Comm., 2015). As it is central in my thesis project, I will introduce in further details Myosin II role in DCs later in this introduction (p.37).

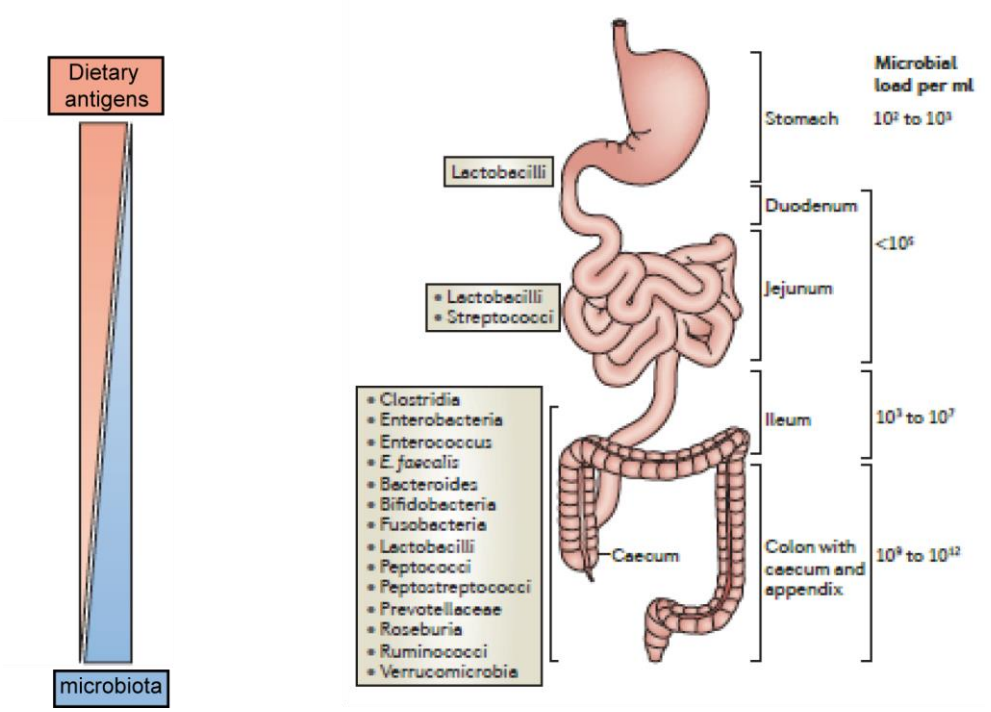

Figure 4. Structure of the small intestine. Dietary antigens and micro-organisms form reciprocal gradients along the small intestine. Adapted from Mowat AM & Agace WW, Nat Rev Immunol., 2014.

B- Mucosal immunology of the small intestine

The classical description of how immune responses are triggered is now enriched by the intensive research focusing on immune cells residing in mucosa. This new field is referred to as mucosal immunology. In the lung for instance, alveolar macrophages are constantly scanning the respiratory track lumen (Lloyd CM & Marsland BJ, Immunity, 2017). In addition, immunological memory exists at mucosal sites in mice and humans (Sathaliwayala T, Immunity, 2013). It can generate local inflammation without activation from secondary lymphoid organs. The precise cell composition and their function depend on the nature of the tissue studied. This section describes the immune specificities of the small intestine, linking them with the specific structure of this organ.

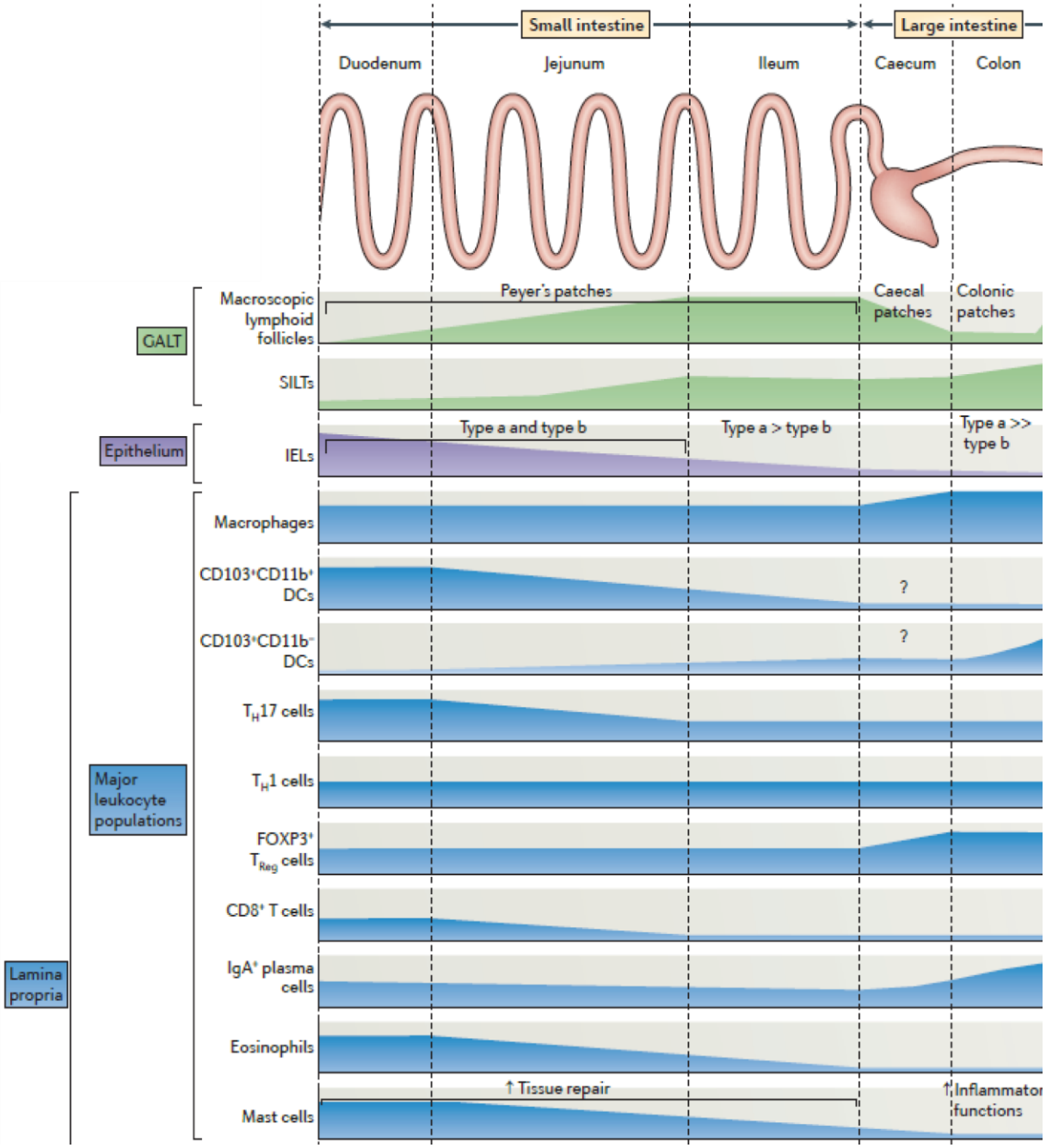

Figure 5. Regional specialization in the gut. Leukocytes populations display heterogeneous repartitions along the small intestine. Gut associated lymphoid tissue (GALT). Intra-epithelial lymphocytes (IELs). Solitary Isolated lymphoid tissue (SILT). Helper T cell (Th). Adapted from Mowat AM & Agace WW, Nat Rev Immunol., 2014.

B-1- In the lumen of the small intestine

The small intestine is the long proximal part of the gut, linking the stomach to the caecum. It has multiple histological specificities. The exchange surface with the lumen is substantially increased thanks to the folding of the organ into villi. From outside to inside, one finds: 1) smooth muscle, 2) submucosa with crypts and 3) lamina propria. Crypts are the circular structures made of stem epithelial cells that give rise to epithelium. The lamina propria is a tissue full of immune cells sitting in between blood and lymph vessels. This structure constitutes the stroma of the villi and is covered by a single epithelial layer. The enterocytes *i.e.* the main cells in the epithelial monolayer, are oriented in the baso-apical direction. On the luminal side, the membrane of enterocytes presents a supplemental folding called the brush border. The duodenum is the most proximal part of the gut and receives the acidic content of the stomach. Therefore, it is full of partly digested food antigens and its microbiotal content is low. Bile acids resulting of heme degradation and cholesterol metabolism are brought by bile ducts and mixed with this food content. The pancreatic duct carries into the duodenum the enzymes required for digestion and produced in the pancreas, such as lipase. The jejunum is the second part of the small intestine where nutrient absorption is very effective. The ileum makes the junction with the caecum. Duodenum, jejunum and ileum form a unique organ since they are not histologically separated but rather assembled with smooth transition between them. The lymph circulating in the small intestine is drained in mesenteric lymph nodes (MLNs) but some gut associated lymphoid tissues (GALTs) are also involved in the gut immune system.

All along the small intestine, some non-encapsulated lymphoid follicles sit right under the epithelium, the main ones are called Peyer Patches and constitute dedicated sites for B cell maturation. This continuum between duodenum, jejunum and ileum promotes gradients formation along the small intestine. In particular, a gradient of pH with a low pH in the duodenum, ranges from 7 to 9 in the jejunum and reaches alkaline values of pH in the ileum. Gradients of metabolites and cells, especially immune cells, are also established as reported in Figure 4. However, how such gradients of immune cells correspond to regions of functional immune specialization remains unclear. I will address this question in my thesis.

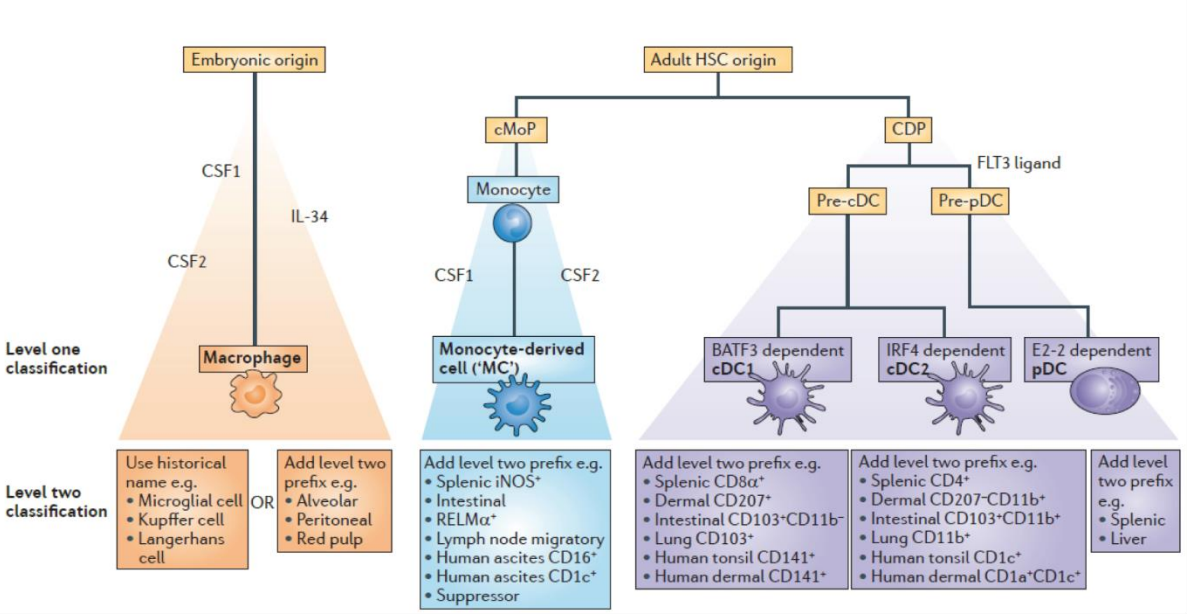

Figure 6. Proposed classification of mononuclear phagocytes. Three main groups of cells are described — namely, common dendritic cell (DC) precursor (CDP)-derived DCs, embryonic-derived macrophages and monocyte-derived cells. DCs are further subdivided into 'classical type 1 DCs (cDC1s)', 'cDC2s' and plasmacytoid DCs (pDCs). BATF3, basic leucine zipper transcriptional factor ATF-like 3; cMoP, common monocyte progenitor; CSF1, colony-stimulating factor 1 (also known as M-CSF); CSF2, colony-stimulating factor 2 (also known as GM-CSF); FLT3, FMS-like tyrosine kinase 3; HSC, haematopoietic stem cell; IL-34, interleukin-34; iNOS, inducible nitric oxide synthase; IRF4, interferon-regulatory factor 4; RELMα, resistin-like molecule-α. Adapted from Guilliams, Nat. Rev. Immunol 2014

B-2- The immune response in the small intestine

B-2-a Antigen presenting cells of the small intestine

DCs and macrophages come from different lineages

Several studies have shown that macrophages and DCs have different origins. First, based on growth factors requirements and second on transcription factors (Murphy TL, Annu Rev Immunol., 2016), the field is now benefiting from transcriptomics approach (Schraml BU & Reis e Sousa C, Curr Op Immunol., 2015). In mouse, tissue macrophages mainly arise from embryonic development and are maintained independently of the postnatal monocytic lineage (Yona S, Immunity, 2013). Haematopoietic stem cells differentiate in granulocytes and lymphoid-primed multipotent progenitor (LMPP). LMPP give rise to two distinct progenitors (Figure 6): a common monocyte progenitor (cMoP) and a common DC precursor (CDP). Different cell lineages develop from these two types of cells develop different cell lineage: monocyte-derived cells from cMoP and DCs from CDP. The main types of DCs residing in tissues are defined as conventional DCs (cDCs). This ontologic model that early separates the monocytic lineage from the DC lineage is validated both in lymphoid organs (Liu K, Science, 2009) and in several peripheral tissues like the skin (Tamoutounour, Immunity, 2013) and the gut (Bain CC, Mucosal Immunol., 2013; Scott CL, Mucosal Immunol., 2015). A lot of efforts have been made to determine the best markers among several candidates (CX3CR1, F4/80, CD64, CD11c) for the different cellular types. Among them, CD64 has been identified to easily distinguish DCs from macrophages and monocyte derived-cells (Tamoutounour S., Eur J Immunol., 2012; Langlet C, J Immunol., 2012). Within CD64 negative cells, cDCs are identified as CD11c positive, MHC II positive cells (Joeris T, Mucosal Immunol., 2017). Additional markers are required to further dissect of the DC landscape in the small intestine (Table 1).

Intestinal mononuclear phagocyte	Main markers (additional markers)	Location	Precursor	Growth/transcription/ environmental factor dependence	Functional specialization	Additional comments	Selected references SI, LI indicate organ of study: small or large intestine
DC	CD103+ CD11b− (CD24+, XCR1+)	Lamina propria, MALT	preDC	Flt-3L Irf8, Id2, Batf-3	Cross-presentation	Equivalent of splenic XCR1+ CD8a+ DC	Edelson et al. (6) SI Ginhoux et al. (7) SI Becker et al. (8) SI Crozat et al. (9) SI Schlitzer et al. (10) SI
	CD103+ CD11b+ (CD24+, Sirpα+)	Lamina propria, MALT	preDC	Flt-3L (partially) Csf-2 (GM-CSF), Irf-4, Notch2, Retinoic acid (ileum)	Required for generation and priming of TH17 cells	More prevalent in ileum	Bogunovic et al. (11) SI, LI Lewis et al. (12) SI, LI Welty et al. (13) SI, LI Schlitzer et al. (10) SI Persson et al. (14) SI, LI Klebanoff et al. (15) SI
	CD103− CD11b+		preDC	Flt-3L, Csf-1 (M-CSF)	Priming of IL-17 and INFγ-producing T cells		Bogunovic et al. (11) SI, LI Cerovic et al. (16) SI Scott et al. (17) SI, LI
	CD103− CD11b-		preDC	Ftl3L	Priming of TH17 *(in vitro)*		Cerovic et al. (16)
Macrophages	CD64+ CX3CR1+ CD11c+ (F4/80+ CD11b+)	Lamina propria	Ly6C+ monocytes	Csf-1 (M-CSF) Csf-2 (GM-CSF) (in colon)			Niess et al. (18) SI Varol et al. (19) SI Bogunovic et al. (11) SI Mortha et al. (20) Cecchini et al. (38)
	CD64+ CX3CR1+ CD11c− (F4/80+ CD11b+)	Lamina propria	Ly6C+ monocytes	Csf-1 (M-CSF) Notch 1/2			Ishifune et al. (21) SI Cecchini et al. (38), SI LI
	CD64+ CX3CR1+ CD169+ (F4/80+ CD11b+)	Crypt proximity	Ly6C+ monocytes	Csf-1 (M-CSF)			Hiemstra et al. (22) LI Cecchini et al. (38), SI LI
	CD64+ CX3CR1+ (F4/80+ CD11b+)	Muscularis layer	Ly6C+ monocytes	Csf-1 (M-CSF)	Communication with neurons		Muller et al. (23) SI, LI Cecchini et al. (38), SI LI

Table 1. Mononuclear phagocytes and their respective subsets in the lamina propria of the mouse intestine. From Gross M, Front Immunol., 2015

Defining DCs of the small intestine

The lamina propria (LP) of the small intestine contains a lot of DCs and macrophages whose functions partially overlap. Thanks to the work on the ontogeny of DCs and macrophages from the gut, and the identification of distinct lineages, the immune gut landscape became clearer (Bogunovic M, Immunity, 2009). In this section, I will focus on the classification of cDCs in the small intestine. Once identified as CD64 negative, CD11c positive and MHC II positive, DCs are split into groups following two additional surface markers: CD103 and CD11b, identifying $CD103^+CD11b^+$, $CD103^+CD11b^-$, $CD103^-CD11b^+$ and $CD103^-CD11b^-$ (Table 1). Thanks to chimeric mice, the contribution of monocytes and CDPs to the different DC subsets was elucidated (Bogunovic M, Immunity, 2009). Monocytes, which produce some $CD103^-CD11b^+$ DCs, do not contribute at all to the CD103+CD11b+ cDC subset. CDPs and pre-DCs give rise preferentially to CD103+CD11b+ DCs in the LP. $CD103^-CD11b^-$cDCs form a small and understudied population.

Monocyte-derived $CD103^-CD11b^+$ are rare in the small intestine but frequent in the colon where they prime pro-inflammatory responses. $CD103^+CD11b^-$ are also derived from pre-DCs under the control of fms-like tyrosine kinase 3 (Flt3) ligand, inhibitor of DNA protein 2 (Id2), IFN regulatory protein 8 (IRF8) (Ginhoux F, J Exp Med., 2009), and Batf3 (Edelson BT, J Exp Med., 2010). They behave similarly to $CD8^+$ DCs of the lymphoid organs and to $XCR1^+$ splenic cells. Intestinal $CD103^+CD11b^-$ cDCs perform cross-presentation of oral antigens to $CD8^+$Tcells in MLNs, which implies their ability to migrate (Becker M, Front Immunol., 2014).

The $CD103^+CD11b^+$ cDC subset is specific to the small intestine LP. It derives from pre-DCs. The development of this subset depends on Irf4 but not on Id2 or IRF8. It relies on environmental cues such as all-trans retinoic acid (AtRA) (Klebanoff CA, J Exp Med., 2013). Parabiontic mice experiments showed that $CD103^+CD11b^+$ DCs had a great turnover rate. This result supports the idea that $CD103^+CD11b^+$ DCs constantly migrate to the MLNs to report information there and stimulate T cells with the latest antigens they have captured. $CD103^+CD11b^+$ cDCs are particularly responsive to fungi and extracellular bacteria through the Notch2 pathway (Lewis KL, Immunity, 2011). They drive Th17 pro-inflammatory response (Persson EK, Immunity, 2013). DC markers now provide us with indications about their function, which is useful for further dissection of the immune system in the small intestine.

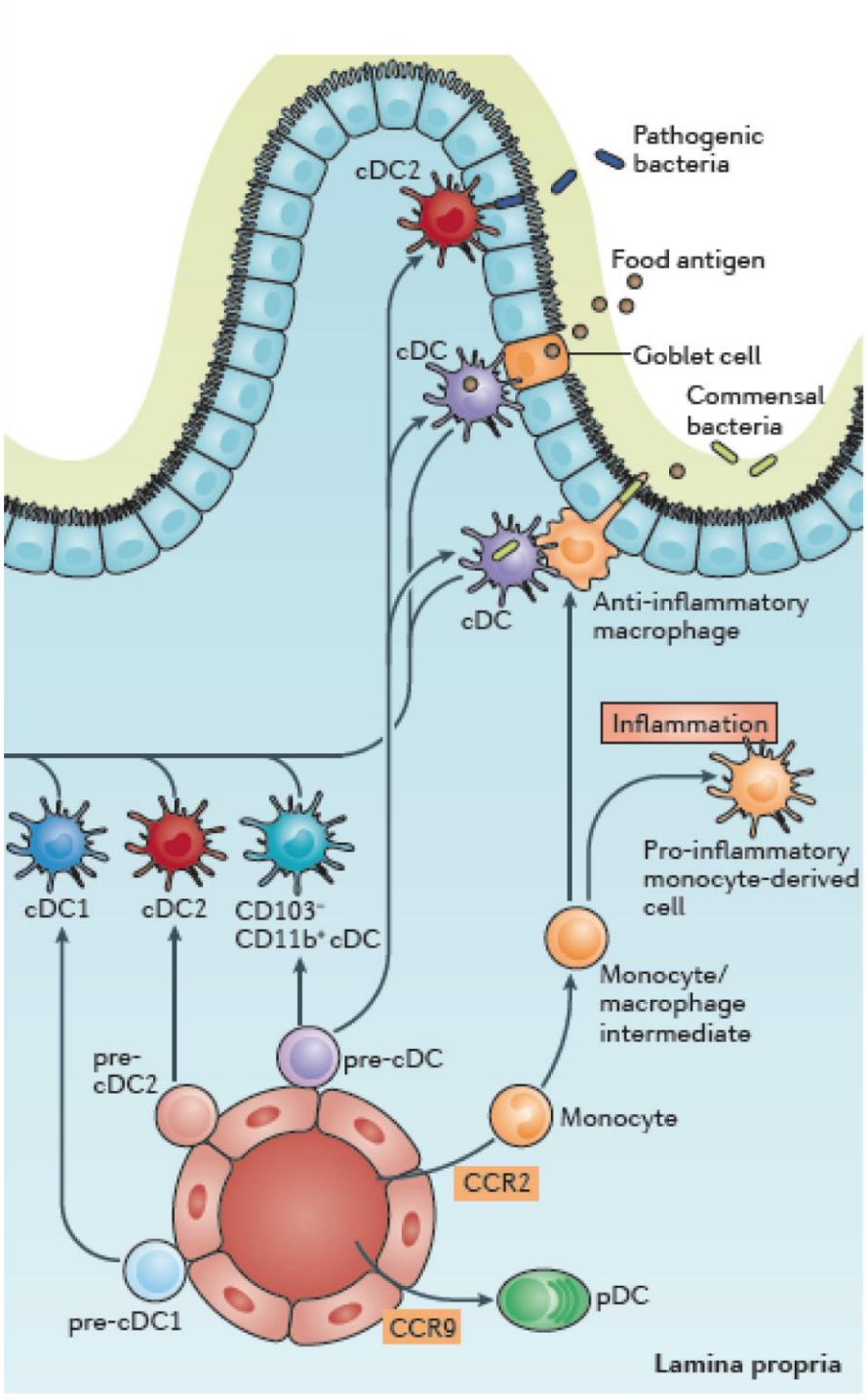

Figure 7. Antigen capture in the small intestine. The small-intestinal LP contains at least three distinct populations of pre-classical dendritic cell (cDC)-derived cDCs (cDC1s, cDC2s and $CD103^{-}$ $CD11b^{+}$ cDCs. LP cDCs acquire antigen by handover, either from epithelial goblet cells or CX_3C-chemokine receptor 1 $(CX_3CR1)^{hi}$ macrophages. LP cDC2s also have the propensity to migrate into the epithelium and extend dendrites into the gut lumen for the capture of pathogenic bacteria. In Peyer's patches, cDCs acquire antigen in the subepithelial-dome (SED) through M cells BCZ, B cell zone; SCS, subcapsular sinus; TCZ, T cell zone. Adapted from Worbs T, Nat. Rev. Immunol. 2017

B-2-b Antigen capture in the small intestine

The intestinal epithelium is rather non permeable to antigens. However, in homeostatic conditions, DCs can sense and capture antigens present in the gut lumen. How do antigens get from the lumen into the LP without requiring any epithelial damage? In this section, I will detail the routes described in the literature as antigen gateways. The relative importance and potential redundancy of these different routes in homeostasis and upon infection remain unknown.

The first proposed ways resemble a passive passage with no particular energy invested by the organism to take up antigens. A possible paracellular leakage of soluble antigens through the epithelium then entering lymphatic vessels is a valid route towards MLNs. In the same line, antigens can enter blood vessels in the LP of the intestinal villi and get direct access to the liver and, if not eliminated at that step, to the general circulation (Pabst O. & Mowat AM., Mucosal Immunol., 2012). Goblet cells can form Goblet cell Associated Antigen Passages (GAPs) and are seen as holes when staining the intestinal epithelial layer as their cytosol is pushed aside by the mucin vesicles. As a result, they deliver soluble antigens to the LP below (Figure 7), in particular to $CD103^+$ DCs. Only small molecules, up to 10kDa according to experiments of dextran internalization, can pass through GAPs (McDole JR, Nature, 2012).

A second proposed mechanism for antigen uptake in the LP is active and direct sampling of the gut lumen by resident immune cells of the LP. Among them, $CD11c^+$ $CX3CR1^+$ cells have been identified to emit trans-epithelial dendrites (TEDs) and sample gut lumen through the epithelium. They emit TEDs as a response to the epithelial secretion by goblet cells of CX3CR1 ligand the chemokine so-called fractalkine (Kim KW, Blood, 2011). $CD11c^+CD103^+$ DCs can also send TEDs through the epithelium. Indeed, they sit at the periphery of the LP where they interact with epithelial cells by opening *adherens* junctions between them (Rescigno M, Nat Immunol., 2001). This mechanism is very likely as CD103 is an integrin whose ligand E-cadherin is present on epithelial surface membranes and might facilitate interactions between CD103+ cells and epithelial cells. It is supported by observations showing that $CD103^+$ cells send dendrites through the epithelium towards the gut lumen both *in vitro* and *in vivo* (Farache J, Immunity, 2013).

TEDs from CD103+ CD11b+ cDCs form especially in the upper gut. Their formation is supposed to depend on the microbiota since they are reduced in germ-free mice and in Specific Pathogen Free (SPF) mice after antibiotic treatment (Chieppa M, J Exp Med., 2006).

A third and last approach is cooperation between cell types. $CD103^{+}CD11b^{-}$ DCs from the Peyer patches can exit the sub-epithelial dome and migrate towards the LP to present antigen to DCs sitting there. Although $CD11c^{+}CX3CR1^{+}$cells have been proposed based on undirect observations to migrate towards MLNs (Diehl GE, Nature, 2013), there is no formal demonstration for this. CD11c+ CX3CR1 cells are now thought of as macrophages with no migratory potential, working as intermediaries between the gut lumen and DCs to which they transfer antigens (Mazzini E, Immunity, 2014).

It is very likely that all proposed routes co-exist and the quantitative contribution of each mechanism is under debate. An immune compartmentalization between colon and small intestine is admitted, due to the differences in both lumen content and the LP DC composition (Mowat AM & Agace WW, Nat Rev Immunol., 2014). Given the metabolic, microbial and immune gradients described into the small intestine, a study comparing the different floors of the small intestine may bring helpful insights in the field.

B-2-c T cell differentiation

After efficient antigen capture, DCs turn into a mature state and migrate to the MLNs to present antigens to T cells. Associated signals, costimulatory molecules, and cytokine secretion are necessary to reach full $CD4^+$ and $CD8^+$ T cell activation. The T cell subsets of the LP may be affected by a modification in DC subsets in the small intestine.

In response to intracellular bacterial infection, antigen presenting cells (APCs) secrete interleukin (IL-)12, enhancing expression of the transcription factor Tbet in CD4+T cells which then differentiate into Th1 cells. Th1 cells promote an immunogenic response through secretion of Interferon γ (IFNγ), IL-2 and tumor necrosis factor α (TNFα), which facilitates the activation of cytotoxic $CD8^+$ T cells and phagocytosis by macrophages. In response to parasite infection, and presence of IL-4 during antigen presentation, $CD4^+$ T cells differentiate into Th2 cells, which depend on the GATA3 transcription factor. In response to extracellular bacteria, APCs secrete low concentrations of TGFβ associated with IL- 6 and IL-21. This triggers the expression of the IL-23 receptor and the RORγt transcription factor promoting differentiation towards Th17 cells (Mangan PR, Nature 2006; Aujla SJ, Nat Med., 2008). Th17 cells secrete IL-17 and IL-22, which favor neutrophil recruitment and stimulate anti-bacterial immunity (Flannigan KL, Mucosal Immunol., 2017). In the presence of high concentrations of Tumor Growth Factor beta (TGFβ) associated with interleukin 6 (IL-6), T cells express the transcription factor FOXP3, which is characteristic of differentiation towards the Treg cell fate. In contrast to the Th subsets previously described, T regs promote tolerance and prevent pro-inflammatory responses. Tregs also suppress T cell pro-inflammatory effects through IL-10 secretion. This reduction of T helper effectors also impacts on antibody production by B cells. As opposed to Th1 and Th2 cell fates that are pretty stable, Th17 and Treg cell fates present some plasticity (Bhaumik S, Front Immunol., 2017).

Besides the induction of T cell proliferation and differentiation, a key function of DCs is to confer T cells the ability to migrate towards the tissue where DCs have detected the antigen that T cells need to eliminate, *i.e.* the small intestine in this case. This phenomenon is referred to as "imprinting of gut homing properties" as DCs will make T cells express surface markers that will trigger their trafficking to the gut, namely the CC chemokine receptor CCR9 and the α4β7

integrin. Upon stimulation, Th cells express CCR9 whose ligand is secreted by epithelial cells only in the small intestine (Kunkel EJ, J Exp Med., 2000). DCs also enhance α4β7 integrin expression on the membrane surface of T cells (Johansson-Lindbom B, J Exp Med., 2005). This integrin binds to the mucosal addressing cell adhesion molecule-1 (MadCam1), which is present on the cellular surface of high endothelial veinules in the small intestine and in the colonic LP. As for differentiation, this phenomenon is facilitated by molecular signals from the microenvironment. Imprinting of gut homing properties to Th cells is more efficient in the presence of TGFβ and all-trans Retinoic Acid (AtRA) (Eksteen B, Gastroenterology, 2009). Once arrived into the tissue they are targeted to, Th cells promote pathogen elimination. In the small intestine their action is further tuned by the DCs that reside in the tissue and by local cues secreted by the epithelium.

B-3- The epithelium maintains the boundary

B-3-a The crosstalk between Intestinal Epithelial cells (IECs) and immune cells

Intestinal epithelium directly and undirectly modifies the local immune system. First, it is itself a barrier against pathogens. Second, it secretes cytokines that affect DC and T cell fates.

IECs constitute a monolayer strongly polarized in an apico-basal manner, the apex being the lumen and the basis corresponding to the basal membrane. IECs form an heterogenous population made of a majority of absorptive cells called enterocytes and a minority of secretory cells: goblet cells, Paneth cells, Tuft cells and enteroendocrine cells. Goblet cells mainly secrete mucus: a network of glycoproteins which form a complex viscous gel on top of the epithelial layer, limiting contacts between the content of the gut lumen and IECs. Mucus is mainly composed of mucins, the main one being MUC2, which is stored in acidic granulae within goblet cells. Release of MUC2 requires local increase of pH and local decrease of calcium to allow its correct unfolding (Ambort D., PNAS, 2012). It is more elaborated in the colon where it consists of two layers: one loose superficial layer that contains some bacteria and a lower thick layer, which sticks to the epithelium and is almost sterile. (Johansson ME, PNAS, 2008). In the small intestine, the mucus structure is drastically different, as it consists of a single thin and loose layer. It is not attached to the epithelium and easy to aspirate during an endoscopic procedure (Johansson ME, Cell Mol Life Sci., 2011). This difference in structure explains that mucus in the small intestine is permeable for nutrients intake and also partly permeable to bacteria. Some adherent bacteria can implant in mucus, such as Segmented Filamentous Bacteria (SFB) in the ileum. Mucus detachment from the epithelium by N-terminal digestion of MUC2 is crucial: it is a way to wash out micro-organisms, preventing them to grow and reach the epithelium (Johansson ME & Hansson GC, Nat Rev Immunol., 2016). Of note, Th2 cells stimulated by parasite infections secrete cytokines, among which IL-13, which enhance mucus secretion and goblet cell hyperplasia, preventing the interaction between parasites and enterocytes (Webb RA, Parasite Immunol., 2007).

The mucus contains molecules secreted by the epithelium that diffuse within the gel. All IECs secrete antimicrobial proteins (AMPs) able to kill bacteria by attacking their wall.

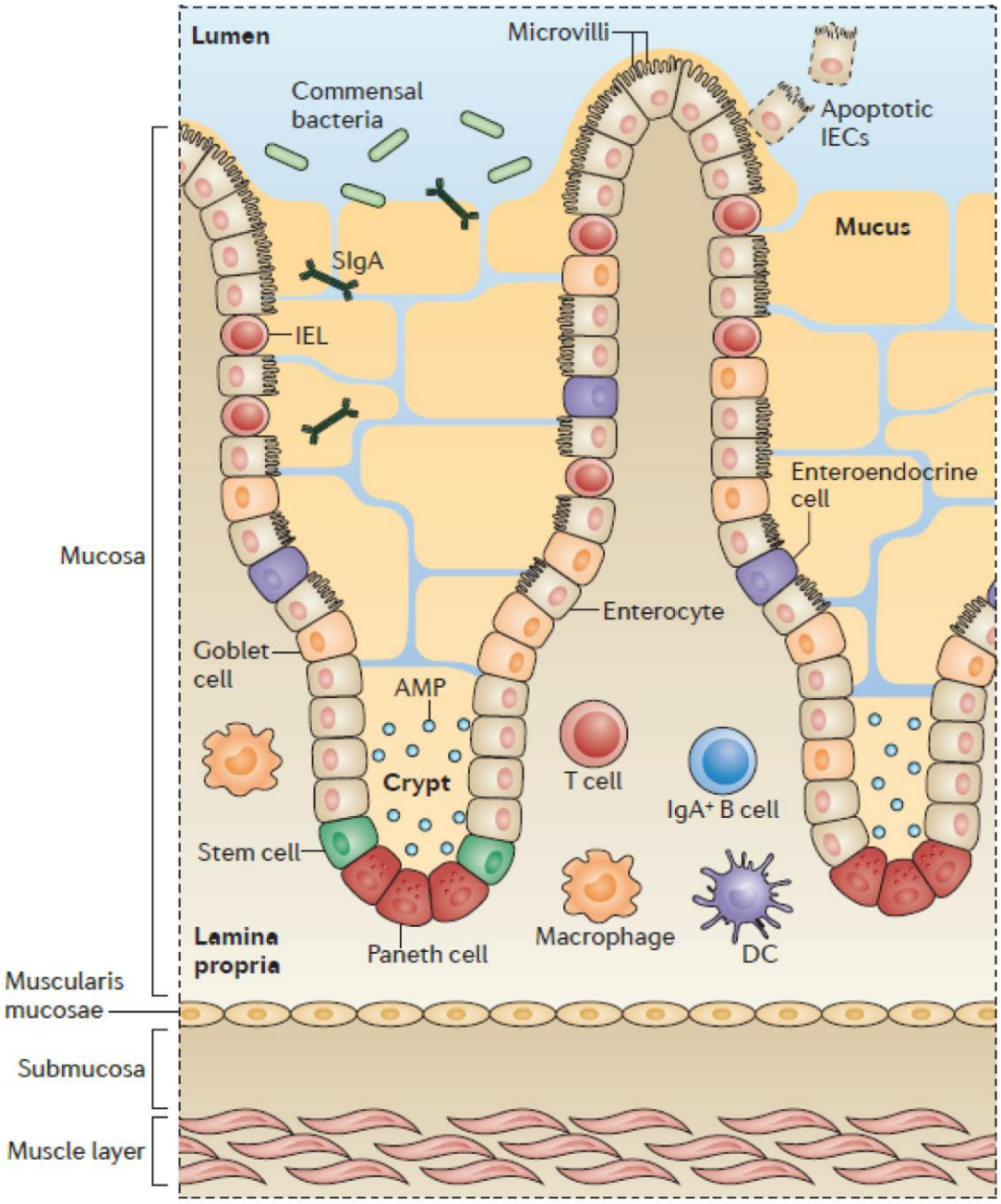

Figure 8. Several lines of defense to prevent bacterial entrance. Intestinal epithelial cells (IECs) are produced from stem cells near the bottom of the crypts. After a few days, IECs are lost from the tip of the villus and are replaced by new cells that are migrating upwards from the crypts. As well as the absorptive epithelial cells, stem cells in the crypts give rise to the mucus-secreting goblet cells found on the villus (indicated by the arrow), and to Paneth cells that migrate downwards to the bottom of the crypt. These Paneth cells are characterized by the presence of dense granules that contain antimicrobial peptides (AMPs). The central part of the villus comprises the LP, where the majority of intestinal immune cells are found, whereas intraepithelial lymphocytes (IELs) are found lying between epithelial cells. DC, dendritic cell; SIgA, secretory immunoglobulin A. Adapted from Mowat AM & Agace WW, Nat. Rev. Immunol. 2014

Paneth cells are the major producers of AMPs, which act as a supplementary protection against bacterial invasion. Paneth cells are produced in the crypts of the small intestine, especially in the ileum, and migrate to the bottom of the crypt. Genetic deletions affecting the pool of Paneth cells, for instance in Nod -/- mice, lead to unadapted reactions to infections as well as to mucosal lesions compatible with Crohn's disease, an inflammatory bowel disease that affects both the small and the large intestine (Clevers, Annu. Rev. Physiol. 2013).

TLR are expressed at low levels at the IECs surface. Thanks to these receptors, epithelial cells are able to sense Pathogens Associated Microbial Peptides (PAMPs). Upon activation, they trigger the NF-κB or Interferon Regulatory Factor (IRF) pro-inflammatory cascade downstream. Some consider epithelial cells as non-professional antigen-presenting cells since they express MHC II. Importantly, IECs also create a microenvironment which is not neutral for immune cells. For instance, it favors differentiation towards one cell fate thanks to their ability to secrete Vitamin A metabolites and cytokines such as TGFβ and Thymic Stromal LymphoProtein (TSLP). DCs cultured in the presence of human IEC supernatants turn into tolerogenic DCs (Iliev ID, Gut, 2009). IECs also shape cells of the adaptative immune system such as the pool of T cells that resides in the epithelium, the intra-epithelial lymphocytes (IELs). These cells form a gradient along the small intestine, being much more numerous in the duodenum. Recently, innate lymphoid cells (ILCs), which have a lymphoid origin and morphology but lack antigen specificity were described. ILCs can be classified into ILC1, which resemble $CD4^+$Th1; ILC2, which resemble $CD4^+$Th2 and ILC3, which resemble $CD4^+$Th17 (Spits H, Nat Rev Immunol., 2013). As for IELs, IECs secrete cytokines that promote ILC2 activation: IL-33, IL-25 and TSLP. In turn, ILC2 act on crypt progenitors to influence IEC differentiation. Furthermore, *in vitro,* $CD4^+$T cells from patients with Crohn disease, which behave like Th17 cells, made intestinal epithelium secrete chemokine (C-X-C motif) ligand 1 (CXCL1), and CXCL8 that attract neutrophils and macrophages (Calderon-Gomez E, Gastroenterology, 2016).

In brief, the epithelium can locally modify immune cell fate and in turn be used as an amplifier of the immune response by effector cells. This close interaction between immune cells and the epithelium raises the hypothesis that a local system refines the immune response programmed in MLNs.

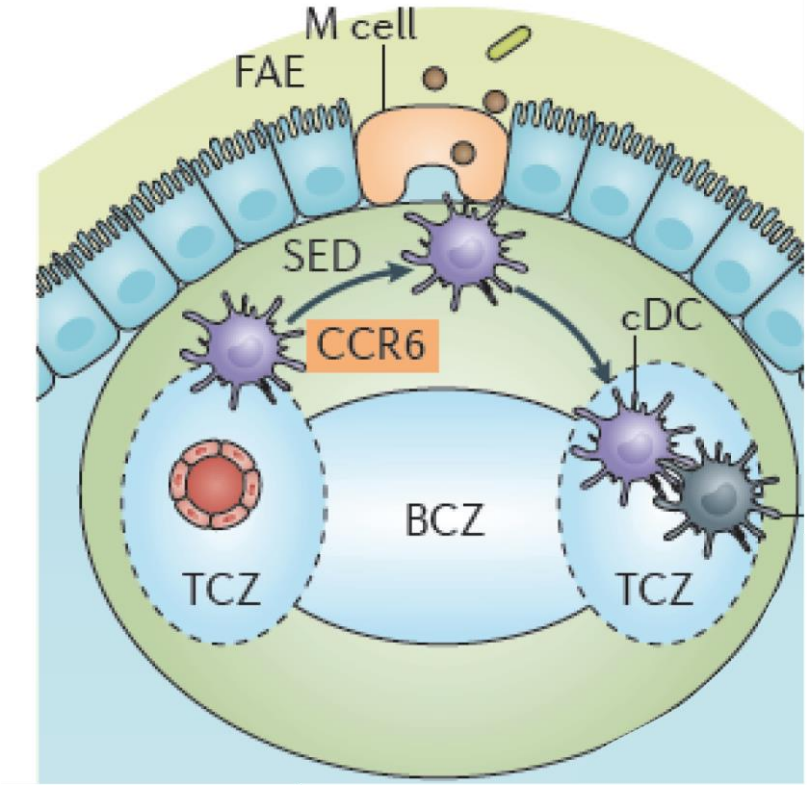

Figure 9. Antigen capture in Peyer's patches. cDCs are recruited in a CCR6-dependent manner towards the follicle-associated epithelium (FAE) where M cells deliver them soluble antigens. They subsequently migrate from the subepithelial dome (SED) into parafollicular T cell areas of Peyer's patches. B cell zone (BCZ); T cell zone (TCZ). Adapted from Worbs T, Nat. Rev. Immunol. 2017

B-2-b The Gut Associated Lymphoid Tissue (GALT)

In addition to the immune cells present in the LP, some non-encapsulated lymphoid organs where T cell activation and B cell maturation take place B cells, are dispersed along the small intestine, in the submucosa. The biggest ones are the Peyer patches. The epithelial layer that covers Peyer patches is specific to these structures: it is enriched with microfold cells called M cells (Figure 9). These M cells transport antigens from the lumen to the stroma, easing antigen presentation to immune cells lying beneath (Owen RL, Sem Immunol., 1999). Therefore, DCs sitting in the sub-epithelial domes in Peyer patches can easily sense the lumen and its microbial content. They present antigens they sample *in situ* to immature B cells enhancing their maturation and class switch to IgA secreting plasma cells (Fagarasan A., Nature, 2001; Mora JR, Science, 2006). IgA plasma cells as they represent 75% of plasma cells in the duodenum and about 90% of the plasma cells in the duodenum. Eosinophils are abundant in Peyer patches and are thought to maintain IgA+ plasma cells. Plasma cells migrate out of Peyer patches in the LP where they secrete IgA (Reboldi A, Science, 2016). IgA are trans-cytosed through the epithelium thanks to a polymeric Ig-receptor, and diffuse into the mucus layer where they bind to the bacterial surface they are targeting. Receptors to IgA have been identified at the membrane surface of eosinophils, DCs and IECs (Wines BD, Tissue Antigens, 2006). Thus, IgA binding to bacteria can result in their endocytosis by IECs or by Peyer patches DCs. The submucosa of the small intestine contains some anatomically well-defined sites dedicated to B cell maturation and high-affinity IgA production. These structures complete the mucosal immune system of the small intestine.

C- The Modulation of mucosal immunity in the small intestine by the lumen content

C-1- Interactions with microbiota

A new paradigm emerged in the 2000s considering that we constantly host trillions of bacteria that do not act as pathogens but as commensals in our organism. The mainstream idea is now that our immune system co-evolved with this flora, implying that it learned to tolerate it and that the flora in turn constantly influences the behavior of immune cells. As the quantity and composition of the flora change along the small intestine, this microbial content of the lumen may contribute to the regionalization of immune cell composition of the LP.

There is a gradient of microbiota from the duodenum to the ileum. Duodenum contains a low bacterial concentration while the ileum is perceived as a reservoir of bacteria containing 10^{12} bacteria per gram of luminal content. It is associated with a parallel gradient of Paneth cells, which are more numerous in the ileum. The diversity of bacteria hosted in our small intestine is huge. Most of them belong to two phylotypes: *Firmicutes* and *Bacteroides.* Very early, studies in germ-free mice have highlighted the importance of the gut microbiota to induce a normal immune response especially in germinal centers formation (Bauer H, Am. J. Pathol., 1963). Upon normal conditions, the microbiota triggers secretory IgA production and regulates the balance between different T cell fates. *Bacteroides fragilis* is able to orientate the differentiation of T cells towards Treg by secreting a specific capsular polysaccharide A (Mazmanian SK, Nature, 2008). Segmented filamentous bacteria (SFB) can colonize the ileum and interact directly with epithelial cells. There, they promote Th17 expansion (Ivanov IL, Cell, 2009; Gaboriau-Routhiau V, Immunity, 2009). SFB deficient mice produce less IgA and respond less to *Citrobacter rodentium* infections. This diverse bacterial population is under environment influence. It can be reversibly manipulated by changes in the diet (Turnbaugh PJ, Cell Host Microbe, 2008) or oral antibiotic treatments. For instance, Streptomycin induces a shift in the inflammation state, allowing *Salmonella Typhimurium* to compete with the original microbiota, thus favoring infection (Stecher B, Plos Biol, 2007).

Clostridium difficile infection, whose major risk factor is treatment with penicillins, illustrates how antibiotics can deeply modify the microbiota. As for prevention, commensal yeast such as *Saccharomyces-boulardii* are associated to antibiotics of the Ampicillin family when they are prescribed to patients with high risk of infection. The latest efficient treatment, fecal transplantation is now performed in routine in case of severe recurrence with excellent results (Van Nood E, NEJM., 2013). It is the best evidence for the reversibility of these antibiotics effects. Besides, it also shows the ability of a healthy human flora to restore diversity in an ill microbiota. These studies revealed that as the microbiota is in close relationship with its host, any alteration in the host microenvironment such as excessive inflammation or injury changes to the microbial composition. However, the reciprocal assumption, *i.e.* changes in the microbiota influence the inflammatory state, is still under debate. Administration of total fecal extracts to mice triggers the production of IL-17 by T cells, TNFα and IL1-β by monocytes, macrophages and DCs. These pro-inflammatory effects are reversed by antibiotic treatments (Bhattacharya N, Immunity, 2016). It is accepted that some bacteria, for instance invasive strains of *Escherichia coli* in patients with Crohn's disease (Darfeuille-Michaud A, Gastroenterology, 2004) maintain unappropriate inflammation. However there are some difficulties to determine whether this is a consequence of inflammation or the cause. Besides, in Crohn's disease, fecal transplantation efficiency is far more controversial than in *C. difficile* infection (Choi HH, Clin. Endosc, 2016). In the cancer field, manipulation of the microbiota can enhance anti-tumoral immune responses (Daillière R, Immunity, 2016) at a systemic level, leading to death of subcutaneous tumors. Consistently, some studies are in favor of a manipulation of the immune response through microbiota. Chemotherapy, for example with cyclophosphamide also alters microbiota composition thus changing adaptive response to cancer (Viaud S, Science, 2013).

These apparent contradictions between cancer, infection and inflammatory bowel disease studies may find a unifying explanation when focusing on epithelial integrity. Indeed, under inappropriate inflammatory conditions such as in Crohn's disease, epithelial barrier is disrupted and loses its power to prevent microbial entrance in the organism.

C-2- Impact of nutrition

C-2-a From oral tolerance to tolerance to food

As previously described, DCs have access to antigens present in the gut lumen. Consequently, they constantly sample dietary antigens, but this permanent intake should not trigger any pro-inflammatory response. Therefore, the small intestine, and especially its upper part is identified as a site where tolerance is particularly efficient. Oral tolerance induction is of particular interest for the immunology community since it would give a simple route for immune manipulation.

Besides anergy *i.e.* absence of immune response by the lack of costimulatory signals, the main mechanism identified is active T cell mediated suppression through Treg expansion (Pabst O. and Mowat A.M., Mucosal Immunol, 2012). DCs are thought to play a crucial role in this process not only by inducing Treg development in MLN but also by recruiting effector T cells to the gut, through imprinting of gut homing receptors (Païdassi H, Gastroenterology, 2011; Mora JR, Nature, 2003; Cassani B, Gastroenterology, 2011). Due to the physiological ingestion of 130-190g of proteins each day (Weiner HL, Immunol Rev 2011), obvious candidates in the small intestine lumen for immune modulation are food proteins.

Food contribution to peripheral Treg expansion has been studied in the gut (Kim KS, Science, 2016) by raising mice under strict control in bacterial content (germ free *vs* specific pathogen free) and food antigen content (milk *vs* antigen-free diet *vs* chow diet after weaning). Antigen-free mice are offsprings from germ free mice raised with an antigen-free diet. This diet impacts on peripheral Treg development in the small intestine but not in the colon where there is a loss in T cell memory, as in the colon of germ free mice. These data suggest regional specificities in the gut, T cell development relying on diet in the small intestine and more on microbiota in the colon. In addition, peripheral Treg depletion leads to stronger immune responses to dietary antigens with more symptoms of intestinal allergy. This work further suggests that both microbial and dietary antigens are required to induce a complete tolerance.

Indeed, by weaning SPF mice onto antigen-free diet or by treating them with antibiotics, the authors show that dietary antigens drive RORγt- peripheral Treg expansion and microbiota drive RORγt+ peripheral Treg expansion.

As far as DCs are concerned, the number $CD103^+$ $CD11b^+$ were reduced in the small intestine of antigen-free mice but not in their MLNs, suggesting a local impact of dietary antigens onto $CD103^+$ $CD11b^+$ cDC expansion.

In brief, the intestine is a route of antigen administration that shapes the immune system through modulation of DC capacity to regulate T cell development and differentiation both in secondary lymphoid organs and in mucosal sites. One well studied nutrient that has multiple effect on DCs and T cell is AtRA,as I will discuss in the next part of the introduction.

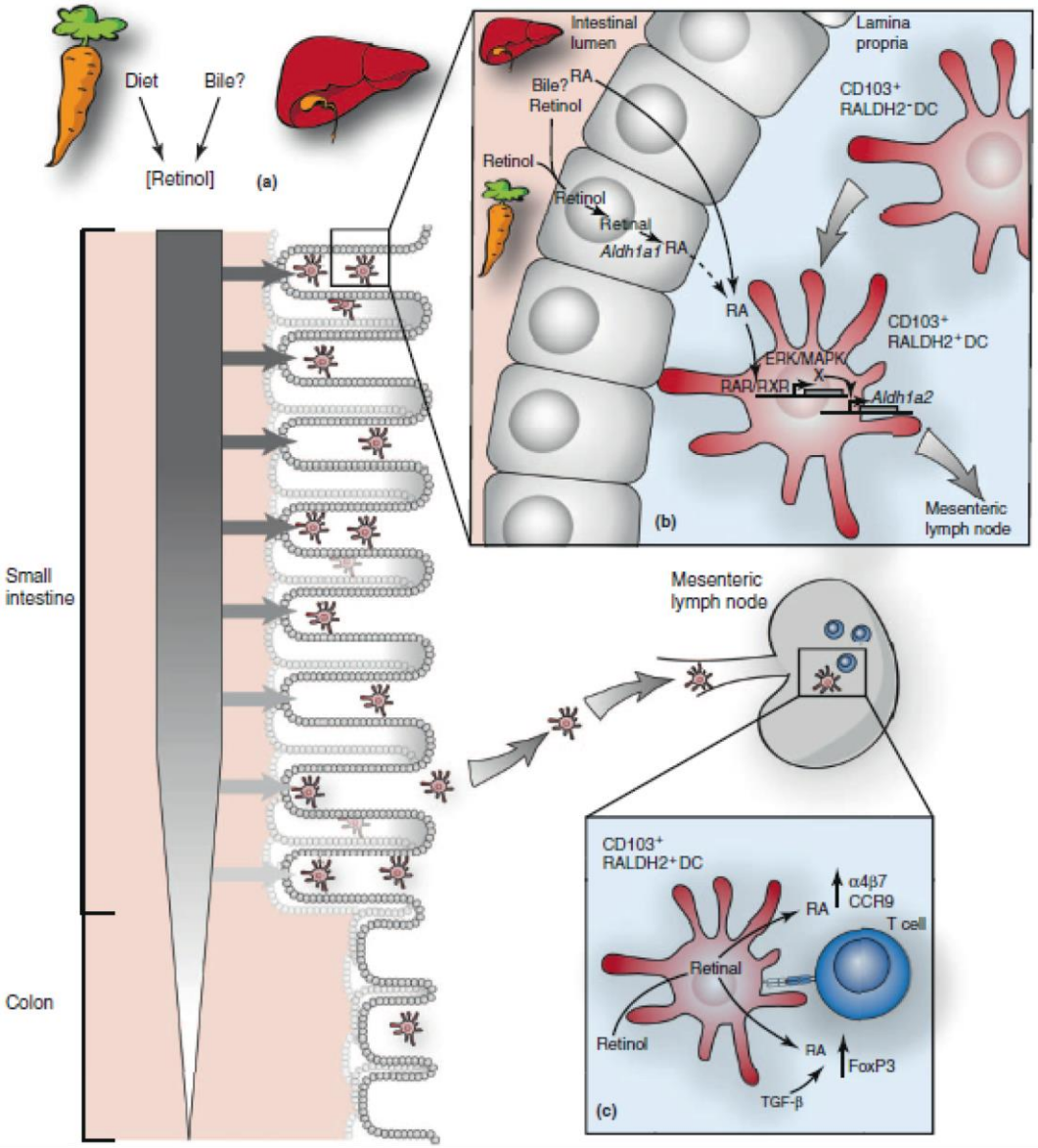

Figure 10. AtRA metabolism in the gut. High retinol concentrations in the small intestine (SI) likely underlie the enhanced *Aldh1a2* expression and ALDH activity of SI CD103$^+$ DCs. **(a)** High concentrations of retinol in the SI and draining MLNs are maintained by the diet and probably also through bile. **(b)**. Which SI cells generate the AtRA that imprints CD103$^+$ DCs *in vivo* are currently unknown but SI epithelial cells likely make an important contribution. Bile directly induces RAR signalling in BM-DCs *in vitro*, suggesting that bile-derived RA may directly contribute to SI CD103$^+$ DCs imprinting. Nevertheless, the *in vivo* role of bile-derived retinol and RA remains to be addressed. RA directly induces *Aldh1a2* expression in SI CD103$^+$ DCs and imprints these cells with vitamin A metabolising activity. RA-induced RAR signalling in DCs appears to require ERK signalling, and RA induction of *Aldh1a2* requires *de novo* protein synthesis and thus functions through additional intermediates. **(c)** Imprinted CD103$^+$ DCs constitutively migrate to draining MLNs and present lumen-derived foreign and intestinal self-antigen to T cells.During T cell priming, vitamin A metabolising CD103$^+$ DCs provide AtRA signals to responding T cells and probably promote the unique nature of the SI immune responses. From Agace WW & Persson EK, Trends Immunol. 2012

C-2-b Focusing on AtRA, a vitamin A metabolite

AtRA is an active vitamin A metabolite whose major clinical application is the treatment of acute promyelocytic leukemia. Vitamin A metabolites such as AtRA or 13-cis retinoic acid, which is used in dermatology, have different targets and, therefore, different effects. They share the property of displaying a narrow therapeutic window, *i.e.* both deficiency and high input of vitamin A are toxic. This phenomenon may explain that vitamin A metabolism that has evolved in a complex pathway of transformation and storage. Besides promoting cell differentiation, AtRA also influences cell migration. The study of AtRA effects on the immune system and especially the gut mucosal immune system became a research field in itself.

AtRA metabolism

Vitamin A is an essential fat-soluble nutrient contained in plant and animal food. It is absorbed when mixed with bile acids (Jaensson-Gyllenbäck, Mucosal Immunol, 2011) in duodenum and jejunum, which contribute to the formation of a gradient all along the small intestine (Villablanca EJ, Gastroenterology, 2011). The word "vitamin A" covers different chemical species mainly all-trans retinol and all-trans retinyl esters. Retinol can diffuse passively through the brush border of enterocytes. All-trans retinyl-esters are converted in all-trans retinol by pancreatic lipases and phospholipase B (Van Bennekum AM., Biochemistry, 2000). Then it can enter freely into enterocytes (Figure 9). The main enzyme involved in retinol conversion to retinal is the lecithin-retinol acyltransferase (Batten ML., J. Biol. Chem., 2004). It is highly specific to retinol and contributes up to 90% to its conversion, rendering its distribution higher in the duodenum as compared to the lower parts of the small intestine. The duodenum thus constitutes a major point in the establishment of the retinoid gradient (Herr FM, J Lipid Res., 1993). For further metabolization, two steps are required. A first set of ubiquitous alcohol dehydrogenases can convert retinol into retinal. Then, a specific retinal dehydrogenase can convert retinal into retinoic acid. Retinaldehyde Dehydrogenase (RALDH) specifically converts all-trans-retinal into all-trans-retinoic acid in an irreversible manner by oxidization. It is the limiting step of retinoic acid metabolism. Retinal deshydrogenase is present in certain cell types only, restricting the target tissues of all-trans-retinoic acid. Several isoforms of RALDH are known. RALDH 1 is expressed by intestinal enterocytes (Iwata M, Immunity, 2004) and hepatic

stellate cells. RALDH 2 is expressed by dendritic cells in the mesenteric lymph node and in the LP (Jaensson-Gyllenbäck, Mucosal Immunol, 2011). Vitamin A metabolites are transported as all-trans retinyl esters in lipid droplets and stored as retinol in different tissues, mostly in the liver (70%). In hepatocytes, retinol is bound to a retinol binding protein and secreted into the circulation and in bile (Jaensson-Gyllenbäck, Mucosal Immunol, 2011). It penetrates cells of peripheral tissues thanks to a Stimulated by Retinoic Acid 6 receptor (STRA 6) and it is stored into retinol esters thanks to LRAT action or metabolized into retinoic acid (Chelstowska S., Nutrients 2016).

AtRA acts both in an autocrine and paracrine manner. AtRA either remains intracellular or passively exits producing cells to enter into neighbor cells or into the blood circulation. In the cytosol, it binds to cellular retinoic acid binding proteins (CRABPs), which allow its transport to the nucleus to activate Retinoic Acid Receptors (RARs). As shown in figure 9, activated RARs associated with Retinoid X Receptors (RXR) act as a transcription factor and promotes the expression of target genes that contain Retinoic Acid Response Elements (RARE). Two isoforms of CRABPs are identified CRABP1 and CRABP2, which is expressed in DCs (Gyöngyösi A, J Lipid Res., 2013). The Cytochrome P 26 (CYP26) family takes in charge AtRA degradation. Interestingly, a nuclear target of AtRA is the promoter of the *cyp26* gene suggesting that AtRA regulates its own catabolism. Besides, AtRA upregulates RALDH2 synthesis in DCs (Villablanca EJ, Gastroenterology, 2011). This evidence claims for a positive feedback-loop of AtRA on its own production and degradation.

AtRA impacts on the immune system

AtRA impacts on all actors of the adaptative immune response in the small intestine. First, it specifically induces the synthesis of RALDH2 isoform in DCs in the LP, turning them into AtRA producers (Molenaar R, J Immunol., 2011; Jaensson-Gyllenbäck, Mucosal Immunol, 2011). AtRA also upregulates CD103 expression in DCs (Iliev ID, Gut, 2009; Feng T, J Immunol., 2010) and promotes imprinting of gut homing markers on T cells through two mechanisms. It directly induces the expression of CCR9 and α4β7 on T cells (Edele F., J Immunol., 2008) and it enhances DC imprinting function on T cells (Saurer L , J. Immunol, 2007). This effect is lost upon treatment with RAR antagonist (Iwata M., Immunity, 2004). AtRA also improves the production of specific antibodies that target the gut lumen content as it promotes B cell conversion into IgA+ plasma cells by $CD103^+$ DCs (Mora JR & Iwata M., Science, 2006; Villablanca EJ., Gastroenterology, 2011).

Finally, AtRA directly impacts T cell fate in the small intestine and in MLNs. The most sensitive T cell subsets to AtRA are Tregs and Th17: AtRA favors tolerance by shifting the Treg/Th17 balance towards Treg cell fate. When combined to TGFβ1, AtRA promotes differentiation of T cells into $FOXP3^+$ T cells through its nuclear receptor RARα. AtRA also stimulates Treg generation by DCs and attenuates co-stimulation signals that alter T cell differentiation (Benson MJ, J Exp. Med., 2007). This effect depends on the presence of interleukin (IL-)2 (Mucida D., Science, 2007). AtRA blocks T cell sensitivity to IL-6 (Mucida D., Science, 2007) and IL-23 by inhibiting IL-6 and IL-23 receptors. As a consequence, it reduces IL-17 secretion. This way, it represses T cell conversion into Th17 and stabilizes the T cell fate towards Treg differentiation even under inflammatory conditions (Benson MJ, J Exp. Med., 2007; Laranche & Cheroutre, Annu Rev Immunol., 2016). In the presence of TGFβ, IL-12 and IL-27, AtRA represses Th17 and Th1 fate but also induces of Tregs and reprograms $CD4^+$ T cells into cytotoxic CD8+ T cells. Of note, AtRA is involved in the survival of T effector memory ($CD8^+$αβ) (Huang Y, Nat. Immunol, 2011). This effect is specifically driven through RARα.

Although AtRA effects in favor of Treg expansion are well admitted by the immunology community, its effects on pro-inflammatory T cell subsets (Th1, Th2, Th17) are more controversial. The repression of reversion from Treg fate to another T cell fate depends on the

doses and inflammatory context (Bono MR, Nutrients, 2016). For instance, in the presence of IL-15, AtRA acts as an adjuvant for pro-inflammatory responses to dietary antigens promoting Th17 expansion and repressing differentiation into Treg (DePaolo RW, Nature, 2011). Th17 and Th1 responses to oral infection are impaired upon vitamin A deficient diet. Indeed, RARα activation by AtRA appears to be crucial to sustain IFNγ secretion by Th1 lymphocytes and IL-17 secretion by Th17 lymphocytes (Hall JA, Immunity, 2011).

These paradoxal effects of AtRA on the immune response lead the community to go beyond the single-gene or single-pathway analysis. In that context, a global transcriptomic analysis of human blood monocytes has been proposed (Klassert, Sci Reports., 2017). They studied the transcriptomic landscape upon different types of infections: invasive fungi with *Aspergillus fumigatus*, tolerated fungi with *Candida albicans* and bacteria with *E. coli*. The effect of vitamin A treatment was compared to vitamin D treatment and lack of vitamin supplementation. Many immune relevant genes were identified especially upon *E. coli* infection (235 genes). Data obtained in this study highlight the role of vitamin A in counteracting pathogens effects on monocytes by modulating cytokine and chemokine activity. Moreover, the AtRA-triggered genetic program appears to be adapted to the encountered pathogen. Interestingly, they found AtRA not only to regulate immune functions genes but also associated to cell migration.

AtRA and the microbiota

Several sources of AtRA are identified in the gut and among them some are linked to the microbiota. Podoplanin positive stromal cells of the LP produce AtRA in a microbiotal dependent manner, even under vitamin A deficient diet. Initial production of AtRA by stromal cells allows DCs of the LP to express RALDH and in turn to produce AtRA (Vicente-Suarez I, Immunity, 2015). Germ-free mice have lower RALDH activity in MLNs and Peyer patches (Zhang Z, Immunity, 2016). Actually, $CD103^+$ $CD11b^+$ $RALDH^+$ cDCs migrate upon microbial colonization after birth to form MLNs and secondary lymph nodes. When transferred to specific pathogen free animal facility, mice displayed increased RALDH activity in secondary lymph nodes compared to mice maintained in germ-free conditions. Antibiotic treatment increases RALDH activity while antifungal treatment decreases RALDH activity in the cells of interest.

Antibiotic treatments in a DSS-induced colitis modulate the expression of enzymes involved in AtRA metabolism. Expression of *aldh1*, which is involved in AtRA production is increased and expression of *Cyp26a1*, which is the major enzyme involved in AtRA degradation, is decreased (Bhattacharya N, Immunity, 2016). Authors concomitantly study distal colon inflammation, which was lowered under antibiotic treatments. They conclude that microbiota enhances inflammation and lowers AtRA production under pro-inflammatory conditions. The reciprocal effect is also observed by generating mice fed with vitamin A deficient diet. AtRA depletion affects microbiota, especially it reduces the amount of SFB which downregulates Th17 cell fate (Cha HR, J Immunol., 2010).

These data strongly support the hypothesis of close interactions between AtRA and the microbiota. However, they do not distinguish the effects that are due to the inflammation state of the intestine from the effects that are directly linked with AtRA and microbiota interactions.

AtRA and cell migration: Matrix Metalloproteinases (MMPs) regulation

AtRA has a different effect on cell migration depending on the cells it targets. The impact of AtRA on DC migration has been deciphered *in vitro* and *in vivo*. These studies provide us with consistent results on the impact of AtRA impact on the mechanism involved.

Some of the AtRA target genes are Matrix Metallo-Proteases (MMPs), the proteases that are in charge of the extracellular matrix degradation (ECM). Their activity is regulated by Tissue Inhibitor of Matrix Proteases (TIMPs). Members of the MMP family, mostly MM9, TIMP 1 and TIMP 2, are secreted by DCs (Osman M, Immunology, 2002; Kouwenhoven M, J Neuroimmunol., 2002). MMP9 cleave proteins of the ECM: gelatin, collagen type I and IV and laminin. MMPs have been shown to be required *in vivo* for DCs migration to the draining lymph node in the skin (Ratzinger G, J.Immunol, 2002). MMP9 is essential to recruit DCs *in vivo* from the lung parenchyma to the broncho-alveolar lumen upon aerosol antigen administration. This ability of MMP9 to locally degrade the ECM is nonetheless dispensable for DC accumulation in the lung parenchyma and for DC migration to draining lymph nodes (Vermaelen KY, J Immunol., 2003). However, AtRA promotes DC migration towards draining lymph node (Darmanin S, J Immunol., 2007). The authors dissected the mechanisms underlying this specific effect of AtRA on DCs: it does not interfere with the expression of CCR7 at the surface of DCs suggesting that it does not act through DC immune maturation pathway. AtRA actually enhances MMP9 transcription and inhibits TIMPs transcription. It downregulates MMP9 in human monocytes infected with two out of the three pathogens used among *A. fumigatus*, *C. albicans*, *E. coli* and downregulates MMP1 upon *E. coli* infection (Klassert T, Sci. Reports, 2017).

To summarize, the effect of AtRA effect on DC migration is independent from its effect on DC maturation, and depends on the infectious status. Due to the numerous targets of ATRA, studies about AtRA effects on cancer cell migration generated heterogeneous results depending on the cancer cell line tested (Liang C, Oncol letter., 2015; Cui J, Int J Oncol., 2016; Quintero-Barceinas RS, Biomed Res Int., 2015). One group focused on the effect of AtRA on the actin associated molecular motor, myosin II. They showed on several cancer cell lines that AtRA actually inhibits their migration but increases their adhesion by interacting with myosin II. It downregulates the expression of the myosin light chain kinase, which results in diminished myosin II activity (Zuo L, Nutr Cancer., 2016; Anla Hu, Oncol Reports., 2014). The *in vivo* effects of a potential interaction between AtRA and myosin II remain to be addressed. As other players influence myosin II activity, I will further develop in the following section the basics of DC migration.

D- Cytoskeleton impact on antigen capture and DC migration

D-1- Cytoskeleton in migration

The network of molecules in charge of maintaining cell shape during division, movement and interaction with neighbors constitutes the cytoskeleton. Components of the cytoskeleton are polymers of actin on one hand and tubulin on the other hand. They assemble and disassemble in a dynamic manner to form filaments referred to as fibrillar-actin (F-actin) and microtubules respectively. Microtubules are involved in intracellular trafficking and cell division. The formation of F-actin networks starts with nucleation promoted by the Arp2/3 complex or proteins from the formin family (Campellone KG, Nat Rev Mol Cell Biol., 2010). Stability of filaments is the result of a balance between F-actin polymerization compensated by a constant disassembly of filaments. In the context of migration, F-actin disassembly generates a retrograde flow of actin monomers, which are used to build new filaments.

F-actin associates with many proteins. Some of these proteins, such as talin, can connect actin to the plasma membrane and/or to transmembrane molecules such as integrins (Sun Z, J Cell Biol., 2016), sensing the adhesion of cells to the extracellular space. Myosins are actin-associated molecular motors that transport vesicles along actin filaments or shape the structure of the actin cytoskeleton. Among myosins, myosin II plays a key role in crosslinking F-actin filaments and thereby contracting actin networks helping force generation. Myosin II is involved in cell migration as well as in phagocytosis and macropinocytosis. In particular, myosin II is essential for the induction and closure of phagosomes and macropinosomes (Mercer & Helenius, Nat. Cell Biol. 2009).

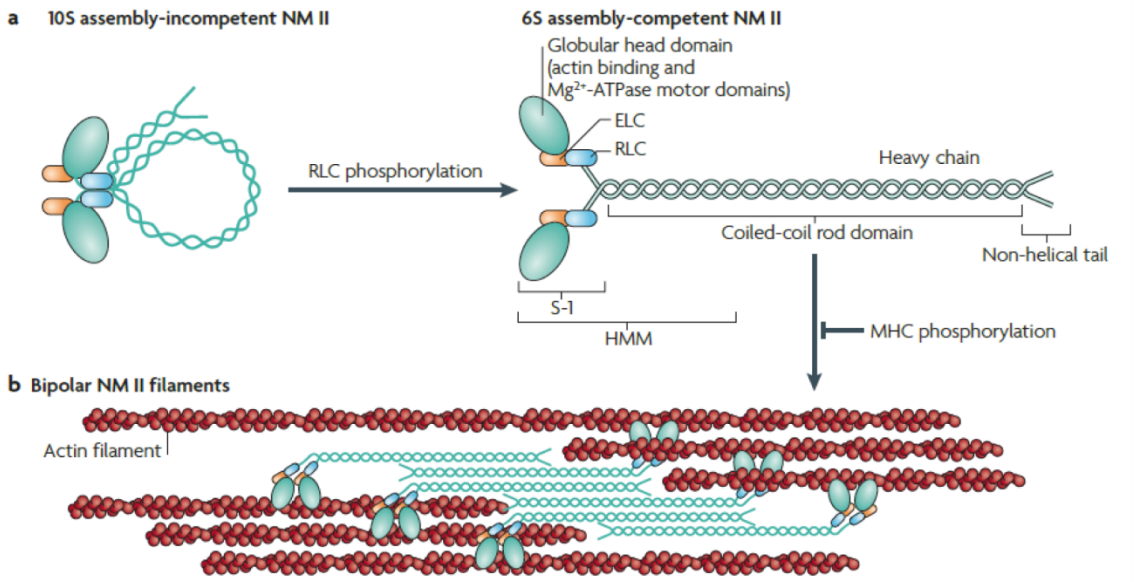

Figure 11. Non-muscle Myosin IIA structure. The subunit and domain structure of non-muscle myosin II (NM II), which forms a dimer through interactions between the α-helical coiled-coil rod domains. The globular head domain contains the actin-binding regions and the enzymatic Mg2+-ATPase motor domains. The essential light chains (ELCs) and the regulatory light chains (RLCs) bind to the heavy chains at the lever arms that link the head and rod domains. In the absence of RLC phosphorylation, NM II forms a compact molecule through a head to tail interaction. It results in an assembly in competent form (10S; left) that is unable to associate with other NM II dimers. On RLC phosphorylation, the 10S structure unfolds and becomes an assembly-competent form (6S). S-1 is a fragment of NM II that contains the motor domain and neck but lacks the rod domain and is unable to dimerize. Heavy meromyosin (HMM) is a fragment that contains the motor domain, neck and enough of the rod to effect dimerization. **b** | NM II molecules assemble into bipolar filaments through interactions between their rod domains. These filaments bind to actin through their head domains and the ATPase activity of the head enables a conformational change that moves actin filaments in an anti-parallel manner. Bipolar myosin filaments link actin filaments together in thick bundles that form cellular structures such as stress fibres. From Vicente-Manzanares M, Nat Cell Biol., 2009

Myosin II presents different isoforms: myosin II A, myosin II B, myosin II C that are encoded by the *myh9*, *myh10* and *myh14* genes respectively. Haematopoietic cells mainly express *myh9*, and among them, DCs only express the *myh9* gene, which corresponds to the myosin IIA isoform (Maravillas-Montero JL, J Leukoc Biol., 2012). As shown in Figure 9, the function of myosin IIA as an actin cross-linker is imprinted in its structure. Each monomer of non-muscle Myosin IIA results from the association of a head at its amino-terminal extremity with an essential light-chain (ELC) and a regulatory MLC, forming a neck and a coiled–coil tail at its carboxy-terminal extremity (Vincente-Manzanares M, Nat Cell Biol., 2009). This coiled-coil forms a supercoil upon dimerization which is required to build a complete Myosin II molecule. Myosin II binds actin filament thanks to the dedicated site at its head. To move or produce tension on actin filaments, it consumes ATP through its ATP catalytic site found also at the head of the molecule. At the steady state, tail and head are connected in a compact way. Upon MLC phosphorylation, the compact form of Myosin II unfolds and the tail of the dimer is released. The oligomerization of Myosin II molecules in an anti-parallel manner produces a contractile unit.

The contribution of each actor of the cytoskeleton to DC migration in one, two and three dimensional environments is a dynamic field of research. Cells in general and DCs in particular must adopt a polarized asymetric phenotype to propel themselves in one direction. In three dimensional environments, this polarization is achieved thanks to the formation of a gradient of molecules in the cytosol, leading to myosin II enrichment at the rear pole of the cell. Such a gradient is maintained thanks to the actin retrograde flow that results from disassembly of filaments. By binding firmly to actin through its light chain, myosin II is transported to the rear of the cell by this flow (Maiuri P, Cell, 2015). Once at the rear, the two cytoskeletal components form active acto-myosin bundles which lead to the contraction of the cell rear (Cramer LP, Nat Cell Biol., 2010). Relaxation of this contraction releases energy producing forward cell movement. Myosin II is thought of as an authentic polarity cue since it also orientates the cell by repositioning the nucleus during migration (Vicente-Manzanares M, Nat Cell Biol., 2009).

A study of mature DC migration has identified the key mechanisms involved depending on the environment (Lämmermann T, Nature 2008). Authors confirm that DC and leukocyte migration in 2D depends on integrin-based adhesion, which are also required for DC extravasation from blood vessels upon inflammation *in vivo* in the skin. Studying 3D migration in collagen gels and *in vivo* shows that DC migrate in an integrin independent manner. They further identify a mechanistic dissociation between front and back of the cell. The front is dynamic, exhibiting with a high rate of protrusion formation facilitated by the cortical actin network, while the rear moves by contraction under the control of myosin II. The integrity of both rear and front actin networks is required to get efficient migration in a 3D collagen gel, that is to say fast and allowing effective displacement of both the nucleus and the cell body. In this set up, when myosin II is inhibited, the cell gets an elongated phenotype since the front is still protruding while the back is not contracting. In that case, the nucleus cannot pass through the pores of the collagen gel unless the density of the mesh is low enough. These data led the authors to conclude that myosin II is required for nucleus propelling through small pores in a 3D environment. The same group studied actin and myosin contribution to mature DC migration in a confined set up under a gradient of chemokines (Renkawitz J, Nat Cell Biol., 2009). They show that myosin II is recruited at the rear of the cell where it contracts the cell body. This myosin II transport backward takes part and occurs through the actin retrograde flow. This was later confirmed in collaboration with our group, who built a physical model demonstrating that polarity cues transported to the cell rear by the actin retrograde flow lead to fast and persistent migration (Maiuri P, Cell, 2015).

Our group further explored the mechanisms involved in the migration of immature DCs under confinement. Data showed localization of myosin IIA is linked to DC speed (Chabaud M, Nat Comm., 2015). During fast migration phases, myosin IIA is located at the rear of the cell. During slow migration phases, myosin IIA is located at the front of the cell. The study shows: 1) myosin II recruitment at the front increases only when cell speed decreases, 2) cell deceleration is due to the loss of myosin II at the rear (Lavi I, Nat Physics, 2016). Experiments about DC migration *in vitro* through small constrictions show the assembly of a confinement induced actin network (CiAN) around the nucleus (Thiam HR, Nat Comm., 2016).

These actin filaments are under the regulation of the actin nucleator Arp2/3. During immature DC passage through small constrictions, myosin IIA is localized at the back of the cell but not around the nucleus. Furthermore, inhibiting myosin IIA does not affect the cell passage rate through constrictions but impacts cell speed, which is consistent with our previous data. This information in microchannels helps us envision myosin IIA role in the migration of immature DCs: it is required for fast migration but not for cell passage through constrictions. In contrast, under similar confinement and in presence of chemokines, mature DCs require myosin IIA to pass through constrictions. These data highlight the influence of the DC maturation state on their migratory profile.

In fibroblasts that, in contrast with DCs, are strongly adhesive cells, another dissociation of back and front is based on pressure. Myosin IIA interacts with nesprin 3 at the front of the nucleus. This generates a high pressure in that part of the cell that maintains the position of the nucleus (Petrie RJ, Science, 2014). To sum up, the literature shows us that the role and the contribution of a cytoskeletal molecule to migration evolve with the cell situation: 2D/3D migration, immature status *vs* mature status. Although the strong impact of myosin IIA on cell speed is admitted in the field of migration in different cell types (Lämmermann T, Nature 2008; Petrie RJ, Science 2014; Thiam HR, Nat Comm 2016), its contribution to DC passage through micrometric pores is still under discussion, as data provide us with different results depending on the *in vitro* experimental set up. Indeed, in a 3D-mesh mimicking extracellular matrix, cell passage through narrow constriction is myosin IIA dependent, whereas under confinement in microchannels mimicking capillaries, cell passage through constrictions relies on actin regulation and not on myosin IIA. In addition, the maturation status of DCs *in vivo* is challenging to define, especially in the small intestine where they are constantly in contact with dietary and microbial antigens. As a consequence, the impact of myosin IIA on DC passage *in vivo* remains unsolved.

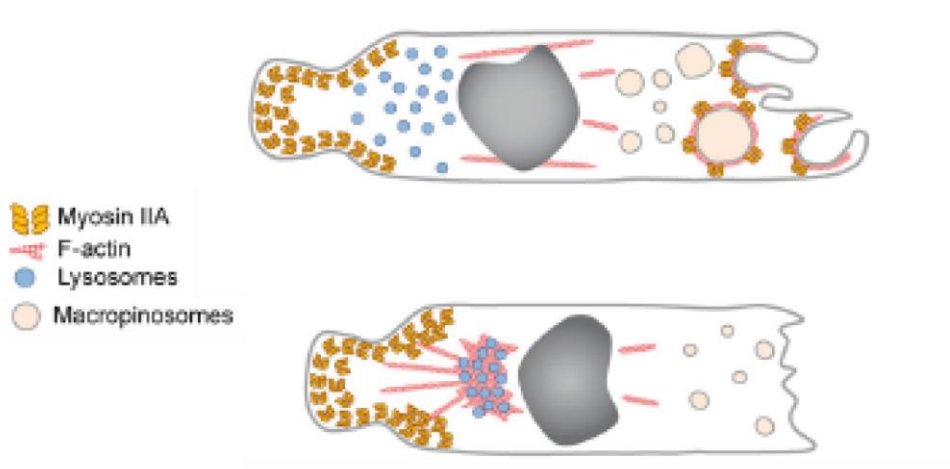

	Dendritic cell	
	Resting	Activated
Macropinocytosis	High	Low
Antigen uptake	High	Low
Polarity	High	High
F-actin	Front	Back
Myosin IIA	Front/back	Back
MTOC	ND	ND
Lysosomes	Back/dispersed	Back/packed

Figure 12. Cytoskeleton and Cell polarization in Dendritic Cells. DCs are highly polarized under resting conditions. At the migrating front of the cell, antigen uptake occurs constantly through macropinocytosis. Macropinosomes form in a F-actin/Arp2/3 and Myosin IIA-dependent manner. In addition, a Myosin IIA-enriched structure is observed at the rear of the cell. Lysosomes are dispersed and located at the rear of the cell behind the nucleus. Upon activation, DCs maintain their polarized phenotype but undergo a major change in F-actin distribution: at the cell front, F-actin is markedly reduced, while at the rear of the cell one observes an F-actin-enriched structure from which actin cables emanate. As a consequence of this change, macropinocytosis is downregulated. Finally, lysosomes are clustered in mature DCs and are closely apposed to the F-actin-enriched structure at the cell rear. (Bottom) The table summarizes the main aspects Ag uptake in DCs. Adapted from Bretou M, Immunol Rev., 2016.

D-2- Myosin is a cell conductor

D-2-a Myosin II in antigen capture

DCs capture antigens thanks to a specific process called macropinocytosis. During macropinocytosis, DCs develop protrusions before engulfment of liquid by closure of the cell membrane onto a nascent macropinosome. Myosin II plays a role in extending protrusions although it is not present at the tip but at the basis of the protrusion. It rather acts indirectly through the force it exerts on actin filaments that form the scaffold of the protrusion. A study of different isoforms shows that myosin IIB is dispensable for protrusion formation in 3D collagen gels while myosin IIA and more precisely, phosphorylation of its heavy chain is required for this process (Rai V, J Bio Chem, 2017). Myosin II also takes part in protrusion dynamics, since cells lacking myosin II can extend protrusions but cannot retract them (Vicente-Manzanares M, J Cell Biol., 2011). Actually, myosin II regulates local actin retrograde flow within the forming protrusion, limiting the formation of actin bundles and thus the elongation of the protrusion. Myosin II prevents not only excessive protrusion elongation but also formation of irrelevant protrusions. This myosin II effect is mediated by two mechanisms. First, myosin II helps forming stable actin bundles that do not polymerize anymore. Second, myosin II promotes the maturation of newly formed adhesions by promoting interaction of actin molecules with vinculin and talin molecules. However, it is not the only step in which myosin II could be involved, since our laboratory lately showed that myosin II is not only essential for motility but also coordinates migration with macropinocytosis antigen processing *in vitro*.

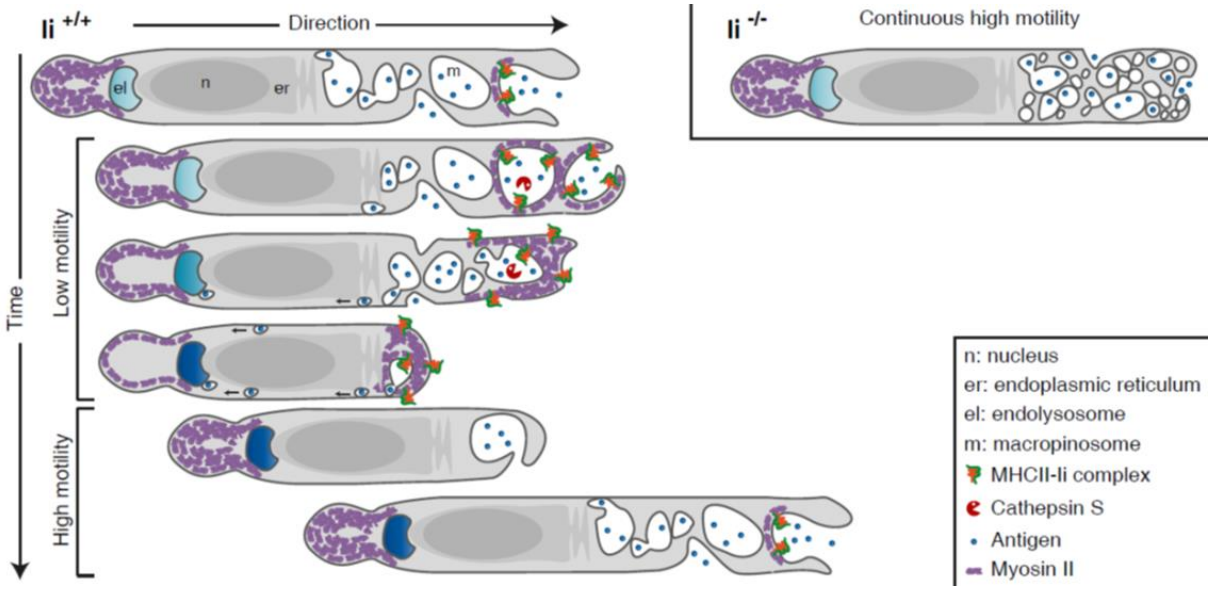

Figure 13. Coupling antigen capture to DC migration. DCs under confinement display a two phase migration mode. The low motility phase when myosin IIA is recruited at the front of the cell corresponds to macropinocytosis and macropinosome maturation. The high motility phase when myosin IIA is recruited at the back of the cell corresponds to few macropinocytosis performed. Ii KO DCs do not have low motility phase. From Chabaud M.

D-2-b Myosin II couples antigen capture and migration

DCs are professional Antigen-Presenting cells (APCs) that is to say they load peptides from the processed antigen on a MHC molecule. Metabolism and protein synthesis get enhanced to provide energy during antigen processing and loading of MHC molecules by exchanging clived Ii with antigenic peptide (see section A-2- and Figure 3). Our group showed Myosin II-Ii complex coordinates antigen processing and immature DC migration under confinement in microchannels (Chabaud M, Nat. Comm., 2016). Macropinosome maturation actually requires the recruitment of myosin IIA at the front of migrating DCs. This Ii-dependent transport of myosin IIA from the rear to the front of DCs disrupts the back-to-front gradient (Figure 13). By breaking polarization, this myosin IIA transport promotes macropinocytosis and slows down immature DCs (Faure-André G, Science 2008). These slow motility phases correlate with transport of antigen from macropinosomes to endolysosomal compartments where they are processed. Upon antigen uptake, DCs sense costimulatory signals leading them to undergo maturation. They engage in a non-reversible pathway and undergo a genetic reprogramming to adapt this new functional status. DC maturation includes downregulation of macropinocytosis and MHC II production and upregulation of adhesion molecules. As they express CCR7 at their membrane surface which ligands CCL19 and CCL25 are expressed on lymphatic endothelial cells, they turn into a fast migrating mode towards lymphatic vessels with Myosin IIA (Chabaud M, Nat Comm., 2016) and actin (Vargas P, Nat Cell Biol., 2016) located at the back of the cell. In the skin, they actively migrate to the draining lymph node of the tissue to present the acquired antigen to T cells (Forster R, Cell, 1999).

Thesis rational and thesis goals

As described above, antigen capture and migration are two major functions that are coupled in DCs. Myosin IIA controls migration of immature DCs in a confined environment and nucleus passage through small pores in mature DCs in the presence of chemokines. Myosin II sub-localization in the cell depends on a sequential regulation: mostly recruited at the back when DCs migrate, mostly recruited at the front when DCs perform macropinocytosis. This dynamic change in polarization is required *in vitro* for a proper coordination of cell migration and antigen capture. Besides, Myosin II controls cell contraction in DCs, especially it concentrates at the origin of dendrites thus controlling their growth and retraction. In the small intestine, a way to capture antigen by phagocytes is to form trans-epithelial dendrites (TEDs) through the gut epithelial monolayer to catch bacterial antigens in the lumen upon infection. These TEDs that are expected to be highly dependent on Myosin II raised our interest in the small intestine.

In vivo, intestinal tissue generates different DC subsets which repartition along the small intestine differs from one subset to another. The tissue has the capacity to locally imprint DC function which might explain variabilities from one subset to another and from one region of the small intestine to another. The impact of tissue cues on the capacity of DCs to migrate and capture antigens remains unclear. Several routes are described for an antigen to get to a lymph node but DCs appear to play a the specific role of capturing antigens in peripheral tissues and bringing it fast to lymph nodes. Antigen presentation by DCs is essential not only for T differentiation but also and more importantly for homing of T cells to the infected or injured tissue.

In that context, what is the myosin IIA contribution to DC function *in vivo* in the specific context of the shaping of the mucosal immune system in the small intestine?

The main goals of my work were, to understand under homeostatic conditions *in vivo* how myosin II impacts on 1) the tissue patrolling function of DC in the small intestine and 2) to evaluate the consequences of such impact on mucosal immunity.

RESULTS

Myosin IIA- and retinoic acid-dependent transmigration defines a unique intra-epithelial population of dendritic cells in the small intestine

Dendritic cells patrol peripheral tissues and transport the antigens they collect to lymph nodes in order to present them to T lymphocytes. This constitutes the first step of adaptive immune responses and relies on two essential cellular functions: (1) the extraordinary ability of DCs to internalize extracellular material and (2) their elevated migratory capacity. In migrating bone-marrow-derived DCs, these two functions are spatiotemporally coordinated by the actin-based motor Myosin II: when Myosin II accumulates at the rear of DCs, it allows forward locomotion, whereas when enriched at their front, Myosin II promotes the internalization of extracellular material. How such coordination impacts the sentinel function of DCs in their natural environment remains unknown. This question is particularly pertinent in view of the existence of DC subtypes with distinct functional specializations in different tissues: whether modulation of antigen uptake and/or migration of DC subtypes by specific cues present in their environment contribute to their functional specialization remains an open question.

Functional specialization of DCs has been extensively studied in the gut, which includes unique DC subtypes that locally control the balance between tolerance and immunity. Importantly, the distribution of DCs along the intestinal tract shows strong compartmentalization. Monocytes can produce $CD103^{-}CD11b^{+}$ DCs but do not contribute to the $CD103^{+}CD11b^{+}$ cDCs. This cDC subset, which is specific to the LP and especially frequent in the upper part of the small intestine, originates from DC precursors (pre-DCs), depends on Notch2 and the transcription factor Irf4 and relies on environmental cues such as the Vitamin A derivative all-trans Retinoic acid (Klebanoff CA, J Exp Med, 2013). $CD103^{+}CD11b^{+}$ cDCs are particularly responsive to fungi and extracellular bacteria (Lewis KL, Immunity, 2011) and drive Th17 pro-inflammatory responses (Persson EK, Immunity, 2013). Parabiontic mice experiments support the hypothesis that $CD103^{+}CD11b^{+}$ cDCs form the main DC subset to migrate to the MLNs in the context of Salmonella infection (Bogunovic M., Immunity, 2009). $CD103^{+}CD11b^{-}$ cDCs also derive from pre-DCs under the control of fms-like tyrosine kinase 3 (Flt3) ligand, the transcription factor Id2, IRF8 (Ginhoux F, J Exp Med, 2009), and Batf3

(Edelson BT, J Exp Med., 2010). Intestinal $CD103^+CD11b^-$ cDCs cross-present oral antigens to $CD8^+$ T cells in MLNs (Becker M, Front Immunol, 2014). The monocyte-derived $CD103^-$ $CD11b^+$ monocyte-derived cells are rare in the small intestine but frequent in the colon where they prime pro-inflammatory responses. $CD103^-CD11b^-$ cDCs form a small and so far understudied population.

Although enterocytes are rather non permeable to antigens, DCs can sense and capture antigens present in the gut lumen. A passive paracellular leakage of soluble antigens through the epithelium has been highlighted for soluble antigen sensing (Pabst O. & Mowat AM., Mucosal Immunol., 2012). In addition, goblet cells form Goblet cell Associated Antigen Passages (GAPs) to deliver soluble antigens to the LP below, in particular to $CD103^+$ DCs (McDole JR, Nature, 2012). Besides, cells residing in the LP such as $CD11c^+$ $CX3CR1^+$ mononuclear phagocytes have been identified to actively and directly sample the gut lumen through the formation of trans-epithelial dendrites (TEDs). They emit TEDs in response to secretion of fractalkine by the epithelium (Kim KW, Blood, 2011) and act as intermediaries between the gut lumen and DCs to which they transfer lumenal antigens (Mazzini E., Immunity, 2014). $CD11c^+CD103^+$ DCs were identified, regardless of their CD11b status, to sit at the periphery of the lamina propria (LP) where they interact with epithelial cells also send TEDs through the epithelium. These cells are eventually found in the epithelium during Salmonella infection (Rescigno M., Nat Immunol., 2001; Chieppa M., J Exp Med. 2006; Farache J., Immunity, 2013). Various antigen capture strategies are differentially used by DCs to patrol the various regions of the gut has not been addressed so far.

We here investigated how modulation of the antigen uptake and/or migratory capacity of DCs impact on their ability to patrol the small intestine *in vivo* by studying their dynamics in myosin IIA-conditional knock out (KO) mice. We found that myosin IIA activity is selectively required for the constitution of an intraepithelial population of DCs, which are $CD11b^{+}CD103^{+}$ and highly motile, suggesting that they actively patrol the epithelial cell layer. Myosin IIA-dependent DC transmigration from the LP to the epithelium requires the production of retinoic acid, and accordingly, occurs preferentially in the upper parts of the small intestine. Noticeably, we found that intraepithelial $CD11b^{+}CD103^{+}$ DCs are an homogenous population that exhibit a distinct transcriptomic signature from the one of LP double-positive DCs. These results suggest that myosin IIA-, retinoic acid-dependent transmigration therefore defines a unique intraepithelial DC population patrolling the upper floors of the gut under homeostatic conditions.

Figure 14. Intra-epithelial cDCs come from the CD103+CD11b+ cDC pool of the lamina propria.
(A) Description of the genetic model. $MyoIIA^{KO}$ refers to Myosin $IIA^{Flox/Flox}$ X CD11c-$Cre^{+/-}$ X $Tomato^{Flox/Flox}$ and $MyoIIA^{WT}$ refers to Myosin $IIA^{WT/WT}$X CD11c-$Cre^{+/-}$ X $Tomato^{Flox/Flox}$.
(B) Left panel: representative image (Z-projection of 6 planes spaced by 2µm) from time lapse movie of Jejunum of $MyoIIA^{WT}$ mouse acquired by intravital microscopy. White arrows highlight GFP^{+} cells in the epithelium. The data are representative of three independent experiments. Right panel: scheme of left panel highlighting the color code: CD11c-GFP (Cyan) and tdTomato (Magenta).
(C) Representative image (Z-projection of 6 planes spaced by 2µm) from time lapse movie of Jejunum of $MyoIIA^{KO}$ mouse acquired by intravital microscopy. Colors represent CD11c-GFP (Cyan) and tdTomato (Magenta). The data are representative of three independent experiments.
(D) Up: time lapse montage on a GFP^{+} cell highlighted in (B) with a white square. Dotted lines mark the borders of the epithelium, white arrow shows a GFP cell entering in the epithelium.
Below: Time lapse montage on a GFP^{+} cell highlighted in (C) with a white square. Dotted lines mark the borders of the epithelium, white star shows a protrusion elongating from the LP into the epithelium.
(E) $MyoIIA^{KO}$ refers to Myosin $IIA^{Flox/Flox}$ X CD11c-$Cre^{+/-}$ and $MyoIIA^{WT}$ refers to Myosin $IIA^{Flox/Flox}$ X CD11c-$Cre^{-/-}$. Number of observed events of cells crossing the basal membrane. Data are pooled from three independent experiments.
Student's t analysis results for this and all subsequent figures are indicated as follows: ***$p < 0.001$, **$p < 0.01$, *$p < 0.05$. A p value of 0.05 or greater was considered non-significant (ns).

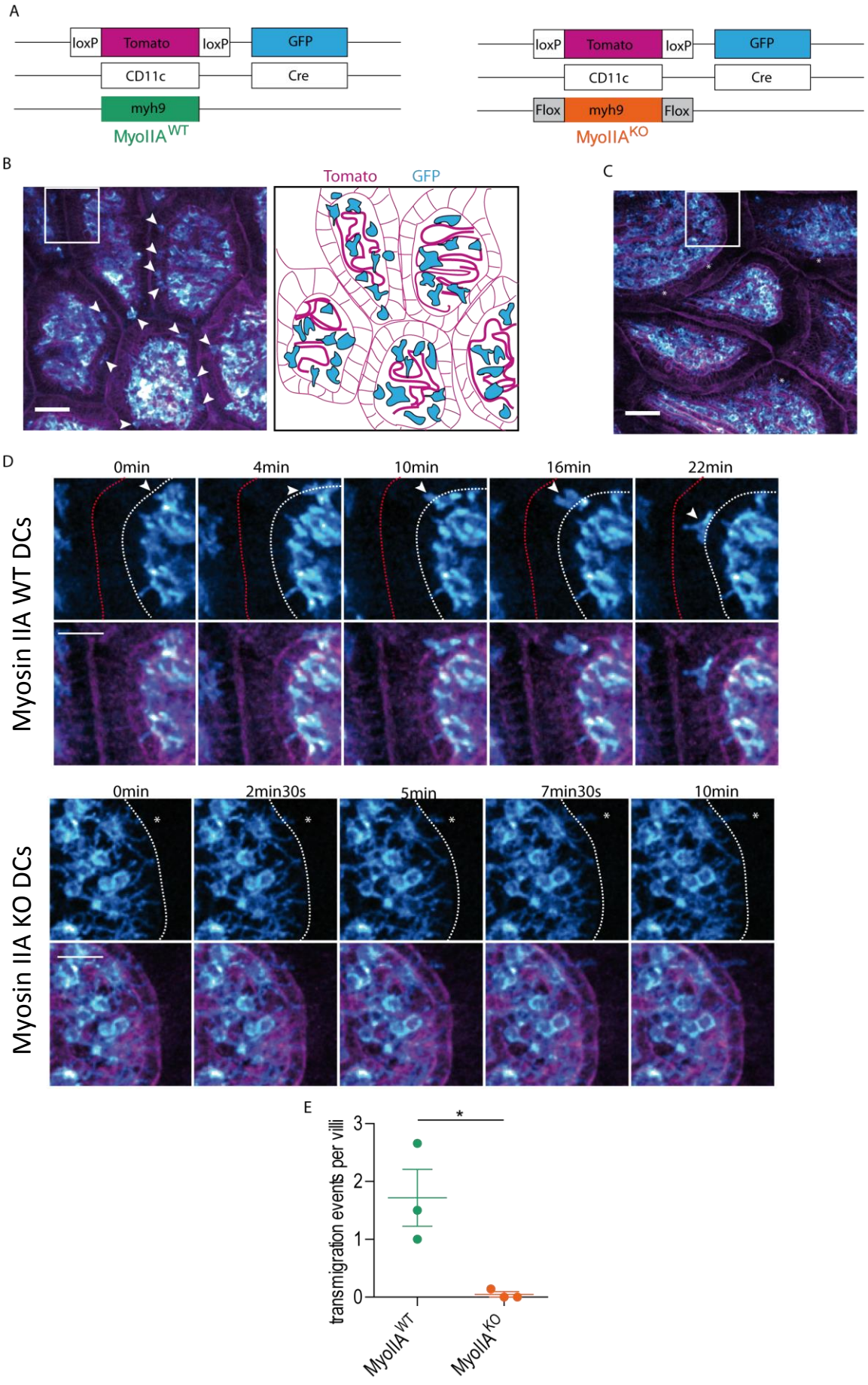
A
loxP
Tomato
loxP
GFP
CD11c
Cre
myh9
MyoIIA WT
loxP
Tomato
loxP
GFP
CD11c
Cre
Flox
myh9
Flox
MyoIIA KO
B
Tomato
GFP
C
D
0min
4min
10min
16min
22min
Myosin IIA WT DCs
0min
2min30s
5min
7min30s
10min
Myosin IIA KO DCs
E
transmigration events per villi
3
2
1
0
*
MyoIIA WT
MyoIIA KO

Intraepithelial DCs originate from CD11b$^+$CD103$^+$ DCs that migrate from the LP in a Myosin IIA-dependent manner

We aimed at investigating how modulation of the capacity of DCs to migrate and capture antigens impacts on their behavior *in vivo* in the small intestine. For this, we generated a mouse model in which CD11c$^+$ cells express GFP while evolving in a TomatoFP+ small intestine, and are or not knock out for Myosin IIA, the main Myosin II heavy chain isoform of mouse DCs (Fig. 14 A) (Shay T & Kang J, Trends in Immunol., 2013; Maravillas-Montero JL, J Leukoc Biol., 2012),. Intra-vital two-photon imaging of the jejunum of wild-type (WT) mice showed numerous GFP$^+$ cells within the LP (Fig. 14 B and supplementary movie 1), as expected. Indeed, the CD11c marker was described as expressed not only in conventional DCs, but also in monocyte-derived DCs and macrophages (Tamoutounour S, Immunity, 2013), as well as in NK cells.

GFP$^+$ cells were highly dynamic: they globally exhibited an elevated protrusive activity, in particular at the border between the LP and the epithelium. In addition, some WT GFP$^+$ cells were highly motile (supplementary movie 1), in agreement with a previous report showing by intravital microscopy that CD11c$^+$ gut DCs identified by histologyand flow cytometry to belong to the CD103$^+$ DC subset can migrate within the LP (Farache J, Immunity, 2013). Noticeably, we found that WT GFP$^+$ motile cells migrated from the LP into the epithelial cell layer. Some were able to establish contacts with GFP$^+$ cells that remained in the LP (supplementary movie 1, Fig. 14 B, and Fig. 14 D for zoom).

Analysis of jejunum slices from Myosin IIA-deficient mice (Fig. 14 B) showed a drastically different picture. First, Myosin IIA-deficient CD11c$^+$ cells lost their locomotion capacity (supplementary movie 2), consistent with previous results showing that this motor protein controls the migration of bone-marrow-derived DCs in confined environments *ex vivo* (Leithner A., Nat Cell Biol, 2016; Chabaud M, Nat Comm, 2015). Second, DCs migrating from the LP into the epithelium were barely observed in Myosin IIA conditional KO mice (Fig. 14 C). Instead, myosin IIA KO CD11c$^+$ cells located within the LP at the frontier with the epithelium extended long membrane protrusions from their cell body towards the lumen of the gut, which were not observed in WT gut DCs (Fig. 14 C and 1A D below for zoom).

This result was confirmed by flow cytometry analysis, which showed that intraepithelial $CD11b^+CD103^+$ DCs were almost totally missing in animals lacking Myosin IIA in their $CD11c^+$ compartment (Fig. 15EF). We conclude that $CD11b^+CD103^+$ double-positive cells need Myosin IIA to migrate from the LP into the gut epithelium, this migration event being required for the establishment of a pool of intraepithelial DCs under homeostatic conditions. Flow cytometry analysis and immuno-staining of fixed gut slices showed that intraepithelial $CD11c^+$ cells mainly corresponded to the $CD11b^+CD103^+$ subset (Fig. 15 A-E), consistent with a previous observation showing that these cells can indeed be found within the epithelial cell layer (Farache J, Immunity, 2013). Our results therefore suggest that the intraepithelial population of DCs originates from $CD11b^+CD103^+$ double-positive cells that migrate from the LP into the gut epithelium.

Figure 15. Myosin IIA deficiency in DC affects only the $CD103^+CD11b^+$ subset.
(A) Gating strategy in epithelium and lamina propria of the small intestine.
(B-D) Plots present percentages and absolute numbers for $CD103^+CD11b^-$ (B), $CD103^-CD11b^+$(C), $CD103^-CD11b^-$ (D) in the lamina propria (left) and in the epithelium (right) of the small intestine. Data are pooled from three independent experiments.
(E) Plots present percentages and absolute numbers for $CD103^+CD11b^+$ in the lamina propria

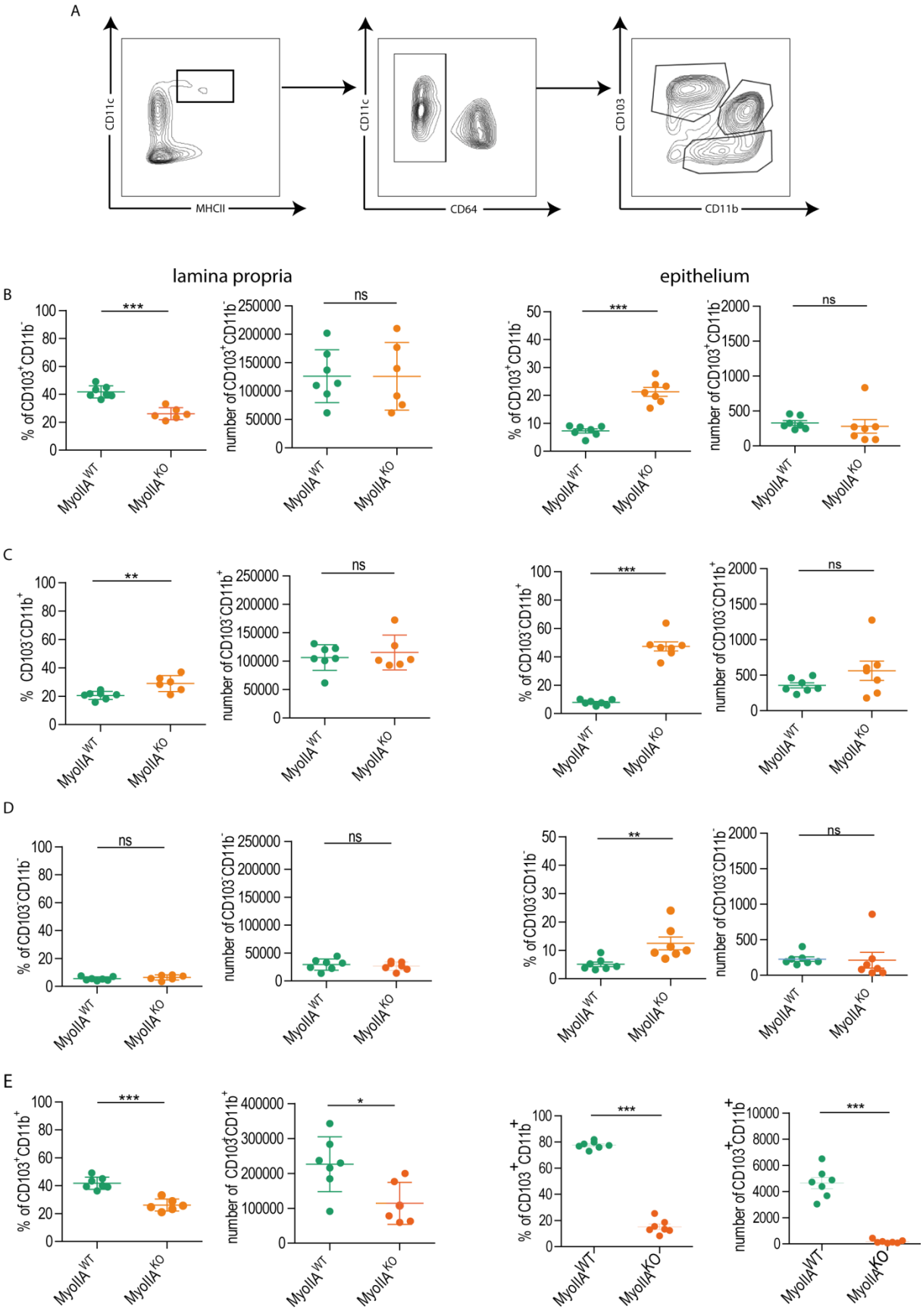
A
CD11c
MHCII
CD11c
CD64
CD103
CD11b
lamina propria
epithelium
B
% of CD103+CD11b-
number of CD103+CD11b-
C
% CD103-CD11b+
number of CD103-CD11b+
D
% of CD103-CD11b-
number of CD103-CD11b-
E
% of CD103+CD11b+
number of CD103+CD11b+
MyoIIA WT
MyoIIA KO
ns
*
**
***

Myosin IIA regulates transmigration of CD11b$^+$CD103$^+$ DCs *in vivo* and *ex vivo*

How does Myosin IIA impact on the migration of CD11b$^+$CD103$^+$ DCs from the LP into the gut epithelium? To address this question, we generated live jejunum slices that can be imaged at higher magnification (40x) as compared to jejunum imaged by intra-vital microscopy (25x). We focused on CD11c$^+$ cells located at the border between the LP and the epithelium. WT CD11c$^+$ DCs exhibited an elevated protrusive activity towards the epithelial cell layer, different type of protrusions being observed, including blebs as well as thinner filopodia-like protrusions (supplementary movie 3 and Fig. 16 A, green stars). Such dynamic short-live protrusions were rare in gut slices from myosin IIA-deficient mice, which displayed a vast majority of long and stable membrane extensions (supplementary movie 4 and Fig. 16 B, orange stars). 3-D reconstructions obtained from such movies showed that protrusions from myosin IIA KO cells penetrated into the epithelial cell layer (supplementary movie 4 and Fig. 16 B). In addition, quantifications performed on fixed jejunum slices confirmed that CD11c$^+$ cells lacking myosin IIA (1) formed more and longer protrusions than their WT counterpart (Fig. 16 C for quantification), and (2) did not cross the basement membrane that separates the LP from the epithelium. However, these protrusions did not increase the permeability of the intestinal (Fig. 17 F) epithelium. These results strongly suggest that DCs first extend protrusions from the LP to the epithelium through the basement membrane in a myosin IIA-independent manner and then move their cell body into the epithelium thanks to the action of the motor protein.

Interestingly, myosin IIA requirement for transmigration was reproduced *ex vivo* when analyzing mature bone marrow DCs derived from KO animals in collagen-coated transwells (Fig. 16 E), indicating that this role of myosin IIA is not restricted to CD11b$^+$CD103$^+$ gut DCs. This result further provided us with a cellular model to address the mechanisms involved in this process. Indeed, Myosin IIA might serve the translocation of the cell body of DCs through the basement membrane by two non-exclusive means: (1) it might promote the retraction of cell front protrusions that are anchored the epithelium and/or (2) it might contract the cell rear to squeeze the nucleus of DCs. To distinguish between these two possibilities, we analyzed the subcellular localization of the motor protein by using bone marrow DCs derived from myosin IIA-GFP knock in (KI) animals migrating into 5x7µm

microchannels that include 2x7µm constrictions. We have previously shown using such device that mature DCs need myosin II activity to go through such small holes (Leithner A., Nat Cell Biol, 2016; Chabaud M, Nat Comm, 2015; Thiam HR, Nat Comm., 2016). We found that myosin IIA-GFP forms a gradient within DCs that pass through constriction, being strongly enriched at the cell rear (supplemental movie 5 and Fig. 16 F). Further analyzing our data on fixed tissue, we showed a significative correlation between the number of protrusions and the number of intra-epithelial DCs in MyoIIA^{WT} mice (Fig. 16 E). We do not observe this correlation in MyoIIA^{KO} mice that display long and numerous protrusions but very few intra epithelial DCs. Taken together, these results suggests that myosin IIA can facilitate the passage of DCs through small holes by contracting their rear, even though we cannot exclude that in CD11b^{+}CD103^{+} gut DCs, Myosin IIA might also promote retraction of cell front protrusions. Anyhow, myosin IIA emerges as a major regulator of DC transmigration *ex vivo* and *in vivo*.

Figure 16. Myosin IIA is required for DC transmigration into the epithelium.
(A) Time lapse montage of 3D-reconstruction of a movie of Jejunum of MyoIIA^{WT} mice acquired by bi-photon microscopy on an *ex vivo* slice. Colors represent CD11c-GFP (Cyan) and tdTomato (Magenta). Green arrows mark blebs and filopodia. The data are representative of three independent experiments.
(B) Time lapse montage of 3D-reconstruction of movie of Jejunum of MyoIIA^{KO} mice acquired by bi-photon microscopy on an *ex vivo* slice. Colors represent CD11c-GFP (Cyan) and tdTomato (Magenta). Orange arrows mark a stable protrusion. The data are representative of three independent experiments.
(C) Distribution of length of the protrusions penetrating the epithelium in MyoIIA^{WT} and MyoIIA^{KO}. Data were pooled from three independent experiments on fixed tissue.
(D) Transmigration assay of bone-marrow derived DCs from MyoIIA^{KO} and MyoIIA^{WT} mice was assessed in Matrigel© coated transwells. Data are representative of three independent experiments, three replicates per experiment.
(E) Correlation analysis of the number of protrusions with the number of intra-epithelial GFP cells between MyoIIA^{WT} and MyoIIA^{KO} villosities. Numbers are normalized by the number GFP cells in the stroma of the villosities. Data were pooled from three independent experiments on fixed tissue.
(F) Left: Timelapse from a movie of a Myosin IIA-GFP DC migrating through a constriction. Right: intensity profile of the GFP signal during migration through the constriction.

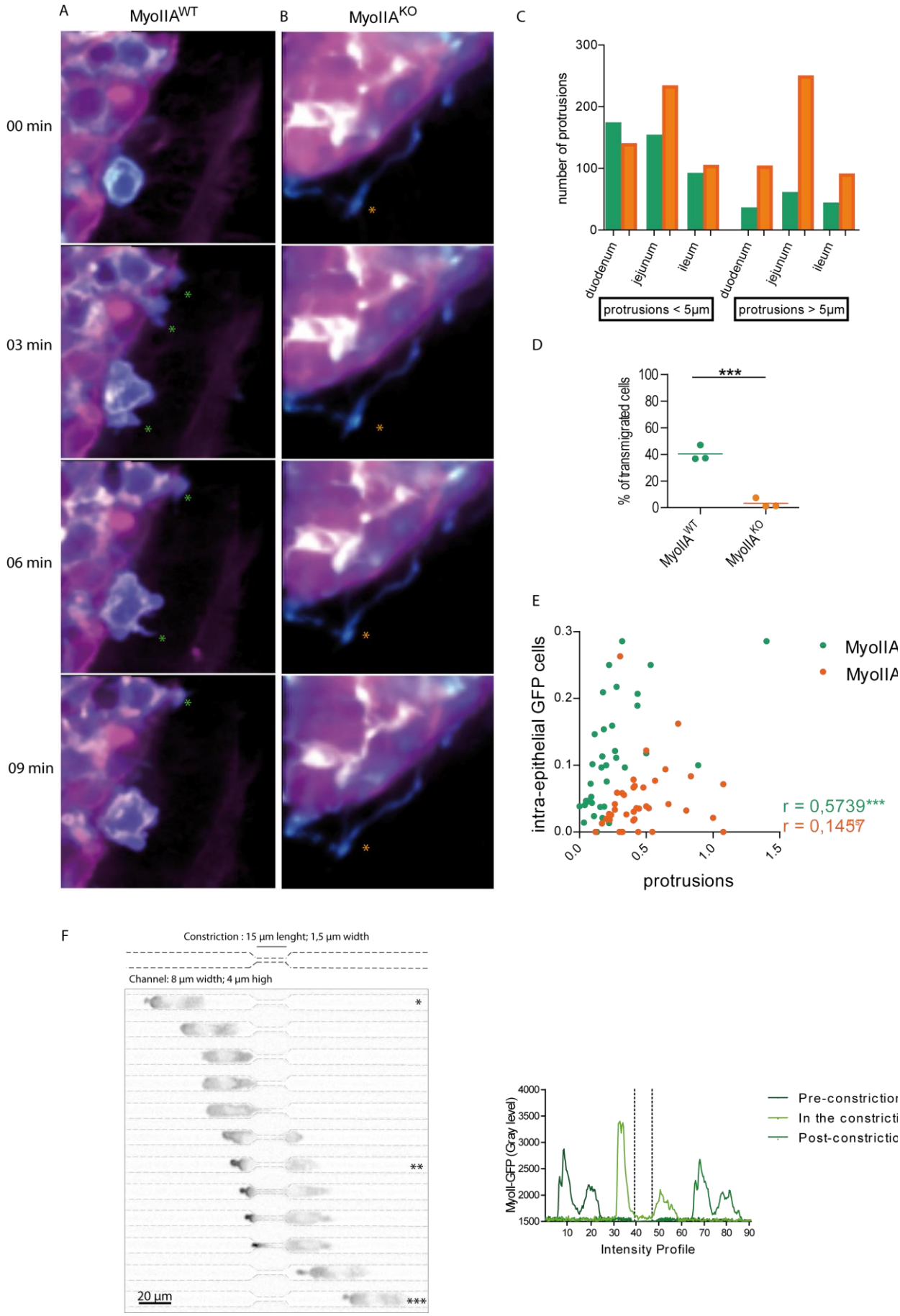
A
MyoIIA^WT
B
MyoIIA^KO
00 min
03 min
06 min
09 min
C
number of protrusions
300
200
100
0
duodenum
jejunum
ileum
duodenum
jejunum
ileum
protrusions < 5µm
protrusions > 5µm
D
% of transmigrated cells
100
80
60
40
20
0
***
MyoIIA^WT
MyoIIA^KO
E
intra-epithelial GFP cells
0.3
0.2
0.1
0.0
0.0
0.5
1.0
1.5
protrusions
MyoIIA
MyoIIA
r = 0,5739***
r = 0,1457
F
Constriction : 15 µm lenght; 1,5 µm width
Channel: 8 µm width; 4 µm high
*
**
***
20 µm
MyoII-GFP (Gray level)
4000
3500
3000
2500
2000
1500
10
20
30
40
50
60
70
80
90
Intensity Profile
Pre-constrictior
In the constricti
Post-constrictic

Myosin IIA-dependent transmigration of CD11b$^+$CD103$^+$ DCs preferentially occurs in the upper region of the small intestine

We next asked whether myosin IIA-dependent transmigration of DCs was homogeneous along the small intestine or preferentially occurred in specific regions. This was motivated by a previous report showing that CD11b$^+$CD103$^+$ DCs were enriched in the upper parts of the gut (Denning T, J Immunol., 2011). To address, this question, we generated fixed gut slices from WT and myosin IIA KO conditional mice, which were immune-stained with a membrane basement marker (Fig. 17 A-B). Numerous intraepithelial CD11c$^+$ cells were detected in the duodenum and jejunum of WT animals (Fig. 17 A). In contrast few CD11c$^+$ cells were observed in the epithelium of the ileum. Accordingly, we found that intraepithelial DCs formed a gradient along the small intestine (Fig. 17 C), which was reminiscent of the gradient reported for CD11b$^+$CD103$^+$ DCs., As expected from our live-imaging results, the number of intraepithelial DCs was drastically reduced in the duodenum and jejunum of myosin IIA conditional KO mice (Fig. 17 B), resulting in the loss of the gradient they exhibit in WT animals (Fig. 17C). Quantifications of protrusions showed that this decrease of intraepithelial DCs in the duodenum and jejunum was accompanied by an increment in the number of protrusions displayed by myosin IIA-deficient DCs (Fig. 17 D). In contrast, no difference in the amount of intraepithelial CD11c$^+$ cells or in the amount of membrane protrusions was observed between the ileum of WT and myosin IIA KO animals (Fig. 17 D). We conclude that myosin IIA-dependent transmigration of DCs from the LP to the epithelium preferentially occurs in the duodenum and jejunum, leading to the formation of a gradient of intraepithelial CD11b$^+$CD103$^+$ DCs along the small intestine.

Figure 17. Intra-epithelial CD11b+CD103+ cDCs display a gradient along the intestine.
(A-B) Representative image of fixed slices from the duodenum of MyoIIA^{WT} mice (A) and MyoIIA^{KO} mice (B). Sections represent tdTomato (magenta), CD11c (cyan), DAPI (blue), laminin (green). The data are representative of three independent experiments.
(C) Number of nuclei of GFP$^+$ cells found in the epithelium per villosity in duodenum, jejunum and ileum of MyoIIA^{WT} and MyoIIA^{KO} mice. Each dot is an intestinal villosity.
(D) Number of GFP$^+$ protrusions found in the epithelium per villosity in duodenum, jejunum and ileum of MyoIIA^{WT} and MyoIIA^{KO} mice. Each dot is an intestinal villosity.
(E) Number of nuclei of GFP$^+$ protrusions found in the epithelium per villosity in the small intestine of MyoIIA^{WT} and MyoIIA^{KO} mice. Each dot is an intestinal villosity, all parts are pooled.
(F) Intestinal permeability assessed by the measurement of FITC-Dextran in the serum from MyoIIA^{WT} and MyoIIA^{KO} mice after gavage. Data pooled from two experiments

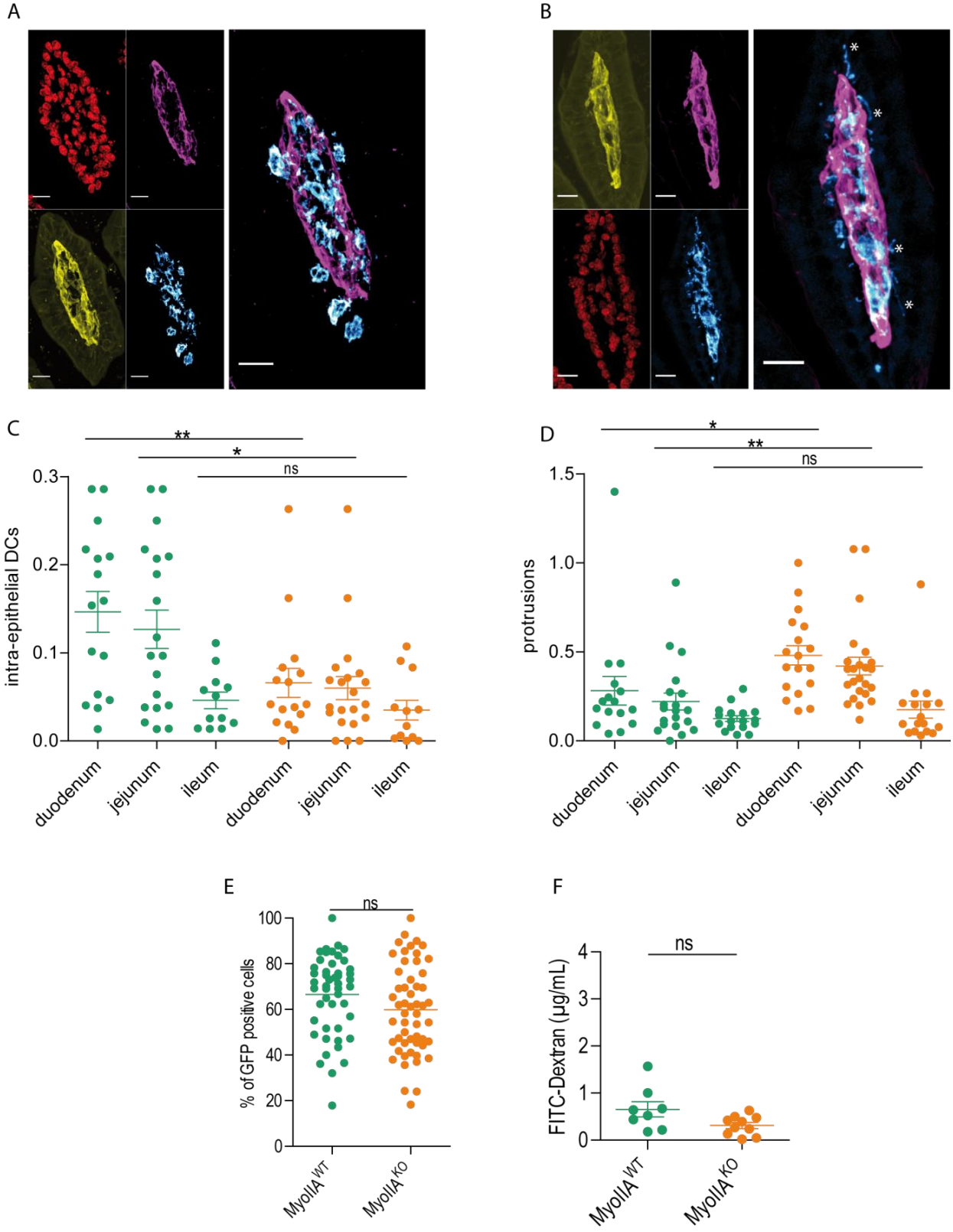
A
B
C
intra-epithelial DCs
0.3
0.2
0.1
0.0
**
*
ns
duodenum
jejunum
ileum
duodenum
jejunum
ileum
D
protrusions
1.5
1.0
0.5
0.0
*
**
ns
duodenum
jejunum
ileum
duodenum
jejunum
ileum
E
% of GFP positive cells
100
80
60
40
20
0
ns
MyoIIA WT
MyoIIA KO
F
FITC-Dextran (µg/mL)
4
3
2
1
0
ns
MyoIIA WT
MyoIIA KO

Transmigration of CD11b$^+$CD103$^+$ DCs from the LP to the epithelium requires retinoic acid production

The existence of a gradient of intraepithelial DCs suggests that there might be extracellular cues present in the upper portions of the intestine that trigger the transmigration of CD11b$^+$CD103$^+$ DCs from the LP to the epithelial cell layer. One valuable candidate is the microbiome as it has been highlighted that the extension of dendrites by gut phagocytes through the epithelium is stimulated by the gut microbiota (Chieppa M, J Exp Med., 2006). This might be particularly relevant in the upper regions of the small intestine as they exhibit a thin mucus layer through which microbial components might more easily diffuse. To assess whether the microbiome promotes the transmigration of DCs from the LP to the epithelium, we treated WT animals with an antibiotic cocktail. We found no significant impact of such treatment on the number of intraepithelial CD11b$^+$CD103$^+$ DCs (Fig. 18 A), the increased in the size of the cecum testifying for antibiotic efficiency (Fig. 18 B). Similarly, mouse treatment with an anti-fungal molecule, Fluconazole, did not have any effect on intraepithelial DC numbers (Fig. 18 A and 18 B). We conclude that the constitution of the intraepithelial pool of DCs in the small intestine does not rely on an intact microbiota.

Alternatively, the trafficking of DCs from the LP to the epithelium might be stimulated by food metabolites, as they are particularly concentrated in the duodenum, i.e. at the crossroad between the stomach and the small intestine. In particular, All-trans Retinoic Acid (AtRA) is an interesting candidate, as this Vitamin A derivative forms a gradient along the gut that parallels the one formed by CD11b$^+$CD103$^+$ DCs (Denning T, J Immunol., 2011). Of note, CD11b$^+$CD103$^+$ DCs have been themselves described as AtRA producers in the LP thanks to their ability to express the enzyme RALDH2 (Jaensson-Gyllenbäck, Mucosal Immunol, 2011). Noticeably, a 4 day treatment of WT mice with the RALDH2 inhibitor Bisdiamine did not affect the CD11b$^+$CD103$^+$ DCs from the LP whereas it was sufficient to decrease the amount of gut intraepithelial DCs (Fig. 18 C). Bisdiamine efficiently decreased RALDH activity in the CD11b$^+$CD103$^+$ DCs from the LP but did not affect their quantity (Fig. 18. C-E). These results indicate that AtRA production is needed to maintain the intraepithelial pool of CD11b$^+$CD103$^+$ DCs in the small intestine, which themselves contribute to the production of this metabolite.

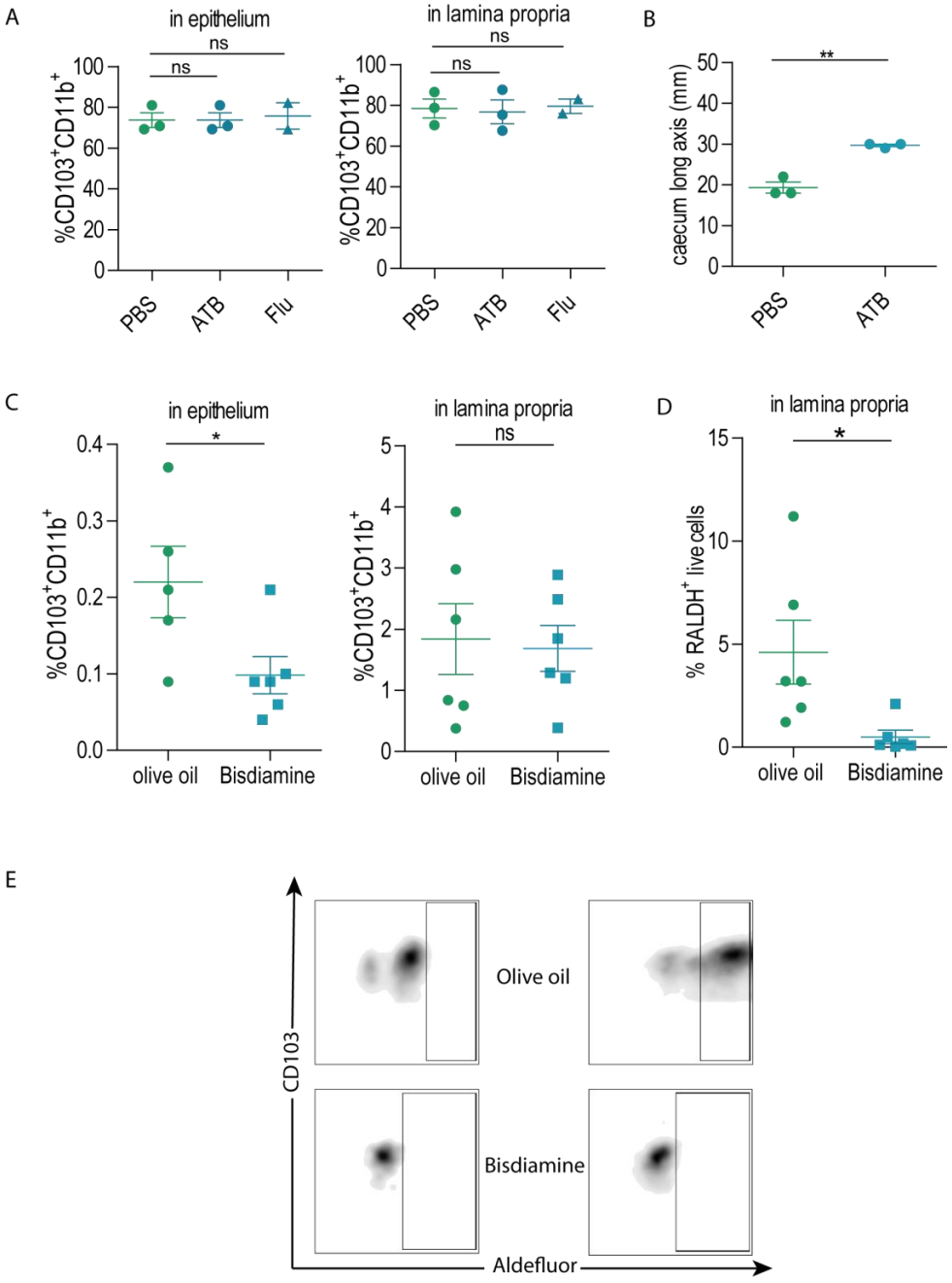

Figure 18. Transmigration of CD11b+CD103+ cDCs in the epithelium depends on AtRA but not on microbiota.

(A) Adult SPF C57/BL6 mice were gavaged with PBS or antibiotic cocktail or fluconazole for 10 days, and the percentages of CD103+CD11b+ cells in epithelium and stroma were determined by flow cytometry. Data are representative of two independent experiments.

(B) Size of the caecum of mice gavaged with PBS or antibiotic cocktail for 10 days.

(C) Adult SPF C57/BL6 mice were gavaged with olive oil or Bisdiamine for 4 days, and the percentages of $CD103^{+}CD11b^{+}$ cells among live CD45+ cells in epithelium and stroma were determined by flow cytometry. Data are representative of two independent experiments.

(D) In same experiments as in (C), percentages of RALDH+ cells were determined by flow cytometry.

(E) Left panel: cell suspension from lamina propria treated with RALDH inhibitor (DEAB) provided with ALDEFLUOR kit was used as a negative control to set up gates for each sample. Right panel: untreated cell suspension from lamina propria.

Intraepithelial CD11b+CD103+ DCs exhibit a distinct and unique transcriptional profile

So far our results show that there is a gradient of intraepithelial $CD11b^+CD103^+$ DCs along the intestine, which relies on Myosin IIA-dependent transmigration from the LP to the epithelium, as well as on the production of AtRA. Does this pool of DCs exhibit a different genetic program than the $CD11b^+CD103^+$ DCs that remain in the LP? To answer this question, we purified LP and intraepithelial $CD11b^+CD103^+$ DCs from WT mice to compare their mRNA expression profiles at the single-cell level. In the case of Myosin IIA KO mice, we only analyzed LP $CD11b^+CD103^+$ DCs, as they lack intraepithelial DCs. Interestingly, when comparing the numbers of $CD11b^+CD103^+$ DCs of the two genotypes, we consistently observed that they were substantially decreased in the LP of Myosin IIA KO mice, although to a lesser extent than in the epithelium (49,6% versus 96,2% decrease) (Fig.15 E). In contrast, we found that myosin IIA had no impact on the amounts of $CD11b^+CD103^-$ and in $CD11b^-CD103^+$ single-positive DCs of the LP (Fig. 15 B-D), excluding a general effect of the motor protein on early precursor proliferation or differentiation. Hence, Myosin IIA deficiency in $CD11c^+$ cells does not only lead to a defect in the transmigration of $CD11b^+CD103^+$ DCs from the LP to the epithelium but also to a decrease in the number of these cells in the LP.

Figure 19. Intra-epithelial CD11b+CD103+ cDCs have an homogenous transcriptomic profile.
(A) Purified $CD103^+CD11b^+$ cDCs were analyzed by single-cell RNA-seq using a drop-seq approach. Colors represent unbiased clustering from graph-based clustering. Each dot represents an individual cell. tSNE analysis of individual cells for total cells (n=731).
(B) Upper panel: percentage of cells from each each cluster found in each sample.
Lower panel: percentage of cells from each sample found in each cluster.
(C-F) Violin plots present levels of expression of ItgaX (C), Itgam (D), ItgaE (E).

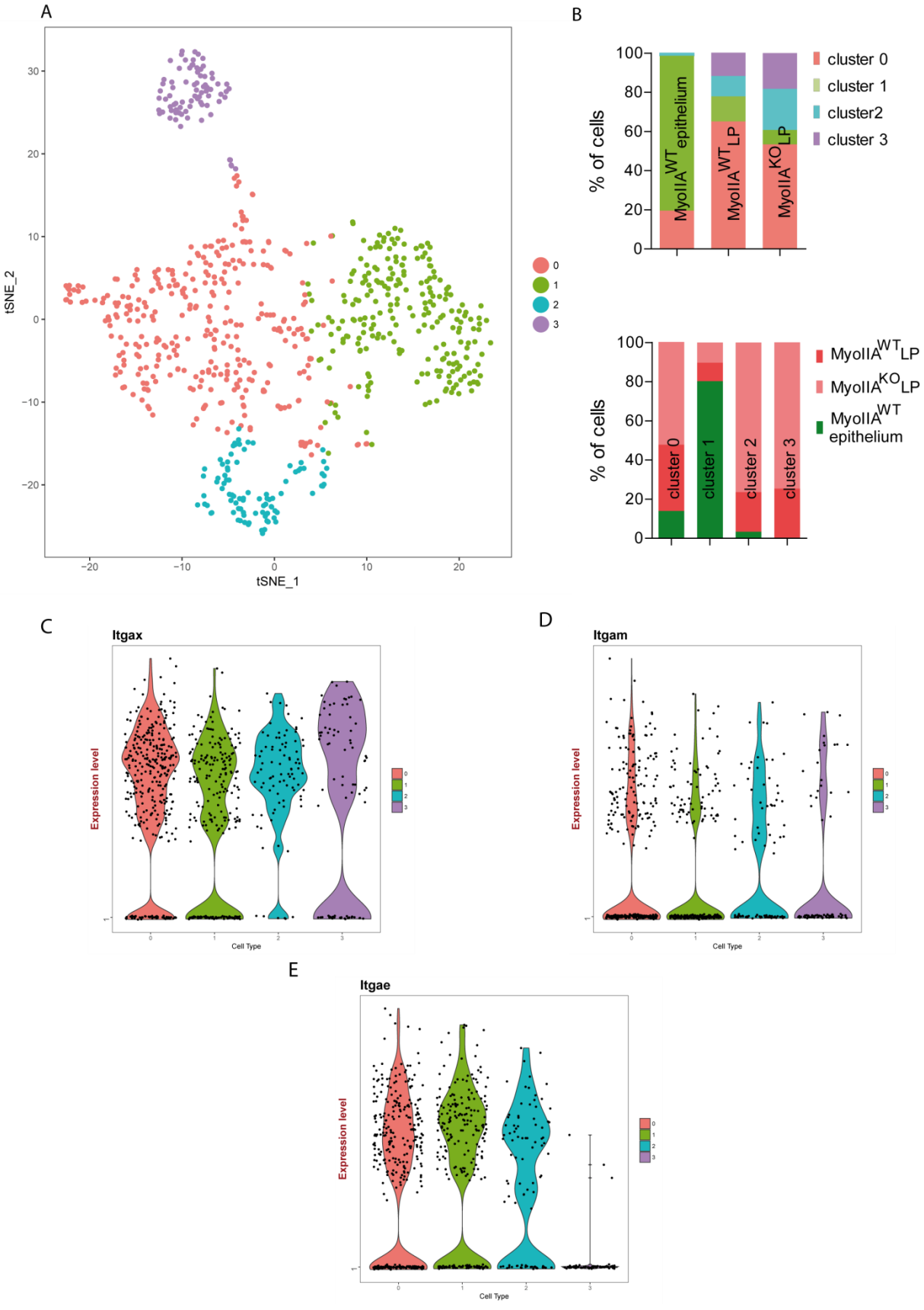
A
tSNE_2
tSNE_1
0
1
2
3
B
% of cells
MyoIIA^WT epithelium
MyoIIA^WT LP
MyoIIA^KO LP
cluster 0
cluster 1
cluster2
cluster 3
MyoIIA^WT LP
MyoIIA^KO LP
MyoIIA^WT epithelium
C
Itgax
Expression level
Cell Type
D
Itgam
E
Itgae

We next generated single-cell transcriptomes from the distinct sorted cells by using a droplet-based method that enables 3' mRNA counting (Zheng D, Methods Mol Biol 2017). Our dataset collected a total of 731 cells (after application of quality filters), distributed as follows: 235 cells from the WT epithelium, 172 cells from the WT LP and 324 cells from the Myosin IIA KO LP. To evaluate the heterogeneity of samples, we used a non-linear dimensionality reduction method. Using t-Distributed Stochastic Neighbor Embedding (tSNE), we detected 4 clusters of cells (Fig. 19 A). Cluster 0 gathers 331 cells, cluster 1 231 cells, cluster 2 89 cells and cluster 3 79 cells. We found that Cdc11c (ItgaX) and CD11b (Itgam) were expressed at similar levels in all clusters (Fig. 19 C-E). Expression of CD103 (ItgaE) was reduced is cluster 3, which corresponds to a contaminating $CD11b^+$ macrophage population (15,9% among the total cells from the LP) (Fig. 20). This cluster displayed a Cx3cr1/Mafb signature specific to the macrophage lineage and was therefore eliminated before Principal Component Analysis (PCA). WT and Myosin IIA KO $CD103^+CD11b^+$ DCs from the LP were evenly distributed between cluster 0 and cluster 2 (Fig. 19 A-B). Cluster 2 corresponded to cells enriched in cell cycle genes, as shown by pathway analysis in Kegg 2016 (p-value=7,402e-27) and Reactome 2016 (p-value=2,175e-94). Myosin IIA KO $CD103^+CD11b^+$ DCs from the LP overlapped with cluster 2 in similar proportions than WT $CD103^+CD11b^+$DCs, suggesting than the loss of myosin IIA gene does not affect the cycling of these (Fig. 19B). Cluster 0, which concerned most $CD103^+CD11b^+$ DCs from the LP exhibited a TNF signature (p-value =1,729e-10), with genes from both PI3k-Akt and NF-κb (p-value =8,405e-10 signaling pathways (canonical and non-canonical) being highly expressed. These pathways were not enriched in cluster 1, *i.e.* in intraepithelial $CD103^+CD11b^+$ DCs. Remarkably, intraepithelial $CD103^+CD11b^+$ DCs overlapped with cluster 1 whereas very few $CD103^+CD11b^+$ DCs from the LP did (Fig. 19 B), suggesting that intraepithelial $CD103^+CD11b^+$ DCs correspond to a homogenous cell population. Strikingly, among the most enriched genes in these cells was the myosin IIA gene (*myh9*, p-value=8,422e-5) (Fig. 19 G), consistent with its essential role in transmigration from the LP to the epithelial cell layer. In addition, intraepithelial $CD103^+CD11b^+$ DCs were enriched for lysosome pathway (p-value=1,573e-3; Kegg 2016), MHCII (H2-Oa: p-value=1,842e-15; H2-Dmb2: p-value=5,976e-07) as well as autophagy related genes (Gabarapl2: p-value=1.355e-09). These results might be indicative

of a role for intraepithelial CD103^{+}CD11b^{+} in antigen processing and presentation. This is consistent with our intra-vital imaging data suggesting that these cells have acquired the ability to patrol the small intestine epithelium. We conclude that Myosin IIA-dependent transmigration of CD11c^{+} cells from the LP to the epithelium defines a pool of intraepithelial CD11b^{+}CD103^{+} DCs that exhibits a distinct gene expression profile than their LP counterpart and might be functionally specialized in epithelium patrolling and antigen presentation for T cell activation.

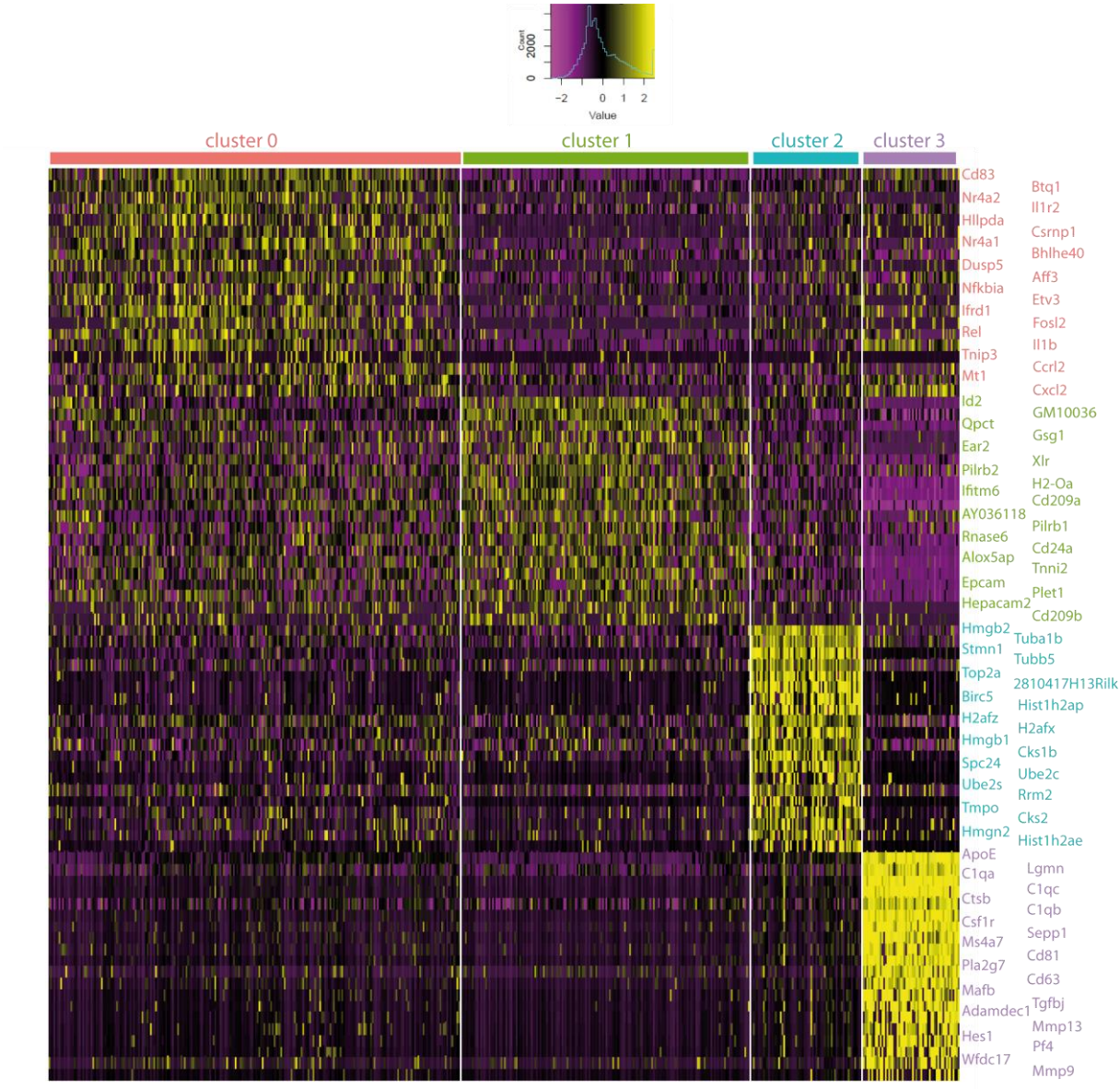

Figure 20. CD103+CD11b+ DCs display different transcriptomic signature in the LP and in the epithelium.
Heat map of scaled expression (log values of transcripts per million) for 20 most expressed genes in each cluster identified in Figure 19.

Lack of intraepithelial CD11b^{+}CD103^{+} DCs in the absence of Myosin IIA is associated to reduced CD4 Intra-epithelial-lymphocyte numbers

We finally investigated whether Myosin IIA deficiency in DCs affects gut lymphocyte homeostasis, as CD11b^{+}CD103^{+} DCs, which are reduced in Myosin IIA conditional KO mice, have been shown to play a key role in Th17, Th2 and Treg differentiation (Fig. 21 A-C)as well as in innate-like cell (ILCs) activation (Fig. 21 D). Comparison of T cell and ILC populations in the LP showed no significant difference between WT and Myosin IIA-deficient animals (Fig. 21 A-D). These data indicate that (1) 50% of CD11b^{+}CD103^{+} DCs are sufficient to regulate lymphocyte differentiation under homeostatic conditions within the LP and (2) this process does not require their transmigration from the LP into the epithelial cell layer. Of note, we do not exclude that the picture might be different under immune stimulation.

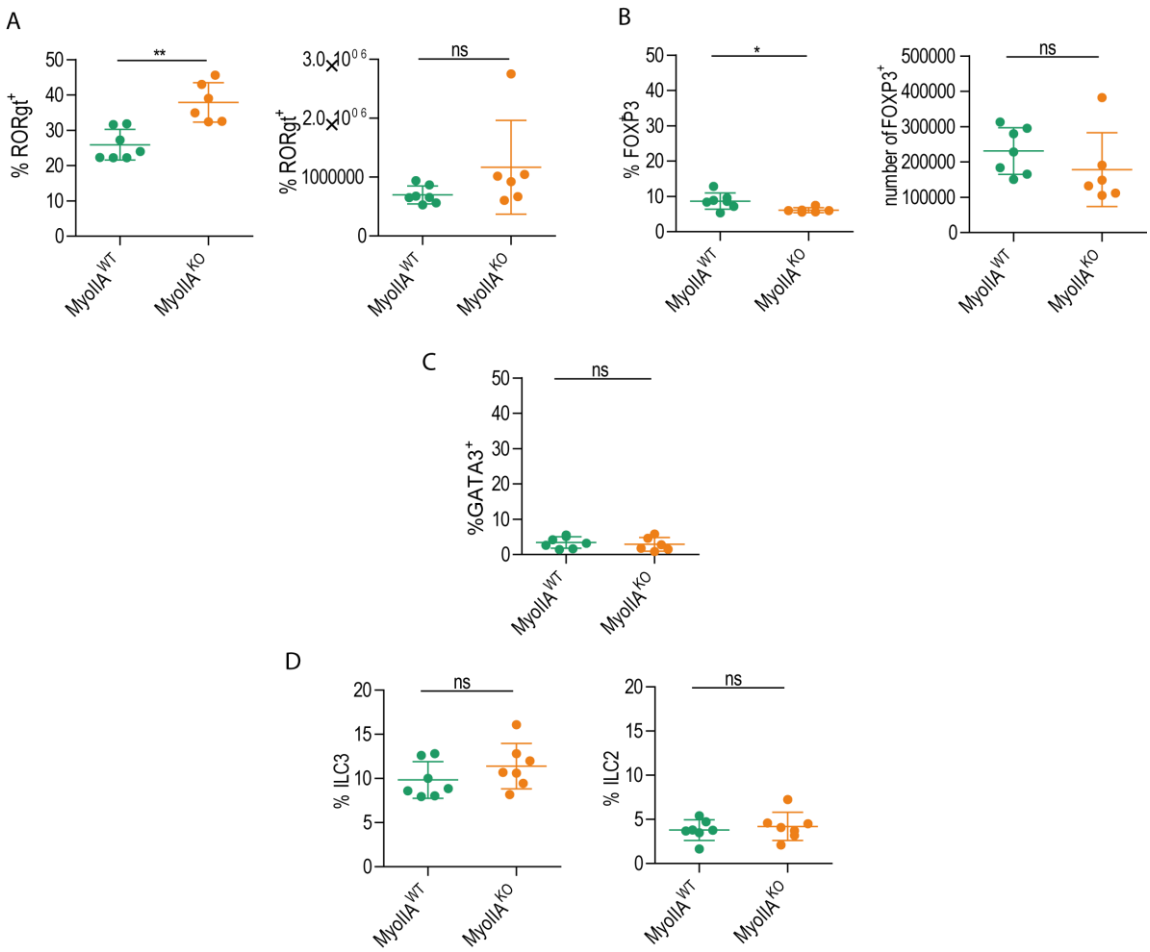

Figure 21. Myosin IIA deficiency in DC does not impact T lymphocytes hoeostasis.
(A-C) T lymphocytes from the lamina propria of MyoIIA^{WT} and MyoIIA^{KO} mice were analyzed by flow cytometry. Plots present percentages and numbers for Th17 (A), Treg (B), Th2 (C).
(D) ILCs from the lamina propria of MyoIIA^{WT} and MyoIIA^{KO} mice were analyzed by flow cytometry. Plots present percentages and numbers for ILC3 (left), ILC2 (right).

More interestingly, when monitoring the epithelium, we found that the number of intra-epithelial lymphocytes (IELs) was reduced in mice whose CD11c$^+$ cells were KO for Myosin IIA. Further analysis of the distinct IELs populations showed that this defect specifically concerned the CD8$^+$αβ IEL subset (Fig 22. B and C), the number of CD8$^+$αα IELs and γδ T cells remaining unaffected (Fig 22. A and D). We conclude that myosin IIA deficiency in CD11c+ cells was associated to a reduction of the small intestine IEL uncer homeostatic conditions. As myosin IIA KO CD11b$^+$CD103$^+$ DCs cannot migrate from the LP to the epithelium, this suggests that intra-epithelial DCs might be needed for maintenance of the IEL pool in the upper part of the gut. As genes controlling lysosome function and antigen processing/presentation are enriched in intraepithelial CD11b$^+$CD103$^+$ DCs, these findings are consistent with a model where these DCs interact with IELs through antigen presentation within the epithelium.

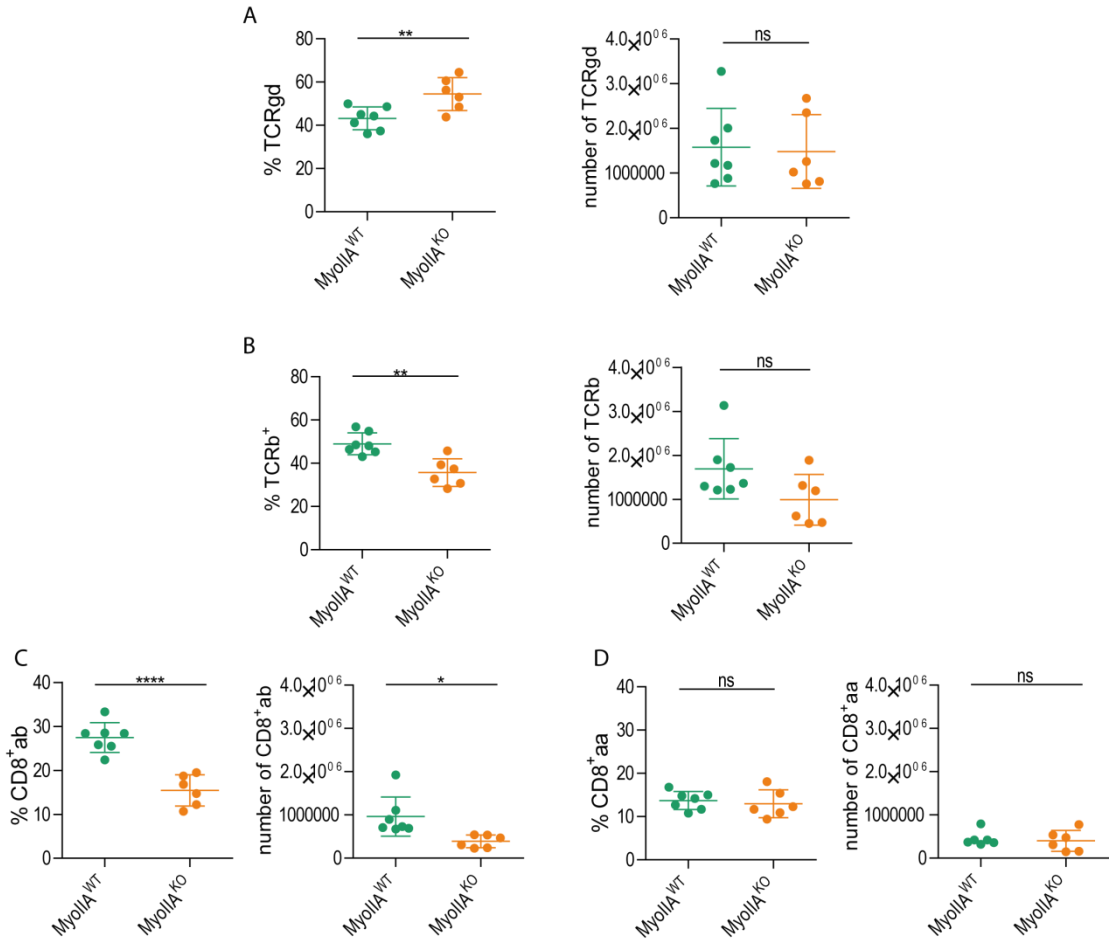

Figure 22. Myosin IIA deficiency in DCs impact IEL homeostasis.
(A-C) IEL from MyoIIA^{WT} and MyoIIA^{KO} mice were analyzed by flow cytometry. Plots present percentages and numbers for γδ T cells (A), classical IEL (B), CD8$^+$αβ IEL (C) and CD8$^+$αα (D) .

Supplementary Movie 1. CD11c$^+$ cells patrol the epithelium of the small intestine at steady-state.
Time-lapse movie acquired by intravital microscopy in the jejunum of a mouse with MyoIIA^{WT} DCs.
Left panel: whole field, white arrows: events of CD11c$^+$ cell transmigration, green arrows: CD11c$^+$ cells residing in the epithelium.
Right panel: zoom on a CD11c$^+$ cell transmigrating from the lamina propria into the epithelium.

Supplementary Movie 2. CD11c$^+$ cells require myosin IIA to transmigrate into the epithelium of the small intestine.
Time-lapse movie acquired by intravital microscopy in the jejunum of a mouse with MyoIIA^{KO} DCs.
Left panel: whole field.
Right panel: zoom on a CD11c$^+$ cell emitting a protrusion in the epithelium while sitting in the lamina propria, white arrow: tip of the growing protrusion.

Supplementary Movie 3. CD11c$^+$ cells sample the epithelium of the small intestine.
Time-lapse movie acquired by two-photon microscopy in a live slice from the jejunum of a mouse with MyoIIA^{WT} mouse.
First part: visualization of 3D-reconstruction of the first time point.
Second part: time-lapse movie, white arrows: dynamic protrusions emitted in the epithelium, green arrow: bleb and filopodia formed in the epithelium.

Supplementary Movie 4. CD11c$^+$ cells require Myosin IIA to sample the epithelium of the small intestine.
Time-lapse movie acquired by two-photon microscopy in a live slice from the jejunum of a mouse with MyoIIA^{WT} mouse.
First part: visualization of 3D-reconstruction of the first time point.
Second part: time-lapse movie, red arrows: stable protrusions emitted in the epithelium.

Supplementary Movie 5. Mysoin IIA is recruited at the back of the cell during DC migration through constrictions.
Time-lapse movie of a bone-marrow derived DC from a Myosin IIA-GFP mouse migrating in a microchannel with constrictions.

Supplementary Movie 6. CD11c$^+$ cells patrol the epithelium of the small intestine at steady-state.
Time-lapse movie acquired by intravital microscopy in the jejunum of a CD11c^{mCherry}-MyosinIIA^{GFP} mouse.
White arrow: CD11c$^+$ cell transmigrating into the epithelium.

Discussion

As illustrated in the first section of this thesis dissertation, DCs are key players of the immune system: they are able to capture antigens in the peripheral tissues they patrol and to trigger adaptative immune responses in lymph nodes. DCs have optimized their patrolling and sensing methods in peripheral tissues. This particularly applies to the intestine, which is constantly exposured to antigens that are taken up orally. We and others have shown the importance of the actin associated molecular motor myosin IIA in both immature and mature DC migration. Immature DCs require myosin IIA to coordinate migration and antigen capture *in vitro* (Faure-André G, Science, 2007; Chabaud M, Nat Comm., 2015) while mature DCs need myosin IIA to achieve fast and directional migration towards lymph nodes (Lämmerman T, Nature, 2008; Renkawitz J, Nat Cell Biol., 2009). The main goal of my project was to assess and dissect myosin IIA contribution to DC function in the small intestine *in vivo*. I focused on $CD103^+CD11b^+$ DCs because they constitute a unique subset, specific of the small intestine, and display a particular competence for direct antigen sampling in the gut lumen (Farache J, Immunity, 2014). I will first summarize the results I obtained in section A and, second, discuss them around 3 specific axes: B) DC transmigration is a key event for intra-epithelial DC homeostasis, C) the function of intra-epithelial $CD103^+CD11b^+$ DCs differs from the function of $CD103^+CD11b^+$ DCs from the lamina propria, D) intra-epithelial $CD103^+CD11b^+$ DCs take part in the immune compartmentalization of the small intestine.

	LP DC2	Epithelial DC	CX3CR1
Cluster	0-2	1	3
Region	Duodenum/jejunum	Duodenum/jejunum	Ileum
Sampling method	TED	epithelium	TED
Environmental cues	_	AtRA	microbiota
Ligand/attractant	?	?	fractalkine
Genes/pathways	NFκb lmnb1	myh9 MHCII Lysosome	mafb
Fonction	Th development	$CD8^{+}$αβ IEL regulation	macrophagic

Table 2. Characteristics of cell populations identified in this study.

A-DCs and intestinal epithelium: more than neighbors

This project has the originality to characterize an understudied DC population in mucosal immunology starting from mechanistic observations collected from the field of cell biology. The combination of several imaging techniques to flow cytometry allowed cell precise identification and localization within the small intestine. The main findings of my work highlight that tissue patrolling by DCs continuously takes place in the epithelium of the small intestine at steady state *i.e.* even in the absence of inflammatory signals. DCs that constantly patrol the epithelium of the small intestine come from the lamina propria and enter the epithelial layer by transmigration through the basal membrane in a myosin IIA dependent manner. DCs with an altered pool of myosin IIA form long protrusions through the epithelium but are not able to cross the basal membrane. DC transmigration observed in $CD11c^{GFP}$-Tomato mice was also observed in $CD11c^{mCherry}$-$MyosinIIA^{GFP}$ mice (supplementary movie 6), which further confirms a DC recruitment in the epithelium under homeostatic conditions. These intra-epithelial DCs are more frequent in the duodenum and jejunum that is to say in the upper part of the small intestine than in the ileum.

The regionalization that we observe suggests that intra-epithelial DCs, mainly from the $CD103^+CD11b^+$ subtype, are under the influence of environmental cues. Indeed, the components of the gut lumen such as microbiota or food metabolites are known to be distributed in gradients along the small intestine, which might drive the regionalization of DC transmigration. We found that the number of $CD103^+CD11b^+$ DCs is not significantly affected by a change in the microbiota. The $CD103^+CD11b^+$ DC subset produces AtRA from retinol thanks to RALDH2 they express in similar proportions in the epithelium and in the lamina propria. *In vivo*, inhibiting RALDH2 activity reduces the number of $CD103^+CD11b^+$ DCs in the epithelium, which suggests that the produced AtRA favors DC transmigration. The compartmentalization of intra-epithelial DCs may therefore result from the variable availability in RALDH2 substrate, the retinal, which is higher in the upper parts of the small intestine.

To elucidate the function of intra-epithelial DCs, we sorted $CD103^+CD11b^+$ DCs from the epithelium and the stroma of the small intestine villi and performed Single Cell RNAseq. The results obtained showed that $CD103^+CD11b^+$ DCs from the epithelium constitute a homogenous cell population whose transcriptomic signature is distinct from the one of LP $CD103^+CD11b^+$ DCs. $CD103^+CD11b^+$ DCs from the epithelium better express genes involved in antigen processing and antigen presentation as compared to LP $CD103^+CD11b^+$ DCs which better express the TNF-associated genes, especially from the NF-κb pathway. In homeostatic conditions, the loss of intra-epithelial $CD103^+CD11b^+$ DCs does not affect LP T subsets but reduces $CD8^+$αβ IEL.

My work therefore highlighted a new mode used by DCs to patrol the small intestine at steady state and dissects the intracellular and extracellular cues driving the generation of intra-epithelial DCs. These findings suggest that DCs use distinct patrolling strategies depending on their localization along the small intestine. This might allow them adapting to the distinct compositions and functions of the different gut regions. This work may open up additional studies in mucosal immunology to further investigate the contribution of the intra-epithelial DC pool to immune defenses.

B- DC transmigration is a key event for intestinal DC homeostasis

B-1- Myosin IIA is essential for DC transmigration into the epithelium

To enter the epithelium, DCs must cross the basal membrane, a dense layer of collagen fibers connected by different sets of proteins such as lamins and integrins. This study shows *in vivo* that myosin IIA is a key regulator of DC transmigration through the basal membrane. Previous studies on mature DC migration in a 3D environment modelled by collagen gels of variable density insisted on a cell front-back dissociation (Lämermann T, Nature, 2008). Intravital microscopy on mice with MyoIIA^{KO} DCs highlighted this cell compartmentalization. Our data show that Myosin IIA is required for membrane contraction to allow protrusion dynamic *in vivo*. Myosin IIA impacts both compartments, MyoIIA^{KO} DCs exhibit longer and less dynamic front protrusions than WT DCs of the small intestine. At the same time, MyoIIA^{KO} DCs are not able to transmigrate through the basal membrane as their nuclei stay stuck at the rear of the elongated cells, in the stroma of the villosities. As far as nucleus passage is concerned, we cannot determine in our set up whether protrusion retraction would be sufficient to allow nucleus passage through small pores or whether the myosin IIA pool located at the back of the cell facilitates contracting the rear of the cell. In the literature, data highly depend on the maturation status of DCs. We have shown previously that, *in vitro*, myosin IIA orchestrates migration and macropinocytosis (Chabaud, Heuzé, Nat Comm., 2015) but was not required for cell passage through constrictions in immature DCs (Thiam, Nat Comm., 2016). In mature DCs, myosin IIA is located at the rear of the cell and its inhibition by blebbistatin prevents nucleus passage through constrictions (Leithner A, Nat Cell Biol., 2016; Renkawitz J, Nat Cell Biol., 2009). Furthermore, mature DCs migrating in collagen gels could not deform their nucleus and make them pass through small pores when their myosin IIA pool was inhibited. To interprete our data in regards with these in vitro data we have to consider the maturation status of DCs patrolling the small intestine in our *in vivo* set up. This maturation status is difficult to define. Although there is no specific stimulation and mice are brought up in SPF facility, they were colonized with microbiota which might be sufficient to convert DCs into a mature state.

Besides, the phenotype we observed is really close to the phenotype of myosin IIA KO mature DCs migrating in collagen gels (Lämmermann T, Nature, 2008). Other groups also showed myosin IIA importance for the passage of mature DCs through narrow spaces (Takamatsu H, Nat Immunol., 2010). An interesting study about kinetics of neutrophil transmigration through basal membrane reported *in vitro* the dramatic decrease of cell transmigration upon blebbistatin treatment *i.e.* upon myosin IIA inhibition. A control neutrophil crosses the basal membrane in 35 seconds while a blebbistatin neutrophil crosses it in about 13 minutes. The critical step that fails in blebbistatin condition is not transmigration initiation but the retraction of the rear of the cell (Stroka KM, Plos One, 2013). Then, our *in vivo* data are consistent with *in vitro* data discussed above and support that myosin IIA is required for the nucleus passage through the basal membrane. These data confirm myosin IIA requirement for intra-epithelial $CD103^{+}CD11b^{+}$ DC recruitment. However, the intracellular mechanism involved remains unclear. We could imagine that the key event to trigger DCs transmigration is back contraction of the cell to push the nucleus, nucleus deformation, front protrusions contraction to pull the nucleus, or a combination of all. More *in vitro* studies with an adapted modeling of the basal membrane that would allow high temporal and spatial resolution imaging are needed.

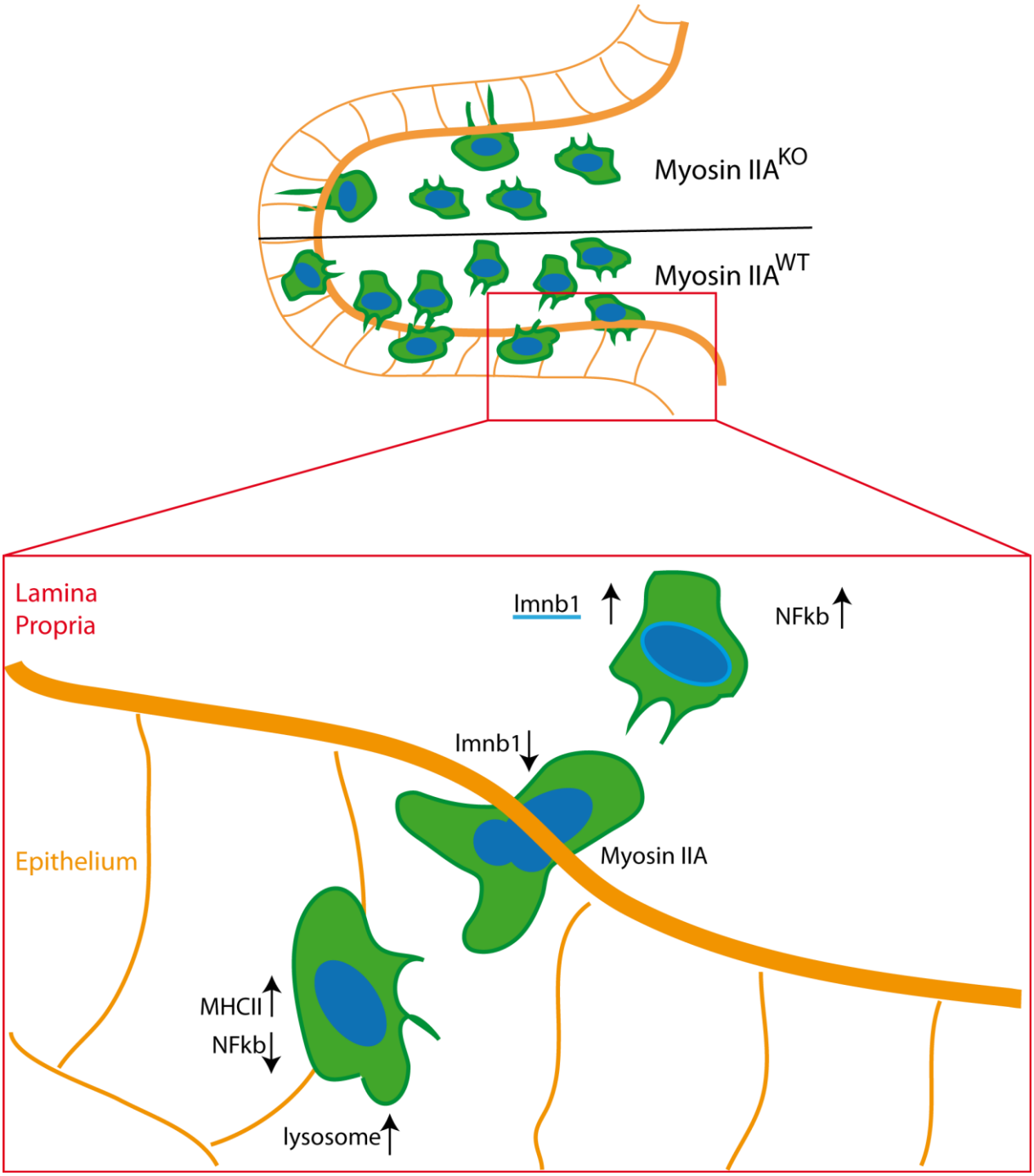

Figure 23. DC transmigration in the small intestine.
Top: Scheme of a typical duodenal villi comparing DC population from mice with MyoIIA^{WT} DCs with mice with MyoIIA^{KO} DCs.
Bottom: Zoom on DC transmigration in the duodenum of mice with MyoIIA^{WT} DCs.

B-2- Which molecules cooperate with myosin IIA to promote DC transmigration?

AtRA has many targets and is known to promote cell migration by enhancing expression of MMPs, which can digest the extra-cellular matrix. This pathway could explain why RALDH+CD103+CD11b+ are more concentrated in the epithelium than in the lamina propria. *In vitro* studies in transwells have particularly adressed the mechanisms by which AtRA impacts on DC migration. One study shows that AtRA impact on DC migration is independent of their maturation (Darmanin, J Immunol., 2007). Indeed, AtRA supplementation does not modulate CCR7 expression in mRNA copy number nor in cell surface staining. Fast migration requires CCR7-ligands but AtRA increases a lot the efficiency of chemotaxis. Moreover, it loses all its impact in the absence of Matrigel, which is used to mimick the basal membrane components. As for the mechanism, AtRA loses its efficiency on DC migration when MMP inhibitors are added to the experimental set up. The fine regulation of AtRA upon the expression of MMPs and their inhibitors could be assessed by performing RNAseq on $CD103^{+}CD11b^{+}$DCs. In Single Cell RNA analysis, *mmp9* and *mmp14* are overexpressed in cluster 3 as compared to other clusters. Unexpectedly, we found that cluster 3 overlaps with LP $CD103^{+}CD11b^{+}$ DCs. This cell subset displays a strong and very specific signature as it is enriched for mRNAs related to the macrophage phenotype: *fcgr1*, *mafb* and *cx3cr1*. Because CX3CR1+ cells are identified as macrophage-like cells forming TEDs in the lamina propria, we hypothesize that these cells use MMPs to digest basal membrane during TED formation. As MMPs are not over expressed in cluster 1, which overlaps with intra-epithelial $CD103^{+}CD11b^{+}$ DCs, it is rather unlikely that AtRA acts through MMPS to promote $CD103^{+}CD11b^{+}$ DCs transmigration though the basal membrane. Whether AtRA promotes $CD103^{+}CD11b^{+}$ DCs transmigration by direct interaction with myosin IIA or any other nuclear target has to be elucidated. This could be addressed by comparing the transcriptome of DCs from wild type mice to DCs from Vitamin A deficient mice.

Another migration facilitator is the *lmnb1* gene that codes for Lamin B1. It is enhanced in LP $CD103^+CD11b^+$ DCs (p-value = 6.607 e-08) as compared to $CD103^+CD11b^+$ DCs from the epithelium. Lamin B1 is involved in the maintenance of nuclear shape and rigidity. Atomic Force microscopy allowed measurement of nuclear rigidity in fibroblasts overexpressing *lmnb1* as compared to control human skin fibroblasts (Ferrera D, FASEB J., 2014). Consistently, transient overexpression of *lmnb1* in different cell lines increased nuclei rigidity. These *in vitro* data on cell lines were confirmed in a later study (Hatch EM, J Cell Biol, 2016) where Lamin B1 synthesis was inhibited by shRNA transfection. This resulted in much more ruptures of the nuclear envelope leading to chromatine herniations. When treated with blebbistatin that inhibits myosin IIA activity, cells transfected with shLmnB1 exhibit less nuclear ruptures. The cells with low translation of Lamin B1 and normal activity of myosin IIA exhibited the more numerous events of nuclear rupture. Taken together, these data suggest that lower expression of *lmnb1* in $CD103^+CD11b^+$ cDCs from the epithelium might result in nuclei that are easier to deform than the ones of $CD103^+CD11b^+$ cDCs from the LP, which express more *lmnb1* (Hatch EM, J Cell Biol, 2016). This higher nuclear deformability may enhance DC migration. Besides, nuclear rupture, which has been shown to occur in DCs migrating through small holes (Raab M, Science, 2016), might be more frequent in $CD103^+CD11b^+$ cDCs. We propose that transmigration promotes differentiation *in vivo*. This is supported by previous *in vitro* data showing that monocytes migrating through a monolayer of endothelial cells differentiate into DCs whereas monocytes that remained below this cell layer resembled macrophages (Randolph GJ, Science, 1998). Deformations and ruptures might lead to chromatin reorganization and enhance the different genetic program at work in $CD103^+CD11b^+$ cDCs from the epithelium.

B-3- Transmigration : a differentiation step?

Unexpectedly, in the intra-epithelial $CD103^+CD11b^+$ DC subset, the most overexpressed gene is the transcription factor *Id2* (p-value = 2.818 e-29) which was reported to drive $CD103^+CD11b^-$ DC differentiation (Li HS, Sci Signal., 2016). This information suggests that intra-epithelial $CD103^+CD11b^+$ DCs undergo further differentiation than their LP counterparts. Although the mean percentage of $CD103^+CD11b^-$ DCs in the epithelium is very low (7,2%) compared to the 77,5% of $CD103^+CD11b^+$ DCs we cannot formally exclude that $CD103^+CD11b^+$ DCs from the epithelium originate from $CD103^+CD11b^-$ DCs from the stroma that acquire CD11b once in the epithelium. Future experiments addressing the numbers of intra-epithelial DCs in Id2 deficient mice shall help address this question.

Mice with $MyoIIA^{KO}$ DCs present also a reduced pool of LP $CD103^+CD11b^+$ DCs. The reduction in the LP (49,6%) is less important than the reduction of $CD103^+CD11b^+$ cDCs in the epithelium (96,2%) that have almost completely disappeared in these animals. The conservation of the other DC subsets suggests that this reduction is not due to an impaired differentiation in the CD11c lineage of mice with myosin IIA deficient DCs. The PCA confirmed the t-SNE analysis showing that intra-epithelial $CD103^+CD11b^+$ DCs form a highly homogenous subset. WT LP $CD103^+CD11b^+$ DCs are very close to this subset while myosin IIA deficient LP $CD103^+CD11b^+$ DCs are more spread along the PC2 and PC3 axis (Fig. 24). This analysis suggests that although Myosin IIA deficient $CD103^+CD11b^+$ DCs do not clusterize differently from LP WT $CD103^+CD11b^+$ DCs, they are more heterogenous and genetically further from intra-epithelial $CD103^+CD11b^+$ DCs that form only when they are WT. Besides, as we could observe both *ex vivo* and by intravital microscopy, intra-epithelial CD11c cells establish contacts with CD11c cells of the LP, it is therefore possible that intra-epithelial DCs deliver signals, such as Notch 2 ligand secreted by the epithelium, we propose that intra-epithelial DCs are needed to maintain the LP $CD103^+CD11b^+$ cDCs.

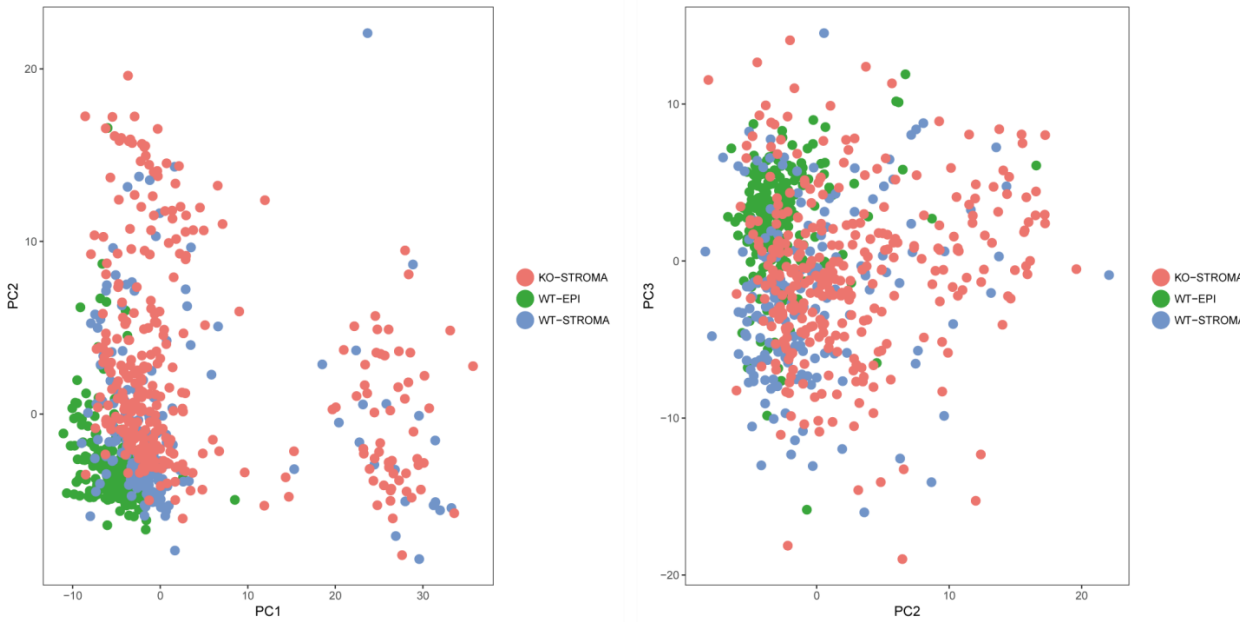

Figure 24. Principal component Analysis (PCA) of CD103⁺CD11b⁺ DCs from the epithelium and the lamina propria.

LP CD103^{+}CD11b^{+} DCs corresponding to cluster 0 are enriched for genes from the TNF signaling pathway in a highly significant manner (p-value =1,729e-10). This includes the PI3k-Akt (*Traf1, Map3K14, NFkbia*) and the NF-κb signaling pathway which is strongly and significantly enriched (p-value =8,405e-10) in this cluster (*Il1b, Nfkb1/2/Rela, Nfkbia, Map3k14, Traf1/2, Bcl2a1a/b/c/d, Gadd45b, Tnfaip3, Ptgs2, Cxcl2, Icam1, Junb, Socs3*).

High NF-κb activity induced in LP CD103^{+}CD11b^{+} DCs may lead to high production and secretion of IL-1β. IL-1β has been shown to increase the expression of myosin II light chain kinase (MLCK) in enterocytes. Increased MLCK activity in enterocytes increases intestinal epithelial tight junctions permeability (Al-Sadi R, J Immunol, 2008). It is known that DCs can open epithelial tight junctions (Rescigno M, Nat Immunol., 2001). These studies, combined with our data, provide us with a model to allow DC transmigration. We propose that elevated expression of *lmnb1* in LP CD103^{+}CD11b^{+} DCs promotes NF-κb pathway, resulting in IL-1β secretion. IL-1β helps DCs to open tight junctions that are available to interact with LP DC integrity. Interestingly, LP CD103^{+}CD11b^{+} DCs over express *lmnb1* that has a crucial role in maintaining nuclear rigidity. As it has been reported that *lmna* induces high NF-κb activity upon IL-1β stimulation (Lammerding J, J Clin Invest., 2004), the high NF-κb activity could result in elevated *lmnb1* expression. In intra-epithelial CD103^{+}CD11b^{+} DCs, the significantly lower expression of the NF-κb pathway genes might be explained by the *lmnb1* lower expression and the Cd24a overexpression (Li W, Mol Neurobiol, 2014). Altogether, these data suggest that a different genetic program is at work in DCs that have transmigrated, which might lead to a different cell function of these cell populations. We hypothesize that intra-epithelial CD103^{+}CD11b^{+} DCs, through antigen presentation, can further amplify the activity of the NF-κb pathway in LP DCs to promote DC transmigration. This hypothesis is supported by our live observations of transient contacts between intra-epithelial and LP DCs and increased intra-epithelial DC pool upon infection previously reported (Farache J, Immunity, 2013).

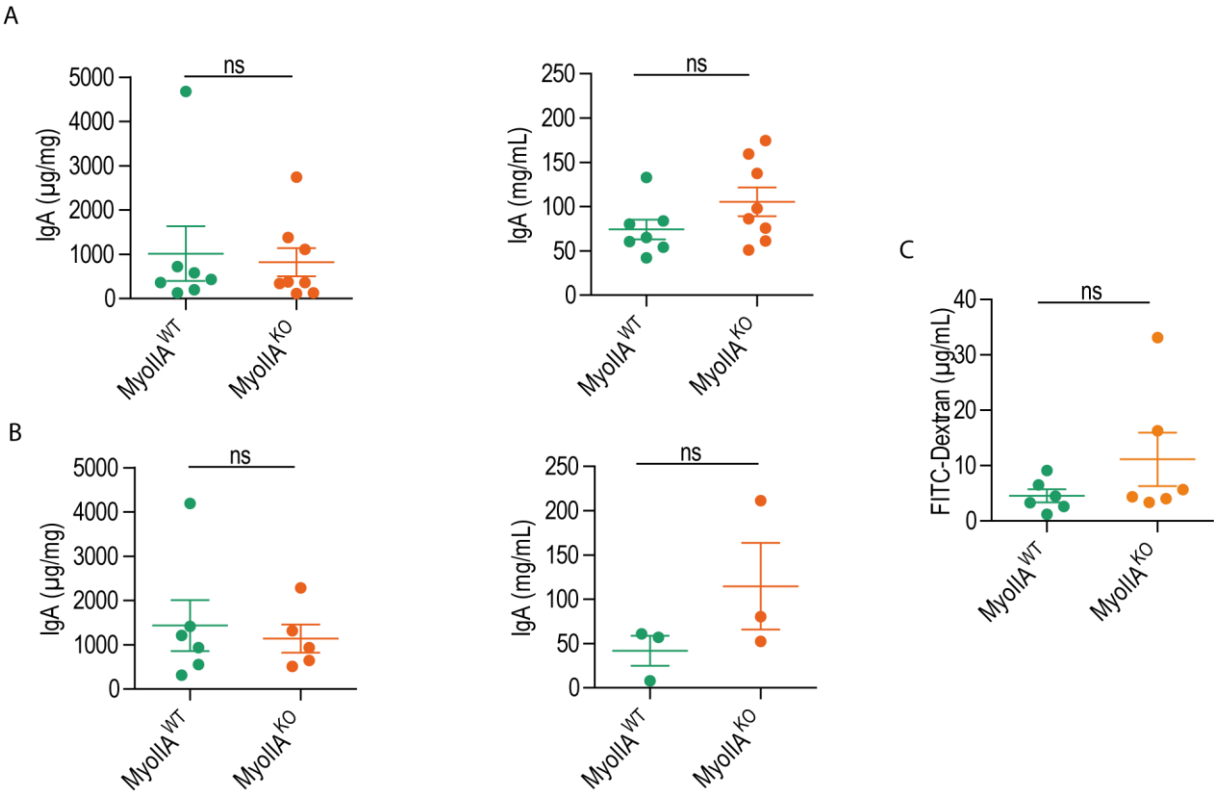

Figure 25. IgA secretion is not affected in mice with MyoIIA^{KO} DCs.
(A) IgA assessed by ELISA in feces (left panel) and serum (right panel) in MyoIIA^{WT} and MyoIIA^{KO} at steady state. Data pooled from three independent experiments.
(B) IgA assessed by ELISA in feces (left panel) and serum (right panel) in MyoIIA^{WT} and MyoIIA^{KO} after seven days of DSS treatment. Data pooled from two independent experiments. (C) FITC-Dextran assessed by fluorescence measurement in serum in MyoIIA^{WT} and MyoIIA^{KO} after seven days of DSS treatment. Data pooled from two independent experiments.

C- Intra-epithelial CD103^{+}CD11b^{+} DCs regulate the immune response in the small intestine epithelium

C-1 Intra-epithelial CD103^{+}CD11b^{+} DCs do not affect LP immune effectors

Over-expressed genes in intra-epithelial CD103^{+}CD11b^{+} DCs are related to antigen sensing, processing and presentation pathways. This includes autophagy (*Gabarapl2*), MHCII presentation (*H2-Oa, H2-Dmb2*) and lysosome genes (*Lamp1, Napsa, Hexb*). The lab lately showed that upon microbial sensing, DCs downregulate macropinocytosis leading to the activation of lysosomal signaling. This lysosome activity promotes myosin IIA activity and results in faster migration to draining lymph nodes (Bretou M, Science Immunol, In Press). Altogether, these data suggest that intra-epithelial CD103^{+}CD11b^{+} DCs have a very high migratory profile.

Due to their localization, we hypothesized that intra-epithelial CD103^{+}CD11b^{+} DCs in the tissue could interact with B cells in the gut associated lymphoid tissue. We assessed IgA levels in feces and serum and observed no significant difference between mice containing MyoIIA^{KO} DCs and co-housed control animals (Fig. 25 A). To test whether mice with MyoIIA^{KO} DCs had a different response to inflammation, we assessed IgA levels after Dextran sulfate salt (DSS) treatment in a longitudinal study. DSS-induced inflammation did not reveal significantly different IgA levels in feces and serum of mice with MyoIIA^{KO} DCs and co-housed control animals (Fig. 25 B). Interestingly, despite the elevated protrusion frequency in the small intestine of mice with MyoIIA^{KO} DCs, they did not present any differences in intestinal permeability upon DSS-induced inflammation (Fig. 25 C). This suggests that cell protrusions do not affect epithelium integrity.

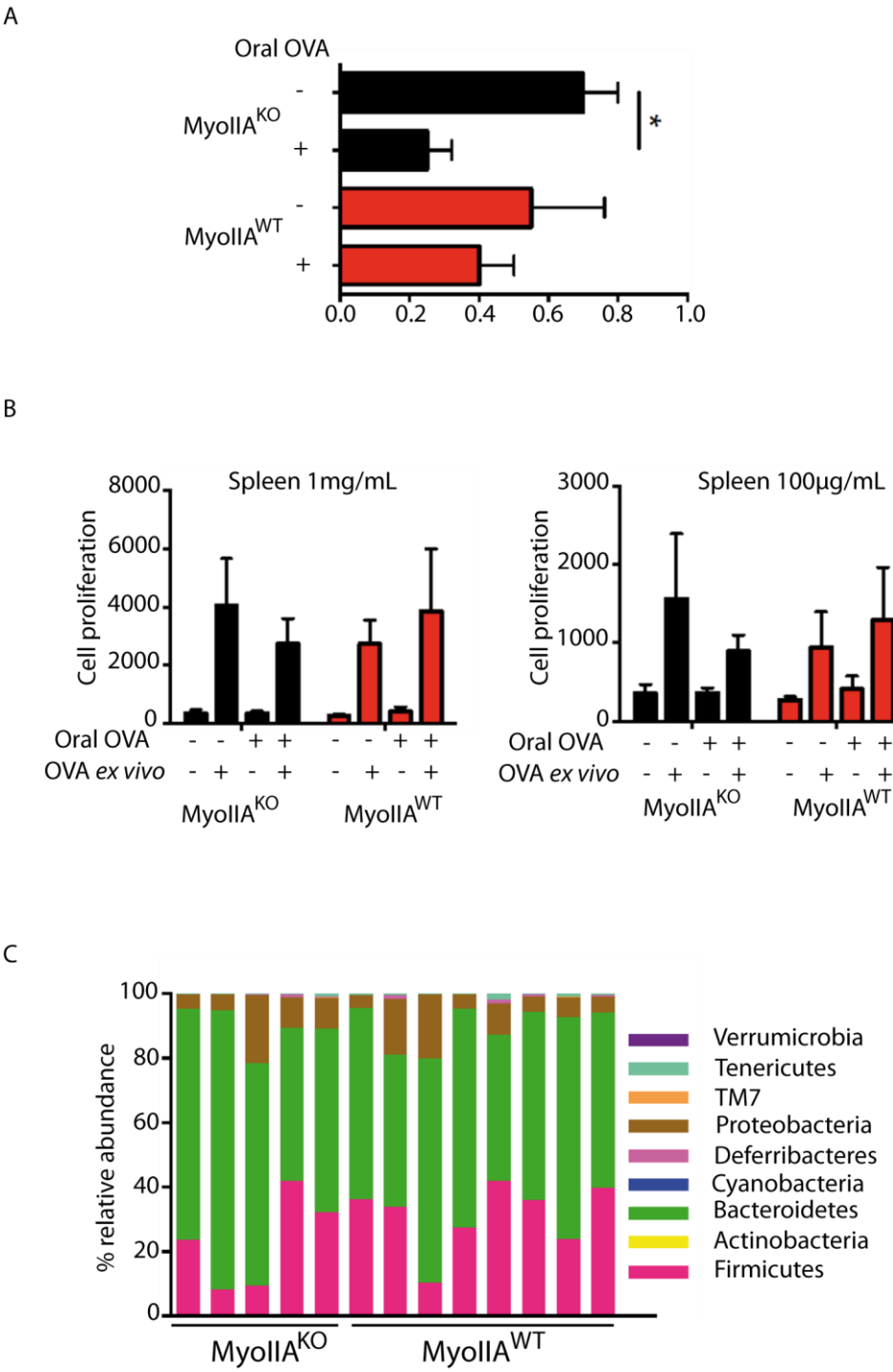

Figure 26. Lack of intra-epithelial CD103⁺CD11b⁺ DCs in MyoIIA^{KO} mice does not affect oral tolerance or commensalism.
(A-C) MyoIIA^{WT} and MyoIIA^{KO} mice were gavaged with Ovalbumin during 8 days and challenged at Day 15. Footpad swelling was measured at Day 16 (A). Proliferation was assessed by measuring Thymidine incorporation after culturing splenic cells with 1mg/mL Ovalbumin (B) or 100µg/mL Ovalbumin (C).
(D) Microbiota from co-housed MyoIIA^{WT} and MyoIIA^{KO} mice was analysed by 16-S sequencing.

Mice with MyoIIA^{KO} DCs had no significant difference in T helper absolute numbers. As some differences appeared in percentages with a significant increase of the Th17 pool and a concomitant decrease of the Treg pool, we tested whether this slight shift in the balance of the Th17/Treg axis could have any functional impact on oral tolerance. We did not observe any significant defect in the induction of oral tolerance assessed by footpad swelling measurement and splenic cell proliferation. Besides, we could not detect any significant difference between the microbiota of mice with MyoIIA^{KO} DCs and control co-housed animals. Taken together, these data suggest that intra-epithelial CD103^{+}CD11b^{+} DCs are not involved in the induction of oral tolerance. This analysis also highlights the redundancy of DCs in the small intestine that are able to compensate the partial reduction of the LP CD103^{+}CD11b^{+} DC subset to drive Th subsets development as previously reported (Welty NE, J Exp Med, 2013). To refine this analysis the production rate of cytokines by the different subsets of LP and intra-epithelial DCs could be assessed in our model.

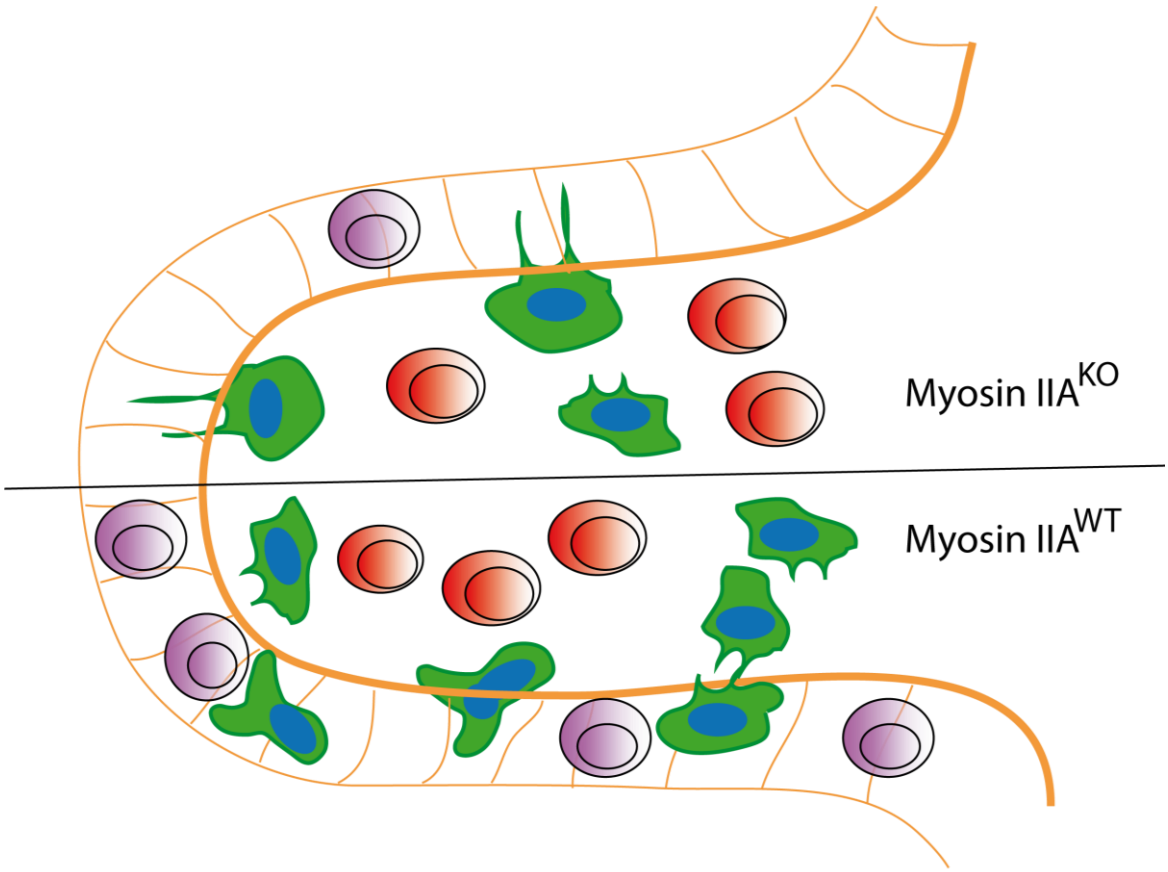

Figure 27. Different immune networks identified in small intestines of MyoIIA^{WT} mice and MyoIIA^{KO} mice.
Green cells represent dendritic cells.
Purple cells represent intrepitheliual lymphocytes.
Red cells represent T lymphocytes.

C-2 Intra-epithelial CD103$^+$CD11b$^+$ DCs affect epithelial immune effectors

Intra-epithelial CD103$^+$CD11b$^+$ DCs may act on innate immunity. They highly express *Pilra*, *Pilrb1* and *Pilrb2* genes, which regulate inflammatory response towards pathogens (Banerjee A, Infect Immunol., 2010). We speculate that intra-epithelial DCs can secrete anti-microbial peptides (AMPs) at the top of the villi. The elevated expression of *Ear2* supports this hypothesis as it is reported to have a strong cytotoxic, antibacterial and anti-parasitic activity (Attery A, Int J Biol Macromol., 2017).

Mice with Myosin IIA deficient DCs lack intra-epithelial cDCs and further show a reduction in the number of TCRαβ CD8$^+$αβ intra-epithelial lymphocytes (IELs) also known as type a IELs (Hayday A, Nat Immunol., 2001). IELs display a gradient, as their number decrease from duodenum to ileum. TCR ab CD8$^+$αβ IELs represent about 40% of this pool in each part of the small intestine of adult mice (Suzuki H, Dev Comp Immunol. 2002). Analyzing variations of IEL repartition according to mice age showed that major variations occur before weaning.

These data suggest that intra-epithelial cDCs are required to get a proper CD8$^+$αβ IEL pool but cannot determine through which mechanism. Do they promote survival, differentiation, expansion or retention of CD8$^+$αβ IEL in the small intestine? Intra-epithelial cDCs were shown to promote CD8$^+$ T cell differentiation and the expression of the gut homing marker CCR9 (Farache J, Immunity, 2013). Intra-epithelial cDCs could specifically attract T cells in the epithelium where they would undergo further differentiation to acquire IEL properties. The overexpression of co-stimulatory molecules such as *Cd48* and the C type lectin receptor *Clec2i* claims for a local expansion triggered by DCs in the epithelium. Another possibility is that intra-epithelial DCs specifically attract T cells in the epithelium where they would undergo further differentiation to acquire IEL properties. Conversion of FOXP3 Tregs into CD4$^+$ IELs after their transmigration into the epithelial layer has been reported (Sujino T, Science, 2016). The question whether a similar process for CD8$^+$ T cells is at work in the small intestinal villosities has not been addressed so far. The same study reports a reduction of CD4$^+$ IELs, and to a lower extent, of CD8$^+$αβ IELs in the epithelium of germ-free mice. We found that myosin IIA deficiency in cDCs affects specifically CD8$^+$αβ IELs in our mice model without any significant change in microbiotal composition our data suggests that IEL maintenance requires different types of stimuli depending on the subset.

Interestingly, $CD8^+\alpha\beta$ IELs express CD103, which is a receptor for E-cadherin. It might help them to interact with epithelial cells and promote their migration into the epithelium (Masopust D, J Immunol., 2006). Upon leukocytis choriomeningitidis viral (LCMV) infection, $CD8^+\alpha\beta$ IELs gradually adapt to their environment and become distinct from splenic $CD8^+$ T cells, although, at day 7 they resemble their splenic counterpart. Consistently, intra-epithelial DCs also overexpress *Cd24*, which is shown to recruit leukocytes by affecting integrin function (Bretz NP, Immunol Lett., 2014). These data suggest a strong impact of the intestinal microenvironment on IELs. We propose that the $CD8^+\alpha\beta$ IEL pool specifically require the presence of intra-epithelial $CD103^+CD11b^+$ cDCs for their recruitment and differentiation.

$CD8^+\alpha\beta$ IEL activity is regulated as $CD8^+\alpha\beta$ IELs efficiently fight against parasitic infections and simultaneously promote tissue damages (Roberts SJ, PNAS, 1996). Interestingly, $CD103^+CD11b^+$ DCs are enriched for a set of C type lectin receptors. Cd209a and Cd209b that code for DC-SIGN molecules (DC-Specific Intercellular adhesion molecule-3-Grabbing Non-integrin) and the Clec4a4 coding for DC immunoreceptor 2 (DCIR2) prevent inflammation and auto-immunity by limiting cytokine production and T cell priming, especially in the context of Th1 response (Uto T, Nat Comm., 2016; Diana J, J Immunol., 2013). Clec4b1, which codes for dendritic cell immunoactivating receptor 2 (DCAR2) is predicted to have an inhibitory activity towards T cell activation (Kanazawa N, J Biol Chem, 2003). This transcriptomic profile of tolerogenic DCs might give them the ability to contain $CD8^+\alpha\beta$ IEL activity (Diana J, J Immunol., 2013). Taken together, our results suggest that intra-epithelial $CD103^+CD11b^+$ DCs are involved in the recruitment, differentiation and activity regulation of $CD8^+\alpha\beta$ IELs.

In brief, intra-epithelial $CD103^+CD11b^+$ DCs appear as key regulators of the epithelial innate aspecific response through AMP secretion and adaptative immune response through $CD8^+\alpha\beta$ IEL regulation .

D- Intra-epithelial CD103$^+$CD11b$^+$ DCs take part in the immune compartmentalization of the small intestine.

Intra-epithelial DCs are more numerous in duodenum and jejunum as compared to the ileum. This repartition is similar to LP CD103$^+$CD11b$^+$ DCs repartition along the small intestine (Denning J, J Immunol., 2011) and parallels the gradient of retinoic acid.

D-1 The intestinal content may drive the gradient of CD103$^+$CD11b$^+$ DCs

CD103$^+$CD11b$^+$ DCs start to express RALDH2 in the LP. Indeed, AtRA has a direct impact on DCs as it can specifically induce the expression of the RALDH2 isoform. (Molenaar, J Immunol 2011) (Jaensson-Gyllenbäck, Mucosal Immunol, 2011). Podoplanin$^+$ LP cells of the small intestine can produce AtRA in a microbiotal dependent manner even under a vitamin A deficient diet. These cells are considered as a first source of AtRA to promote RALDH expression in DCs. Podoplanin+ LP cells would be the first ones to imprint the functional phenotype to LP CD103$^+$CD11b$^+$ DC. Then CD103$^+$CD11b$^+$ DC would take part in a positive feedback loop, increasing AtRA production in the lamina propria (Vicente-Suarez I, Mucosal Immunol, 2015). This first source of AtRA could drive a first epithelial colonization by CD103$^+$CD11b$^+$ DCs. Further dissection of DC interactions with LP cells in the lamina propria of the small intestine and colon might provide us with information about how the mucosal immune system is shaped.

The upper vs lower regionalization is associated with retinol availability that imprints CD103$^+$CD11b$^+$ DCs the ability to convert into AtRA thanks to RALDH2, which is specific to intestinal DCs. Retinal is highly available in the upper parts of the small intestine, since a great part of its stock is contained in bile (Jaesson-Gÿllenback, Mucosal Immunol., 2011). Lumenal retinoids act through the epithelium to imprint DCs with AtRA producing properties. A parallel has been observed between the expression of the Cytosolic Retinoid Chaperone Cellular Retinol Binding Protein II (CRBPII) in the epithelium and the expression of RALDH by LP DCs. CRBPII expression exhibits a gradient from the duodenum where it is highly expressed, to the colon where it is not expressed. RALDH positive DCs display the same gradient (McDonald KG, Am J Pathol., 2012). Intra-epithelial CD103$^+$CD11b$^+$ DCs could be involved in this close interaction between epithelium and DCs of the stroma as they form contacts with both of them.

We observe that the pool of intra-epithelial DCs is higher in the upper gut that is to say in a portion where bacterial load is lower. Furthermore, we found that the pool of intra-epithelial $CD103^+CD11b^+$ DCs was not affected by a reduction in bacterial or fungal load in adult mice. As it was demonstrated in the colon (Bhatthacharya N, Immunity, 2016), bacteria may have an impact on AtRA metabolism in the small intestine, being able to increase its degradation and lower the epithelial production of All-*trans* Retinal, which is one of the RALDH substrate required to produce AtRA. This phenomenon might explain a lower epithelial colonization by $CD103^+CD11b^+$ DCs in regions with a high bacterial load such as the ileum and the almost complete absence of $CD103^+CD11b^+$ DCs in the colonic lamina propria. Taken together, these data suggest that lumenal RALDH2 substrate contained in the bile maintains the pool of $CD103^+CD11b^+$ DCs in the epithelium that give survival signals to their LP counterparts.

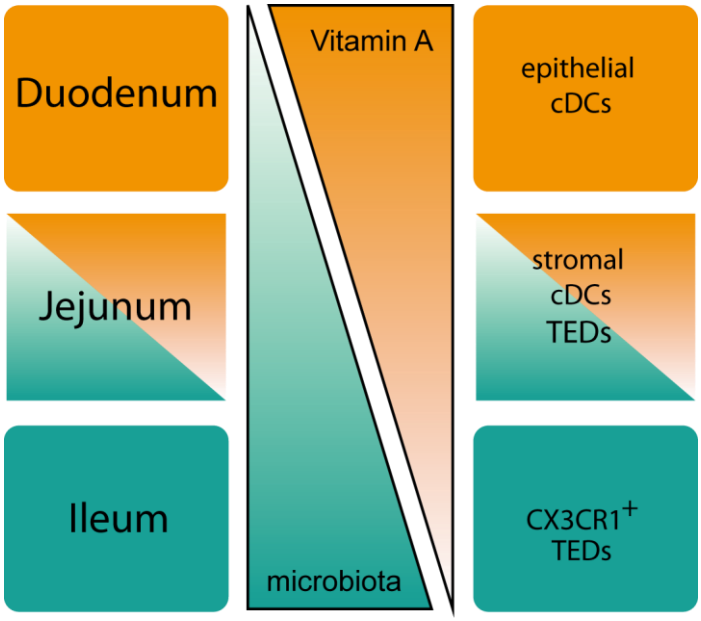

Figure 28. Proposed model of antigen sampling in the different regions of the small intestine taking into account the lumen content.

D-2 The regionalization of intra-epithelial CD103$^+$CD11b$^+$ DCs underlies regionalized strategies for antigen sampling

Intra-epithelial CD103$^+$CD11b$^+$ DCs are more frequent in the duodenum and jejunum, which is consistent with previous observations about trans-epithelial dendrites (TEDs) emitted by DCs that are more frequent in the upper parts of the small intestine, especially in the proximal jejunum (Chieppa M, J Exp Med, 2006). This gradient of intra-epithelial CD103$^+$CD11b$^+$ DCs can result in a differential scheme for antigen sampling depending on the region of the small intestine. LP CD103$^+$CD11b$^+$ DCs might contribute themselves to facilitate their transmigration into the epithelial layer. In our model, LP CD103$^+$CD11b$^+$ DCs overexpress *Il1b* that codes for IL-1β. As they are more frequent in the duodenum, IL-1β secretion might be higher in that part of the small intestine. Upon IL-1β stimulation, epithelial Myosin Light Chain Kinase (MLCK) regulates tight junctions of the intestinal epithelium *in vitro* (Al-Sadi R, J Immunol, 2008). Neutrophil epithelial transmigration experiments showed that epithelial myosin IIA could act by opening occluding tight junctions without affecting the epithelial permeability (Lapointe TK, Am J Physiol Gastrointest Liver Physiol., 2012). Then, cell cooperation within CD103$^+$CD11b$^+$ DCs could occur to facilitate transmigration of some.

CX3CR1$^+$ cells have been reported to form TEDs to uptake luminal antigen following the expression of the CX3CR1 ligand (CX3CL1) (Niess JH, Science, 2005). Notably, CX3CL1 is expressed at the basolateral surface of intestinal epithelial cells exclusively in the ileum and not in the upper parts of the small intestine. Conversely, in the upper parts of the intestine, no attractant has been identified so far for TED formation by LP CD103$^+$CD11b$^+$ DCs. We propose that AtRA favors the presence of intra-epithelial CD103$^+$ CD11b$^+$ DCs. Given their high potential for antigen processing and presentation, we hypothesize that those intra-epithelial DCs may signal LP CD103$^+$CD11b$^+$ DCs to emit TEDs. The nature of this signal (cytokine secretion, antigen presentation) has to be defined.

These findings modify the typical scheme of tissue patrolling of the small intestine and may open up additional studies in mucosal immunology to further investigate the contribution of this intra-epithelial DC pool to both innate and adaptative immune defenses. In particular, the precise interactions of these cells with the intestinal epithelium and LP DCs would be of great interest.

Immune responses are classically thought to be triggered in secondary lymph nodes. The field of mucosal immunology has underlined the importance of immune interactions taking place in peripheral tissues to finely tune immune responses. My work brings new pieces in the puzzle of gut immunology. This work shows that a constant pool of DCs is constantly patrolling the epithelium of the small intestine in homeostasis, which deeply modifies the actual scheme of antigen capture in the small intestine. We provide the first characterization of intra-epithelial DCs and give insights for their regulation and function in the gut immune landscape. Furthermore, this study shows that the epithelium is not only an extension of the stroma of intestinal villosities but a tissue where an additional immune network is at work. To obtain these data we combined cytometry and live imaging. The histo-cytometry method fuses both approaches in lymph nodes (Gerner MY, Immunity, 2012). Overcoming technical limitations due to tissue specificities to apply this method to the small intestine would bring great insights into the field.

First, we showed the essential role of myosin IIA in $CD103^+$ $CD11b^+$ DC transmigration from the LP to the epithelium. This *in vivo* demonstration brings clues about the mechanisms by which myosin IIA facilitates $CD103^+$ $CD11b^+$ DC passage through the basal membrane. In addition, *in vitro* studies are now needed to decipher properly the intracellular mechanisms involved in that crucial migration step. Second, we highlight that through the deformations it imposes to the nucleus, transmigration initiate a new transcriptomic program in $CD103^+$ $CD11b^+$ DCs confering them new competences. Indeed, we showed that intra-epithelial $CD103^+$ $CD11b^+$ DCs maintain the pool of IELs and may regulate their activity. Our RNA sequencing data thus suggest that, intra-epithelial cDCs might regulate the local immune system. Third, this work deciphers how the intestinal environment and its changes along the different parts of the small intestine influence intra-epithelial DC pool and its compartmentalization.

Taken together, these findings shift once again the balance towards peripheral tissues to regulate adaptative immune responses. They also open new challenges to understand how intra-epithelial DCs interact with the epithelium: how does this intra-epithelial pool react to acute infection? How does it adapt to chronic inflammation?

MATERIALS and METHODS

Mice

MyoIIA $^{flox/flox}$ X CD11c$^{Cre+/-}$ mice were generated by crossing *MyoIIA$^{flox/flox}$* mice (Jacobelli J. et al., Nat Immunol., 2011) with *CD11c$^{Cre+/-}$* mice (Caton ML et al., J Exp Med., 2007). These mice were crossed with the tdTomato/GFP reporter previously described (Muzumdar MD, Genesis, 2007) to obtain MyoIIA $^{flox/flox}$ X CD11c$^{Cre-GFP}$ X Tomato$^{flox/flox}$. Myosin IIA heavy Chain-GFP knock-in mice (referred to as myosin IIA-GFP) were previously described (Zhang Y. et al., Blood, 2012). Experiments were performed on 8 to 14 weeks-old male or female mice. For animal care, we strictly followed the European and French National Regulation for the Protection of Vertebrate Animals used for Experimental and other Scientific Purposes (Directive 2010/63; French Decree 2013-118).

Antibodies and Reagents

The following reagents were used : OCT (1507701005 from Sakura Tissue-tek). Bovine Serum Albumine Standard (BSA, 04-100-812-C from Euromedex), EGF (Peprotech, ref.315-09), Transferrine (Calbiochem, ref.616397), Insulin (Sigma-Aldrich, ref.i1882-100mg). Fetal Bovine Serum (Biowest, S1810-500) was decomplemented at 56°C and filtered before use as FBS. Used antibodies were PE anti-CD103 (eBioscience, clone 2E7), PECy7 anti-CD11b (eBioscience, clone M1/70), APC anti-CD11c (BD Bioscience, clone HL3), Alexa Fluor 700 anti-IA/IE (BioLegend, clone M5/114.152), BV421 anti-CD64 (BioLegend, clone X54-5/7.1), PE-Cy5.5 anti-CD45 (eBioscience, clone 30-F11), APC/Cy7 anti-CD19 (BioLegend, clone 6D5), APC/Cy7 anti-CD3ε (Biolegend, clone 145-2C11), LiveDead (eBioscience, ref.65-0865-14), APC anti-FOXP3 (eBioscience, clone FJK-16s), PE anti-GATA3 (eBioscience, clone TWAJ), PE anti-RORγt (BD Horizon, clone Q31-378), Per-CP anti-CD4 (BD Horizon, clone RMA-5), Rabbit anti-laminin (SIGMA, L9393-2ML), Alexa 647 Goat anti-Rabbit (Life Technologies, A21245). Tissues were embedded in tissue cassettes from Electron Microscopy Sciences, at least 5mm deep.

Isolation of Intestinal Cell Suspensions

For preparation of single-intestinal-cell suspension the small intestines were extracted from mice by separation from the mesentery. Peyer Patches were removed and Intestines were opened with scissors along the intestinal length, then washed in PBS. Next, intestinal tissues were incubated on a magnetic shaker incomplete medium (CM, 2% FBS in Ca2+, Mg2+-free Phenol Red 10X HBSS; H4385 Sigma-Aldrich, St. Louis, MO, USA diluted in filtered H2O) in the presence of 1 mM DTT (D9779, Sigma-Aldrich, St. Louis, MO, USA) at 37°C for 30 min and subsequently incubated with 1 mM EDTA (15575-038 from Invitrogen) in 5% FBS/ PBS at 37°C for 10min. This was followed by incubation inthen in 15mM Hepes (15630-056 from Gibco) in 1% FBS/PBS at room temperature for 7min without agitation. The supernatants containing intestinal epithelial cell (IEC) were collected and analyzed by flow cytometry. Isolated tissues were collected and digested using 0.15 mg/ml Liberase (054010200001from Roche) and 0.1mg/ml DNAse1 (10104159001 from Roche) in HBSS at 37°C for 45min with magnetic agitation. Tissues were then homogenized, filtered on 100µm cell strainer, and washed in HBSS. Gradient was performed on both epithelial fraction and lamina propria to further eliminate fat in 44% and 67% fractions of Percoll (17-0891-01, GE Healthcare) prepared in 100mM Hepes in HBSS. MLNs cell suspensions were prepared by digestion with Liberase and Dnase1 for 45min. Single-cell suspensions were stained with mouse antibodies and analyzed by flow cytometry.

Flow cytometry analysis

Cells were stained with 2mM EDTA, 5%FBS in PBS and RALDH activity in individual cells was measured using an Aldefluor kit according to the manufacturer's protocol. 7.5 µM of DEAB was added in different tubes at 37°C for 15 min as Aldefluor fluorescent baseline control. Flow cytometry was performed on Fortessa (BD) and analyzed using FlowJo software. Percentage values were charted with Graphpad Prism.

Tissue immunofluorescence

The small intestine was extracted and washed by flushing the lumen with cold Leibovitz's L-15 medium (L5520, SIGMA). 5mm fragments from each region of the small intestine (I.e. duodenum, jejunum, ileum). Tissue was fixed in the fixative solution (4% PFA/0.05 M L-Lysine/12mM NaH_2PO_4/50mM Na_2HPO_4/H_2O) at 4°C overnight, and dehydrated 20% sucrose/PBS for 4h at room temperature. After washing twice with 40 mM NaH_2PO_4/160 mM Na_2HPO_4/H_2O samples were embedded with OCT in tissue cassettes, snap frozen using liquid nitrogen, and stored at -80°C. Samples were incubated in permeabilization buffer (1% Triton X100/PBS) for 1h (1ml/10 slices), then in blocking buffer (1% BSA/3%FCS/0,2% Triton-X100/PBS) for 1h. Tissue staining was performed by incubating gut slices with primary antibodies overnight in 0,2% Tx100/PBS (100µL/3slices), using the following dilutions: 1/50 for anti-CD103; 1/100 for all other antibodies diluted. Samples were washed 3 times 0,2%Tx100/PBS for 1h (each wash), with mild shaking rocking. When required, samples were incubated with secondary antibodies and DAPI overnight (both diluted 1/100) and then washed as described before. Samples were kept at room temperature during all steps before louting with Aqua Polymount medium. Z-stacks consisting of 1024*1024 pixels (150nm pixel size) images spaced by 0.35µm were acquired using an inverted confocal microscope (Leica DMi8, SP8 scanning head unit) equipped with a 63Xoil immersion objective, pixel size 1024*1024, z-step 0,35mm.

Ex vivo microscopy

The gut region was extracted and washed by flushing the lumen with L-15 Leibowitz's L-15 medium and then cut into ~1mm slices using a sterile scalpel. Gut slices were placed in a cell culture dish (35mm, Fluorodish, World Precision Instruments) containing 500µL ofimaging medium (50ng/ml EGF/100mg/ml Transferrin/0,25U/ml Insulin/ 1% Penicillin-Streptamycin/2,5% FBS/DMEM-Glutamax). A tissue anchor (SHD-26GH/10; Harvard Apparatus, UK) was placed above the slices to minimize the drift. Time lapse movies were acquired with a two-photon laser scanning microscope: inverted Leica SP8 microscope coupled to a femtosecond Chameleon Vision II Laser (680-1350nm; Coherent Inc.) equipped with a 40xoil immersion objective. Tissue was maintained at 37°C in 95%O2/5%CO2 with 95% humidification inside a top stage incubator (Okolab).

Fluorescence was monitored on non-descanned Hybrid detectors through filters: 525/25nm (GFP), 575/25 (Tomato). Excitation wave length was set at 960nm. Z-stack were acquired every 45seconds, z-step 1µm.

Intravital microscopy

Myosin $IIA^{WT/WT}$X $CD11c^{Cre\text{-}GFP}$ X $Tomato^{Flox/Flox}$ and Myosin $IIA^{Flox/Flox}$ X $CD11c^{Cre\text{-}GFP}$ X $Tomato^{Flox/Flox}$ were used to image DCs. Anesthesia was initiated with a 3% isoflurane/ air mixture. The mouse was kept anesthesized throughout the procedure with a 1,5% isoflurane/air mixture. A loop of the ileum was exposed through a small ventral incision and an incision was made along the intestine to expose the mucosal side. The anesthesized mouse was mounted on a custom built holder placed on a heated pad. The holder keeps the intestine outside of the body to limit the drift due to breathing movements during imaging and it also keeps the tissue flat under the lens of the microscope. The holder and the mice were placed in a thermostated chamber to keep the temperature of the mouse at 37°C during the imaging. The time lapse movies are acquired with an upright multiphoton microscope (A1R MP, Nikon operating with NIS software), coupled with an IR laser (insight deepsee, spectra physics), equipped with a 2mm working distance, 25X water objective (Nikon). The excitation wavelength was 960nm. The fluorescence was collected through a two non descanned GaAsP detectors with band pass filters (525/50 for the GFP and 575/50 for the tdTomato signals). Z stacks were acquired every 2minutes, z-step 2µm.

Image analysis and processing

Image analysis and processing was performed using Fiji software (ref: *Schindelin, J.; Arganda-Carreras, I. & Frise, E. et al. (2012), "Fiji: an open-source platform for biological-image analysis", Nature methods 9(7): 676-682, PMID 22743772* (on Google Scholar). Two photon stacks were registered to correct tissue movement. First, "Correct 3D Drift" plugin on tdTomato channel was apply to correct each Zstack. Then a custom macro was use to correct drift between time points: briefly, a well identify structure position was measured for all time and stacks were aligned on those positions. Movies and montage shown correspond to a maximum intensity Z-projection of 5 planes spaced by 2µm.

3D reconstructions of in-vitro stacks was achieved using 3D viewer plugin.

Quantification of intra-epithelial GFP cells was performed on IF 3D stacks. Intra-epithelial GFP cells manually count and normalized by the number of GFP cells found inside the stroma. To determine the number of GFP positives cells inside, an homemade macro was used. First seeds corresponding to nuclei center were determined using Log detection of TrackMate plugin apply on the Dapi channel. Then the volume of the stroma was divided according to those seeds usind 3D watershed function of the ImageJ 3D suite and thus, individuals cell's volumes were obtained. To finish, a mean GFP intensity was measured on each cell's volume and a threshold was apply on those intensities to determine the number of GFP positive cells inside the vilosity.

The 3D protrusions were manually defined on each stack and their length was computed.

Single cell RNA-seq library preparation

Cells were isolated from the lamina propria of 2 pooled SI of Myosin $IIA^{Flox/Flox}$ X $CD11C^{Cre+/-}$ and from the epithelium and the lamina propria of 2 pooled SI of Myosin $IIA^{Flox/Flox}$ X $CD11C^{Cre-/-}$ Cellular suspensions (1700 cells) were loaded on a 10X Chromium instrument (10X Genomics) according to manufacturer's protocol based on the 10X GEMCode proprietary technology. Single-cell RNA-Seq libraries were prepared using Chromium Single Cell 3' v2 Reagent Kit (10X Genomics) according to manufacturer's protocol as described in Goudot C. et al., Immunity, 2017. Using a full Rapid flow cell, a coverage around 100M reads per sample (around 1000 cells) were obtained corresponding to 100,000 reads/cell. Data were analyzed with a Seurate package.

Antibiotic and anti-fungal treatment

C57/BL6 were gavaged during 10 days with 200µL per day of PBS or 0.5mg/mL Fluconazole (F8929) in PBS or antibiotic cocktail in PBS of Ampicillin A9393 1mg/mL+ Gentamicin sulfate G4918 1mg/mL+ Vancomycin 861987 0,5mg/mL+ Metronidazole M1547 1mg/mL+ Neomycin trisulfate salt N1876 1mg/mL (all products purchased at Sigma-Aldrich). Stools were collected before treatment and right before sacrifice.

Microbiota analysis

DNA was extracted from stools using Qiamp DNA stool mini kit (51504 from Qiagen)

Gut Inflammation induction

2% Dextran sulfate sodium salt (DSS, 42867 from Sigma-Aldrich) was admnistered in drinking water during 7 days. Feces were collected at Day 0, Day 7 and Day 14.

Intestinal permeability assessment

Mice were gavage with 60mg/100g of FITC-Dextran 4kDa (46944 from Sigma-Aldrich) at 100mg/mL in H20. Mice were sacrified 4 hours later and blood was collected into microtainer tubes (ref 365968 from BD) by heart puncture to recover serum. Sera were plated in black plates. FITC-dextran amount in serum was measured with a fluorescence spectrophotometer setup with emission and excitation wavelengths of respectively 490 nm and 520 nm. FITC-dextran concentration was determined from standard curves generated by serial dilution of FITC-dextran in serum.

Enzyme-linked immunosorbent assay (ELISA)

Microtitre plates (96 wells, Maxisorb, Nunc) were coated overnight at 4°C with unlabeled goat anti-mouse Ig/H-L (1010.01 from Southern Biotech) in carbonate buffer pH 9.6. For the measurement of background binding, wells without coated antigens were used. Reagents, sera and fecal lysates were diluted in PBS/bovine serum albumin (BSA) 1%. Between all following steps, microtitre plates were washed with 200 µl of 0,01% Tween in PBS. Plates were coated with serial dilutions of sera (1:5000 and then 1:10) or feces lysates (1:2000 and then 1:5). After 3 washesPlates were blocked with 200 µl PBS/BSA 5% for 2 h at 37°C. Plates were then coated with horseradish peroxidase -Goat anti-mouse IgA (ab97235 from abcam) After 10 washes, plates were incubated with 100 µl TMB (3,3′ – 5,5′-Tetramethylbenzidin; ref 555214 from BD Biosciences) for 10–15 min. 2-fold serial dilution curve of unlabeled mouse-IgA (Southern Biotech, clone S107) served as standard. The reaction was stopped by adding 50 µl 2N H_2SO_4. Optical density was read photometrically at 450 nm. Total IgA were measured in 1:1000 diluted serum and fecal homogenates prepared in Cocktail Protease 1x (11697498001 from Roche) + 1% BSA in PBS.

Inhibition of RALDH activity

Mice were gavaged during 4 days with 230µL olive oil or 0,1mg/kg of Bisdiamine (WIN 18446, ref 1477-57-2 from Tocris) diluted in olive oil. RALDH activity was assessed by flow cytometry with the ALDEFLUOR kit (StemCell).

Induction of oral tolerance

Mice were gavaged during five days with 20mg/mL Ovalbumin in PBS. On day 8 mice were immunized by subcutaneous injection of 100µL 2,5mg/mL Ovalbumin+CFA(Complete Freund Adjuvant from Sigma F5881) in the tail. AT Day 15 mice were challenged with with 100µL of 1mg/mL Ovalbumin in right footpad and 100µL PBS in left footpad. Footpad swelling was measured at day 16, before sacrifice. Cell suspension obtained from Spleen was plated (2.10^5 per well) and cultured during three with either 0,1mg/mL or 1mg/mL solutions of Ovalbumin. Cell Proliferation of MLNs and restimulated splenic cells was assessed by thymidine incorporation.

Cells and Cell culture

Mouse bone marrow-derived dendritic cells (BMDCs) were obtained by culturing bone marrow precursors for 10 in IMDM medium containing FBS (10%), glutamine (20 mM), penicillin–streptomycin (100 U ml^{-1}), 2-Mercapto-ethanol (50 µM) and further supplemented with granulocyte-macrophage colony-stimulating factor (50 ng ml^{-1})-containing supernatant obtained from transfected J558 cells, as previously described in Faure-André G. et al., Science, 2008. Immature DCs were obtained by gentle recovery of semi-adherent cells from culture dishes. Mature DCs were obtained by treating iDCs with LPS from *Salmonella enterica* serotype typhimurium (Sigma) (100 ng ml^{-1}) for 30 min and washing 3 times with complete medium.

Confined migration assay

Microchannel were prepared as previously described (Thiam HR, Nat Comm., 2016; Sáez PJ, Methods in Molecular Biology., submitted). Briefly, 8X4µm microchannels with constrictions of 1.5X4 µm were prepared in PDMS (RTV) using a custom-made mold. PDMS chamber were stick to 35mm glass bottom dish after plasma activation. Devices were incubated 1h in the oven at 70°C to reinforce the binding. After a second plasma activation, microchannels were coated with 10µg/ml of fibronectin (Sigma) and 200ng/ml of chemokine CCL21 (R&D System) for 1h at RT, then washed in PBS and incubated 30 min with BMDCs medium at 37°C, and 5% CO2. 100 000 MyoII-GFP mDCs were load at the microchannels entry and imaged during 18h using a Leica video microscope. One representative cell were isolated and analyses using imageJ.

Transmigration experiments

ECM (Matrigel) invasion assays for mature DCs were performed using Transwell cell culture chambers (polycarbonate filters, 3µm pore size;ref. **353096 from Corning**) placed in 24 well plates (ref. 353047 from Falcon). As previously described (Darmanin S. et al., J Immunol., 2016) the filters were coated with 40µl of Matrigel (BD Biosciences) (diluted 1/3 (v/v) in cold serum-free medium) and incubated at 37°C for 60min. Recombinant murine CCL19and CCL21 (both from R&D Systems) were diluted in complete medium at a concentration of 100 ng/ml and placed in the lower chamber of the Transwell in a volume of 600µl. Mature DCs (1.10^5) were suspended in 100µl of complete medium and placed in the upper chamber of the Transwell. Transmigration was assessed by manual counting of live cells in medium recovered in the lower chamber in Trypan blue medium (v/v: 1:2).

REFERENCES

Agace, W.W., and Persson, E.K. (2012). How vitamin A metabolizing dendritic cells are generated in the gut mucosa. Trends in Immunology *33*, 42–48.

Al-Sadi, R., Ye, D., Dokladny, K., and Ma, T.Y. (2008). Mechanism of IL-1β-Induced Increase in Intestinal Epithelial Tight Junction Permeability. The Journal of Immunology *180*, 5653–5661.

Ambort, D., Johansson, M.E.V., Gustafsson, J.K., Nilsson, H.E., Ermund, A., Johansson, B.R., Koeck, P.J.B., Hebert, H., and Hansson, G.C. (2012). Calcium and pH-dependent packing and release of the gel-forming MUC2 mucin. PNAS *109*, 5645–5650.

Attery, A., and Batra, J.K. (2017). Mouse eosinophil associated ribonucleases: Mechanism of cytotoxic, antibacterial and antiparasitic activities. International Journal of Biological Macromolecules *94*, *Part A*, 445–450.

Aujla, S.J., Chan, Y.R., Zheng, M., Fei, M., Askew, D.J., Pociask, D.A., Reinhart, T.A., McAllister, F., Edeal, J., Gaus, K., et al. (2008). IL-22 mediates mucosal host defense against Gram-negative bacterial pneumonia. Nat. Med. *14*, 275–281.

Bain, C.C., Scott, C.L., Uronen-Hansson, H., Gudjonsson, S., Jansson, O., Grip, O., Guilliams, M., Malissen, B., Agace, W.W., and Mowat, A.M. (2013). Resident and pro-inflammatory macrophages in the colon represent alternative context-dependent fates of the same Ly6Chi monocyte precursors. Mucosal Immunol *6*, 498–510.

Banerjee, A., Stevenaert, F., Pande, K., Haghjoo, E., Antonenko, S., Gorman, D.M., Sathe, M., McClanahan, T.K., Pierce, R., Turner, S.P., et al. (2010). Modulation of Paired Immunoglobulin-Like Type 2 Receptor Signaling Alters the Host Response to Staphylococcus aureus-Induced Pneumonia. Infect. Immun. *78*, 1353–1363.

Batten, M.L., Imanishi, Y., Maeda, T., Tu, D.C., Moise, A.R., Bronson, D., Possin, D., Gelder, R.N.V., Baehr, W., and Palczewski, K. (2004). Lecithin-retinol Acyltransferase Is Essential for Accumulation of All-trans-Retinyl Esters in the Eye and in the Liver. J. Biol. Chem. *279*, 10422–10432.

Bauer, H., Horowitz, R.E., Levenson, S.M., and Popper, H. (1963). The Response of the Lymphatic Tissue to the Microbial Flora. Studies on Germfree Mice. The American Journal of Pathology *42*, 471.

Becker, M., Güttler, S., Bachem, A., Hartung, E., Mora, A., Jäkel, A., Hutloff, A., Henn, V., Mages, H.W., Gurka, S., et al. (2014). Ontogenic, Phenotypic, and Functional Characterization of XCR1+ Dendritic Cells Leads to a Consistent Classification of Intestinal Dendritic Cells Based on the Expression of XCR1 and SIRPα. Front. Immunol. *5*.

van Bennekum, A.M., Fisher, E.A., Blaner, W.S., and Harrison, E.H. (2000). Hydrolysis of Retinyl Esters by Pancreatic Triglyceride Lipase. Biochemistry *39*, 4900–4906.

Benson, M.J., Pino-Lagos, K., Rosemblatt, M., and Noelle, R.J. (2007). All-trans retinoic acid mediates enhanced T reg cell growth, differentiation, and gut homing in the face of high levels of co-stimulation. Journal of Experimental Medicine *204*, 1765–1774.

Bhaumik, S., and Basu, R. (2017). Cellular and Molecular Dynamics of Th17 Differentiation and its Developmental Plasticity in the Intestinal Immune Response. Front. Immunol. *8*.

Bogunovic, M., Ginhoux, F., Helft, J., Shang, L., Hashimoto, D., Greter, M., Liu, K., Jakubzick, C., Ingersoll, M.A., Leboeuf, M., et al. (2009). Origin of the Lamina Propria Dendritic Cell Network. Immunity *31*, 513–525.

Bono, M.R., Tejon, G., Flores-Santibañez, F., Fernandez, D., Rosemblatt, M., and Sauma, D. (2016). Retinoic Acid as a Modulator of T Cell Immunity. Nutrients *8*, 349.

Bretou, M., Kumari, A., Malbec, O., Moreau, H.D., Obino, D., Pierobon, P., Randrian, V., Sáez, P.J., and Lennon-Duménil, A.-M. (2016). Dynamics of the membrane–cytoskeleton interface in MHC class II-restricted antigen presentation. Immunol Rev *272*, 39–51.

Bretz, N.P., Salnikov, A.V., Doberstein, K., Garbi, N., Kloess, V., Joumaa, S., Naumov, I., Boon, L., Moldenhauer, G., Arber, N., et al. (2014). Lack of CD24 expression in mice reduces the number of leukocytes in the colon. Immunology Letters *161*, 140–148.

Calderón-Gómez, E., Bassolas-Molina, H., Mora-Buch, R., Dotti, I., Planell, N., Esteller, M., Gallego, M., Martí, M., Garcia-Martín, C., Martínez-Torró, C., et al. (2016). Commensal-Specific CD4+ Cells From Patients With Crohn's Disease Have a T-Helper 17 Inflammatory Profile. Gastroenterology *151*, 489–500.e3.

Cassani, B., Villablanca, E.J., Quintana, F.J., Love, P.E., Lacy–Hulbert, A., Blaner, W.S., Sparwasser, T., Snapper, S.B., Weiner, H.L., and Mora, J.R. (2011). Gut-Tropic T Cells That Express Integrin α4β7 and CCR9 Are Required for Induction of Oral Immune Tolerance in Mice. Gastroenterology *141*, 2109–2118.

Cha, H.-R., Chang, S.-Y., Chang, J.-H., Kim, J.-O., Yang, J.-Y., Kim, C.-H., and Kweon, M.-N. (2010). Downregulation of Th17 Cells in the Small Intestine by Disruption of Gut Flora in the Absence of Retinoic Acid. The Journal of Immunology *184*, 6799–6806.

Chabaud, M., Heuzé, M.L., Bretou, M., Vargas, P., Maiuri, P., Solanes, P., Maurin, M., Terriac, E., Berre, M.L., Lankar, D., et al. (2015). Cell migration and antigen capture are antagonistic processes coupled by myosin II in dendritic cells. Nature Communications *6*, ncomms8526.

Chelstowska, S., Widjaja-Adhi, M.A.K., Silvaroli, J.A., and Golczak, M. (2016). Molecular Basis for Vitamin A Uptake and Storage in Vertebrates. Nutrients *8*, 676.

Chieppa, M., Rescigno, M., Huang, A.Y.C., and Germain, R.N. (2006). Dynamic imaging of dendritic cell extension into the small bowel lumen in response to epithelial cell TLR engagement. J Exp Med *203*, 2841–2852.

Choi, H.H., and Cho, Y.-S. (2016). Fecal Microbiota Transplantation: Current Applications, Effectiveness, and Future Perspectives. Clinical Endoscopy, Clinical Endoscopy *49*, 257–265.

Clevers, H.C., and Bevins, C.L. (2013). Paneth Cells: Maestros of the Small Intestinal Crypts. Annual Review of Physiology *75*, 289–311.

Cramer, L.P. (2010). Forming the cell rear first: breaking cell symmetry to trigger directed cell migration. Nat Cell Biol *12*, 628–632.

Daillère, R., Vétizou, M., Waldschmitt, N., Yamazaki, T., Isnard, C., Poirier-Colame, V., Duong, C.P.M., Flament, C., Lepage, P., Roberti, M.P., et al. (2016). Enterococcus hirae and Barnesiella intestinihominis Facilitate Cyclophosphamide-Induced Therapeutic Immunomodulatory Effects. Immunity *45*, 931–943.

Darfeuille-Michaud, A., Boudeau, J., Bulois, P., Neut, C., Glasser, A.-L., Barnich, N., Bringer, M.-A., Swidsinski, A., Beaugerie, L., and Colombel, J.-F. (2004). High prevalence of adherent-invasive Escherichia coli associated with ileal mucosa in Crohn's disease. Gastroenterology *127*, 412–421.

Darmanin, S., Chen, J., Zhao, S., Cui, H., Shirkoohi, R., Kubo, N., Kuge, Y., Tamaki, N., Nakagawa, K., Hamada, J., et al. (2007). All-trans Retinoic Acid Enhances Murine Dendritic Cell Migration to Draining Lymph Nodes via the Balance of Matrix Metalloproteinases and Their Inhibitors. J Immunol *179*, 4616–4625.

Denning, T.L., Norris, B.A., Medina-Contreras, O., Manicassamy, S., Geem, D., Madan, R., Karp, C.L., and Pulendran, B. (2011). Functional Specializations of Intestinal Dendritic Cell and Macrophage Subsets That Control Th17 and Regulatory T Cell Responses Are Dependent on the T Cell/APC Ratio, Source of Mouse Strain, and Regional Localization. J Immunol *187*, 733–747.

DePaolo, R.W., Abadie, V., Tang, F., Fehlner-Peach, H., Hall, J.A., Wang, W., Marietta, E.V., Kasarda, D.D., Waldmann, T.A., Murray, J.A., et al. (2011). Co-adjuvant effects of retinoic acid and IL-15 induce inflammatory immunity to dietary antigens. Nature *471*, 220.

Diana, J., Moura, I.C., Vaugier, C., Gestin, A., Tissandie, E., Beaudoin, L., Corthésy, B., Hocini, H., Lehuen, A., and Monteiro, R.C. (2013). Secretory IgA Induces Tolerogenic Dendritic Cells through SIGNR1 Dampening Autoimmunity in Mice. The Journal of Immunology *191*, 2335–2343.

Diehl, G.E., Longman, R.S., Zhang, J.-X., Breart, B., Galan, C., Cuesta, A., Schwab, S.R., and Littman, D.R. (2013). Microbiota restricts trafficking of bacteria to mesenteric lymph nodes by CX3CR1hi cells. Nature *494*, 116–120.

Dranoff, G. (2004). Cytokines in cancer pathogenesis and cancer therapy. Nat Rev Cancer *4*, 11–22.

Edele, F., Molenaar, R., Gütle, D., Dudda, J.C., Jakob, T., Homey, B., Mebius, R., Hornef, M., and Martin, S.F. (2008). Cutting Edge: Instructive Role of Peripheral Tissue Cells in the Imprinting of T Cell Homing Receptor Patterns. The Journal of Immunology *181*, 3745–3749.

Edelson, B.T., Kc, W., Juang, R., Kohyama, M., Benoit, L.A., Klekotka, P.A., Moon, C., Albring, J.C., Ise, W., Michael, D.G., et al. (2010). Peripheral CD103+ dendritic cells form a unified subset developmentally related to CD8α+ conventional dendritic cells. Journal of Experimental Medicine *207*, 823–836.

Eksteen, B., Mora, J.R., Haughton, E.L., Henderson, N.C., Lee–Turner, L., Villablanca, E.J., Curbishley, S.M., Aspinall, A.I., von Andrian, U.H., and Adams, D.H. (2009). Gut Homing Receptors on CD8 T Cells Are Retinoic Acid Dependent and Not Maintained by Liver Dendritic or Stellate Cells. Gastroenterology *137*, 320–329.

Fagarasan, S., Kinoshita, K., Muramatsu, M., Ikuta, K., and Honjo, T. (2001). In situ class switching and differentiation to IgA-producing cells in the gut lamina propria. Nature *413*, 639–643.

Farache, J., Koren, I., Milo, I., Gurevich, I., Kim, K.-W., Zigmond, E., Furtado, G.C., Lira, S.A., and Shakhar, G. (2013). Luminal bacteria recruit CD103+ dendritic cells into the intestinal epithelium to sample bacterial antigens for presentation. Immunity *38*, 581–595.

Faure-André, G., Vargas, P., Yuseff, M.-I., Heuzé, M., Diaz, J., Lankar, D., Steri, V., Manry, J., Hugues, S., Vascotto, F., et al. (2008). Regulation of Dendritic Cell Migration by CD74, the MHC Class II-Associated Invariant Chain. Science *322*, 1705–1710.

Feng, T., Cong, Y., Qin, H., Benveniste, E.N., and Elson, C.O. (2010). Generation of Mucosal Dendritic Cells from Bone Marrow Reveals a Critical Role of Retinoic Acid. The Journal of Immunology *185*, 5915–5925.

Ferrera, D., Canale, C., Marotta, R., Mazzaro, N., Gritti, M., Mazzanti, M., Capellari, S., Cortelli, P., and Gasparini, L. (2014). Lamin B1 overexpression increases nuclear rigidity in autosomal dominant leukodystrophy fibroblasts. FASEB J *28*, 3906–3918.

Flannigan, K.L., Ngo, V.L., Geem, D., Harusato, A., Hirota, S.A., Parkos, C.A., Lukacs, N.W., Nusrat, A., Gaboriau-Routhiau, V., Cerf-Bensussan, N., et al. (2017). IL-17A-mediated neutrophil recruitment limits expansion of segmented filamentous bacteria. Mucosal Immunol *10*, 673–684.

Förster, R., Schubel, A., Breitfeld, D., Kremmer, E., Renner-Müller, I., Wolf, E., and Lipp, M. (1999). CCR7 Coordinates the Primary Immune Response by Establishing Functional Microenvironments in Secondary Lymphoid Organs. Cell *99*, 23–33.

Gerner, M.Y., Kastenmuller, W., Ifrim, I., Kabat, J., and Germain, R.N. (2012). Histo-Cytometry: A Method for Highly Multiplex Quantitative Tissue Imaging Analysis Applied to Dendritic Cell Subset Microanatomy in Lymph Nodes. Immunity *37*, 364–376.

Ginhoux, F., Liu, K., Helft, J., Bogunovic, M., Greter, M., Hashimoto, D., Price, J., Yin, N., Bromberg, J., Lira, S.A., et al. (2009). The origin and development of nonlymphoid tissue CD103+ DCs. The Journal of Experimental Medicine *206*, 3115.

Gross, M., Salame, T.-M., and Jung, S. (2015). Guardians of the gut – murine intestinal macrophages and dendritic cells. Front. Immunol. 254.

Gyöngyösi, A., Szatmari, I., Pap, A., Dezső, B., Pos, Z., Széles, L., Varga, T., and Nagy, L. (2013). RDH10, RALDH2, and CRABP2 are required components of PPARγ-directed ATRA synthesis and signaling in human dendritic cells. J. Lipid Res. *54*, 2458–2474.

Hall, J.A., Cannons, J.L., Grainger, J.R., Dos Santos, L.M., Hand, T.W., Naik, S., Wohlfert, E.A., Chou, D.B., Oldenhove, G., Robinson, M., et al. (2011). Essential Role for Retinoic Acid in the Promotion of CD4+ T Cell Effector Responses via Retinoic Acid Receptor Alpha. Immunity *34*, 435–447.

Hatch, E.M., and Hetzer, M.W. (2016). Nuclear envelope rupture is induced by actin-based nucleus confinement. J Cell Biol *215*, 27–36.

Hayday, A., Theodoridis, E., Ramsburg, E., and Shires, J. (2001). Intraepithelial lymphocytes: exploring the Third Way in immunology. Nat Immunol *2*, 997–1003.

Herr, F.M., Wardlaw, S.A., Kakkad, B., Albrecht, A., Quick, T.C., and Ong, D.E. (1993). Intestinal vitamin A metabolism: coordinate distribution of enzymes and CRBP(II). J. Lipid Res. *34*, 1545–1554.

Huang, Y., Park, Y., Wang-Zhu, Y., Larange, A., Arens, R., Bernardo, I., Olivares-Villagómez, D., Herndler-Brandstetter, D., Abraham, N., Grubeck-Loebenstein, B., et al. (2011). Mucosal CD8 Memory T Cells are selected in the periphery by an MHC Class I Molecule. Nature Immunology *12*, 1086.

Iliev, I.D., Spadoni, I., Mileti, E., Matteoli, G., Sonzogni, A., Sampietro, G.M., Foschi, D., Caprioli, F., Viale, G., and Rescigno, M. (2009a). Human intestinal epithelial cells promote the differentiation of tolerogenic dendritic cells. Gut *58*, 1481–1489.

Iliev, I.D., Spadoni, I., Mileti, E., Matteoli, G., Sonzogni, A., Sampietro, G.M., Foschi, D., Caprioli, F., Viale, G., and Rescigno, M. (2009b). Human intestinal epithelial cells promote the differentiation of tolerogenic dendritic cells. Gut *58*, 1481–1489.

Iwata, M., Hirakiyama, A., Eshima, Y., Kagechika, H., Kato, C., and Song, S.-Y. (2004). Retinoic Acid Imprints Gut-Homing Specificity on T Cells. Immunity *21*, 527–538.

Jaensson-Gyllenbäck, E., Kotarsky, K., Zapata, F., Persson, E.K., Gundersen, T.E., Blomhoff, R., and Agace, W.W. (2011). Bile retinoids imprint intestinal CD103+ dendritic cells with the ability to generate gut-tropic T cells. Mucosal Immunology *4*, 438.

Joeris, T., Müller-Luda, K., Agace, W.W., and Mowat, A.M. (2017). Diversity and functions of intestinal mononuclear phagocytes. Mucosal Immunol *10*, 845–864.

Johansson, M.E.V., and Hansson, G.C. (2016). Immunological aspects of intestinal mucus and mucins. Nat Rev Immunol *16*, 639–649.

Johansson, M.E.V., Phillipson, M., Petersson, J., Velcich, A., Holm, L., and Hansson, G.C. (2008). The inner of the two Muc2 mucin-dependent mucus layers in colon is devoid of bacteria. PNAS *105*, 15064–15069.

Johansson, M.E.V., Ambort, D., Pelaseyed, T., Schütte, A., Gustafsson, J.K., Ermund, A., Subramani, D.B., Holmén-Larsson, J.M., Thomsson, K.A., Bergström, J.H., et al. (2011). Composition and functional role of the mucus layers in the intestine. Cell. Mol. Life Sci. *68*, 3635.

Johansson-Lindbom, B., Svensson, M., Pabst, O., Palmqvist, C., Marquez, G., Förster, R., and Agace, W.W. (2005). Functional specialization of gut CD103+ dendritic cells in the regulation of tissue-selective T cell homing. Journal of Experimental Medicine *202*, 1063–1073.

Kanazawa, N., Tashiro, K., Inaba, K., and Miyachi, Y. (2003). Dendritic Cell Immunoactivating Receptor, a Novel C-type Lectin Immunoreceptor, Acts as an Activating Receptor through Association with Fc Receptor γ Chain. J. Biol. Chem. *278*, 32645–32652.

Kim, K.S., Hong, S.-W., Han, D., Yi, J., Jung, J., Yang, B.-G., Lee, J.Y., Lee, M., and Surh, C.D. (2016). Dietary antigens limit mucosal immunity by inducing regulatory T cells in the small intestine. Science *351*, 858–863.

Kim, K.-W., Vallon-Eberhard, A., Zigmond, E., Farache, J., Shezen, E., Shakhar, G., Ludwig, A., Lira, S.A., and Jung, S. (2011). In vivo structure/function and expression analysis of the CX3C chemokine fractalkine. Blood *118*, e156–e167.

Klassert, T.E., Bräuer, J., Hölzer, M., Stock, M., Riege, K., Zubiría-Barrera, C., Müller, M.M., Rummler, S., Skerka, C., Marz, M., et al. (2017). Differential Effects of Vitamins A and D on the Transcriptional Landscape of Human Monocytes during Infection. Scientific Reports *7*, srep40599.

Klebanoff, C.A., Spencer, S.P., Torabi-Parizi, P., Grainger, J.R., Roychoudhuri, R., Ji, Y., Sukumar, M., Muranski, P., Scott, C.D., Hall, J.A., et al. (2013). Retinoic acid controls the homeostasis of pre-cDC–derived splenic and intestinal dendritic cells. Journal of Experimental Medicine *210*, 1961–1976.

Kouwenhoven, M., Özenci, V., Tjernlund, A., Pashenkov, M., Homman, M., Press, R., and Link, H. (2002). Monocyte-derived dendritic cells express and secrete matrix-degrading metalloproteinases and their inhibitors and are imbalanced in multiple sclerosis. Journal of Neuroimmunology *126*, 161–171.

Kunkel, E.J., Campbell, J.J., Haraldsen, G., Pan, J., Boisvert, J., Roberts, A.I., Ebert, E.C., Vierra, M.A., Goodman, S.B., Genovese, M.C., et al. (2000). Lymphocyte Cc Chemokine Receptor 9 and Epithelial Thymus-Expressed Chemokine (Teck) Expression Distinguish the Small Intestinal Immune Compartment: Epithelial Expression of Tissue-Specific Chemokines as an Organizing Principle in Regional Immunity. Journal of Experimental Medicine *192*, 761–768.

Lammerding, J., Schulze, P.C., Takahashi, T., Kozlov, S., Sullivan, T., Kamm, R.D., Stewart, C.L., and Lee, R.T. (2004). Lamin A/C deficiency causes defective nuclear mechanics and mechanotransduction. J Clin Invest *113*, 370–378.

Lämmermann, T., Bader, B.L., Monkley, S.J., Worbs, T., Wedlich-Söldner, R., Hirsch, K., Keller, M., Förster, R., Critchley, D.R., Fässler, R., et al. (2008). Rapid leukocyte migration by integrin-independent flowing and squeezing. Nature *453*, 51–55.

Langlet, C., Tamoutounour, S., Henri, S., Luche, H., Ardouin, L., Grégoire, C., Malissen, B., and Guilliams, M. (2012). CD64 Expression Distinguishes Monocyte-Derived and Conventional Dendritic Cells and Reveals Their Distinct Role during Intramuscular Immunization. The Journal of Immunology *188*, 1751–1760.

Lapointe, T.K., and Buret, A.G. (2012). Interleukin-18 facilitates neutrophil transmigration via myosin light chain kinase-dependent disruption of occludin, without altering epithelial permeability. American Journal of Physiology - Gastrointestinal and Liver Physiology *302*, G343–G351.

Larange, A., and Cheroutre, H. (2016). Retinoic Acid and Retinoic Acid Receptors as Pleiotropic Modulators of the Immune System. Annual Review of Immunology *34*, 369–394.

Lavi, I., Piel, M., Lennon-Duménil, A.-M., Voituriez, R., and Gov, N.S. (2016). Deterministic patterns in cell motility. Nat Phys *12*, 1146–1152.

Leithner, A., Eichner, A., Müller, J., Reversat, A., Brown, M., Schwarz, J., Merrin, J., de Gorter, D.J.J., Schur, F., Bayerl, J., et al. (2016). Diversified actin protrusions promote environmental exploration but are dispensable for locomotion of leukocytes. Nat Cell Biol *18*, 1253–1259.

Lewis, K.L., Caton, M.L., Bogunovic, M., Greter, M., Grajkowska, L.T., Ng, D., Klinakis, A., Charo, I.F., Jung, S., Gommerman, J.L., et al. (2011). Notch2 Receptor Signaling Controls Functional Differentiation of Dendritic Cells in the Spleen and Intestine. Immunity *35*, 780–791.

Li, H.S., Liu, C., Xiao, Y., Chu, F., Liang, X., Peng, W., Hu, J., Neelapu, S.S., Sun, S.-C., Hwu, P., et al. (2016). Bypassing STAT3-mediated inhibition of the transcriptional regulator ID2 improves the antitumor efficacy of dendritic cells. Sci. Signal. *9*, ra94-ra94.

Li, W., Ling, H.-P., You, W.-C., Liu, H.-D., Sun, Q., Zhou, M.-L., Shen, W., Zhao, J.-B., Zhu, L., and Hang, C.-H. (2014). Elevated Cerebral Cortical CD24 Levels in Patients and Mice with Traumatic Brain Injury: A Potential Negative Role in Nuclear Factor Kappa B/Inflammatory Factor Pathway. Mol Neurobiol *49*, 187–198.

Liang, C., Yang, L., and Guo, S. (2015). All-trans retinoic acid inhibits migration, invasion and proliferation, and promotes apoptosis in glioma cells in vitro. Oncology Letters *9*, 2833.

Liu, K., Victora, G.D., Schwickert, T.A., Guermonprez, P., Meredith, M.M., Yao, K., Chu, F.-F., Randolph, G.J., Rudensky, A.Y., and Nussenzweig, M. (2009). In Vivo Analysis of Dendritic Cell Development and Homeostasis. Science *324*, 392–397.

Lloyd, C.M., and Marsland, B.J. (2017). Lung Homeostasis: Influence of Age, Microbes, and the Immune System. Immunity *46*, 549–561.

Maiuri, P., Rupprecht, J.-F., Wieser, S., Ruprecht, V., Bénichou, O., Carpi, N., Coppey, M., De Beco, S., Gov, N., Heisenberg, C.-P., et al. (2015). Actin Flows Mediate a Universal Coupling between Cell Speed and Cell Persistence. Cell *161*, 374–386.

Mangan, P.R., Harrington, L.E., O'Quinn, D.B., Helms, W.S., Bullard, D.C., Elson, C.O., Hatton, R.D., Wahl, S.M., Schoeb, T.R., and Weaver, C.T. (2006). Transforming growth factor-β induces development of the TH17 lineage. Nature *441*, 231–234.

Maravillas-Montero, J.L., and Santos-Argumedo, L. (2012). The myosin family: unconventional roles of actin-dependent molecular motors in immune cells. J Leukoc Biol *91*, 35–46.

Masopust, D., Vezys, V., Wherry, E.J., Barber, D.L., and Ahmed, R. (2006). Cutting Edge: Gut Microenvironment Promotes Differentiation of a Unique Memory CD8 T Cell Population. The Journal of Immunology *176*, 2079–2083.

Mazmanian, S.K., Round, J.L., and Kasper, D.L. (2008). A microbial symbiosis factor prevents intestinal inflammatory disease. Nature *453*, 620–625.

Mazzini, E., Massimiliano, L., Penna, G., and Rescigno, M. (2014). Oral Tolerance Can Be Established via Gap Junction Transfer of Fed Antigens from CX3CR1+ Macrophages to CD103+ Dendritic Cells. Immunity *40*, 248–261.

McDole, J.R., Wheeler, L.W., McDonald, K.G., Wang, B., Konjufca, V., Knoop, K.A., Newberry, R.D., and Miller, M.J. (2012). Goblet cells deliver luminal antigen to CD103+ DCs in the small intestine. Nature *483*, 345–349.

McDonald, K.G., Leach, M.R., Brooke, K.W.M., Wang, C., Wheeler, L.W., Hanly, E.K., Rowley, C.W., Levin, M.S., Wagner, M., Li, E., et al. (2012). Epithelial Expression of the Cytosolic Retinoid Chaperone Cellular Retinol Binding Protein II Is Essential for in Vivo Imprinting of Local Gut Dendritic Cells by Lumenal Retinoids. The American Journal of Pathology *180*, 984–997.

Mercer, J., and Helenius, A. (2009). Virus entry by macropinocytosis. Nat Cell Biol *11*, 510–520.

Mintern, J.D., Macri, C., and Villadangos, J.A. (2015). Modulation of antigen presentation by intracellular trafficking. Current Opinion in Immunology *34*, 16–21.

Molenaar, R., Knippenberg, M., Goverse, G., Olivier, B.J., Vos, A.F. de, O'Toole, T., and Mebius, R.E. (2011). Expression of Retinaldehyde Dehydrogenase Enzymes in Mucosal Dendritic Cells and Gut-Draining Lymph Node Stromal Cells Is Controlled by Dietary Vitamin A. The Journal of Immunology *186*, 1934–1942.

Mora, J.R., Bono, M.R., Manjunath, N., Weninger, W., Cavanagh, L.L., Rosemblatt, M., and von Andrian, U.H. (2003). Selective imprinting of gut-homing T cells by Peyer's patch dendritic cells. Nature *424*, 88–93.

Mora, J.R., Iwata, M., Eksteen, B., Song, S.-Y., Junt, T., Senman, B., Otipoby, K.L., Yokota, A., Takeuchi, H., Ricciardi-Castagnoli, P., et al. (2006). Generation of Gut-Homing IgA-Secreting B Cells by Intestinal Dendritic Cells. Science *314*, 1157–1160.

Mucida, D., Park, Y., Kim, G., Turovskaya, O., Scott, I., Kronenberg, M., and Cheroutre, H. (2007). Reciprocal TH17 and Regulatory T Cell Differentiation Mediated by Retinoic Acid. Science *317*, 256–260.

Murphy, T.L., Grajales-Reyes, G.E., Wu, X., Tussiwand, R., Briseño, C.G., Iwata, A., Kretzer, N.M., Durai, V., and Murphy, K.M. (2016). Transcriptional Control of Dendritic Cell Development. Annual Review of Immunology *34*, 93–119.

Niess, J.H., Brand, S., Gu, X., Landsman, L., Jung, S., McCormick, B.A., Vyas, J.M., Boes, M., Ploegh, H.L., Fox, J.G., et al. (2005). CX3CR1-Mediated Dendritic Cell Access to the Intestinal Lumen and Bacterial Clearance. Science *307*, 254–258.

van Nood, E., Vrieze, A., Nieuwdorp, M., Fuentes, S., Zoetendal, E.G., de Vos, W.M., Visser, C.E., Kuijper, E.J., Bartelsman, J.F.W.M., Tijssen, J.G.P., et al. (2013). Duodenal infusion of donor feces for recurrent Clostridium difficile. N. Engl. J. Med. *368*, 407–415.

Osman, M., Tortorella, M., Londei, M., and Quaratino, S. (2002). Expression of matrix metalloproteinases and tissue inhibitors of metalloproteinases define the migratory characteristics of human monocyte-derived dendritic cells. Immunology *105*, 73–82.

Owen, R.L. (1999). Uptake and transport of intestinal macromolecules and microorganisms by M cells in Peyer's patches— a personal and historical perspective. Seminars in Immunology *11*, 157–163.

Pabst, O., and Mowat, A.M. (2012). Oral tolerance to food protein. Mucosal Immunology *5*, 232.

Persson, E.K., Uronen-Hansson, H., Semmrich, M., Rivollier, A., Hägerbrand, K., Marsal, J., Gudjonsson, S., Håkansson, U., Reizis, B., Kotarsky, K., et al. (2013). IRF4 Transcription-Factor-Dependent CD103+CD11b+ Dendritic Cells Drive Mucosal T Helper 17 Cell Differentiation. Immunity *38*, 958–969.

Petrie, R.J., Koo, H., and Yamada, K.M. (2014). Generation of compartmentalized pressure by a nuclear piston governs cell motility in a 3D matrix. Science *345*, 1062–1065.

Quintero Barceinas, R.S., Garc&#xed, a-Regalado, A., Ar&#xe9, chaga-Ocampo, E., Villegas-Sep&#xfa, Lveda, N., s, Gonz&#xe1, lez-De la Rosa, C.H., et al. (2015). All-Trans Retinoic Acid Induces Proliferation, Survival, and Migration in A549 Lung Cancer Cells by Activating the ERK Signaling Pathway through a Transcription-Independent Mechanism.

Raab, M., Gentili, M., Belly, H. de, Thiam, H.-R., Vargas, P., Jimenez, A.J., Lautenschlaeger, F., Voituriez, R., Lennon-Duménil, A.-M., Manel, N., et al. (2016). ESCRT III repairs nuclear envelope ruptures during cell migration to limit DNA damage and cell death. Science *352*, 359–362.

Rai, V., Thomas, D.G., Beach, J.R., and Egelhoff, T.T. (2017). Myosin IIA Heavy Chain Phosphorylation Mediates Adhesion Maturation and Protrusion in Three Dimensions. J. Biol. Chem. *292*, 3099–3111.

Randolph, G.J., Beaulieu, S., Lebecque, S., Steinman, R.M., and Muller, W.A. (1998). Differentiation of Monocytes into Dendritic Cells in a Model of Transendothelial Trafficking. Science *282*, 480–483.

Ratzinger, G., Stoitzner, P., Ebner, S., Lutz, M.B., Layton, G.T., Rainer, C., Senior, R.M., Shipley, J.M., Fritsch, P., Schuler, G., et al. (2002). Matrix Metalloproteinases 9 and 2 Are Necessary for the Migration of Langerhans Cells and Dermal Dendritic Cells from Human and Murine Skin. The Journal of Immunology *168*, 4361–4371.

Reboldi, A., Arnon, T.I., Rodda, L.B., Atakilit, A., Sheppard, D., and Cyster, J.G. (2016). IgA production requires B cell interaction with subepithelial dendritic cells in Peyer's patches. Science *352*, aaf4822.

Renkawitz, J., Schumann, K., Weber, M., Lämmermann, T., Pflicke, H., Piel, M., Polleux, J., Spatz, J.P., and Sixt, M. (2009a). Adaptive force transmission in amoeboid cell migration. Nat Cell Biol *11*, 1438–1443.

Renkawitz, J., Schumann, K., Weber, M., Lämmermann, T., Pflicke, H., Piel, M., Polleux, J., Spatz, J.P., and Sixt, M. (2009b). Adaptive force transmission in amoeboid cell migration. Nat Cell Biol *11*, 1438–1443.

Rescigno, M., Urbano, M., Valzasina, B., Francolini, M., Rotta, G., Bonasio, R., Granucci, F., Kraehenbuhl, J.-P., and Ricciardi-Castagnoli, P. (2001). Dendritic cells express tight junction proteins and penetrate gut epithelial monolayers to sample bacteria. Nat Immunol *2*, 361–367.

Sathaliyawala, T., Kubota, M., Yudanin, N., Turner, D., Camp, P., Thome, J.J.C., Bickham, K.L., Lerner, H., Goldstein, M., Sykes, M., et al. (2013). Distribution and Compartmentalization of Human Circulating and Tissue-Resident Memory T Cell Subsets. Immunity *38*, 187–197.

Saurer, L., McCullough, K.C., and Summerfield, A. (2007). In Vitro Induction of Mucosa-Type Dendritic Cells by All-Trans Retinoic Acid. The Journal of Immunology *179*, 3504–3514.

Schraml, B.U., and Reis e Sousa, C. (2015). Defining dendritic cells. Current Opinion in Immunology *32*, 13–20.

Scott, C.L., Bain, C.C., Wright, P.B., Sichien, D., Kotarsky, K., Persson, E.K., Luda, K., Guilliams, M., Lambrecht, B.N., Agace, W.W., et al. (2015). CCR2+CD103|[minus]| intestinal dendritic cells develop from DC-committed precursors and induce interleukin-17 production by T cells. Mucosal Immunol *8*, 327–339.

Shay, T., and Kang, J. (2013). Immunological Genome Project and systems immunology. Trends in Immunology *34*, 602–609.

Spits, H., Artis, D., Colonna, M., Diefenbach, A., Di Santo, J.P., Eberl, G., Koyasu, S., Locksley, R.M., McKenzie, A.N.J., Mebius, R.E., et al. (2013). Innate lymphoid cells — a proposal for uniform nomenclature. Nat Rev Immunol *13*, 145–149.

Steinman, R.M., and Cohn, Z.A. (1973). Identification of a Novel Cell Type in Peripheral Lymphoid Organs of Mice: I. Morphology, Quantitation, Tissue Distribution. Journal of Experimental Medicine *137*, 1142–1162.

Stroka, K.M., Hayenga, H.N., and Aranda-Espinoza, H. (2013). Human Neutrophil Cytoskeletal Dynamics and Contractility Actively Contribute to Trans-Endothelial Migration. PLOS ONE *8*, e61377.

Sujino, T., London, M., Konijnenburg, D.P.H. van, Rendon, T., Buch, T., Silva, H.M., Lafaille, J.J., Reis, B.S., and Mucida, D. (2016). Tissue adaptation of regulatory and intraepithelial CD4+ T cells controls gut inflammation. Science *352*, 1581–1586.

Suzuki, H., Jeong, K., and Doi, K. (2002). Age-related changes in the regional variations in the number and subsets of intraepithelial lymphocytes in mouse small intestine. Dev. Comp. Immunol. *26*, 589–595.

Takamatsu, H., Takegahara, N., Nakagawa, Y., Tomura, M., Taniguchi, M., Friedel, R.H., Rayburn, H., Tessier-Lavigne, M., Yoshida, Y., Okuno, T., et al. (2010). Semaphorins guide the entry of dendritic cells into the lymphatics by activating myosin II. Nat Immunol *11*, 594–600.

Tamoutounour, S., Henri, S., Lelouard, H., de Bovis, B., de Haar, C., van der Woude, C.J., Woltman, A.M., Reyal, Y., Bonnet, D., Sichien, D., et al. (2012). CD64 distinguishes macrophages from dendritic cells in the gut and reveals the Th1-inducing role of mesenteric lymph node macrophages during colitis. Eur. J. Immunol. *42*, 3150–3166.

Tamoutounour, S., Guilliams, M., Montanana Sanchis, F., Liu, H., Terhorst, D., Malosse, C., Pollet, E., Ardouin, L., Luche, H., Sanchez, C., et al. (2013). Origins and Functional Specialization of Macrophages and of Conventional and Monocyte-Derived Dendritic Cells in Mouse Skin. Immunity *39*, 925–938.

Thiam, H.-R., Vargas, P., Carpi, N., Crespo, C.L., Raab, M., Terriac, E., King, M.C., Jacobelli, J., Alberts, A.S., Stradal, T., et al. (2016). Perinuclear Arp2/3-driven actin polymerization enables nuclear deformation to facilitate cell migration through complex environments. Nature Communications *7*, ncomms10997.

Uto, T., Fukaya, T., Takagi, H., Arimura, K., Nakamura, T., Kojima, N., Malissen, B., and Sato, K. (2016). Clec4A4 is a regulatory receptor for dendritic cells that impairs inflammation and T-cell immunity. Nature Communications *7*, ncomms11273.

Vargas, P., Maiuri, P., Bretou, M., Sáez, P.J., Pierobon, P., Maurin, M., Chabaud, M., Lankar, D., Obino, D., Terriac, E., et al. (2016). Innate control of actin nucleation determines two distinct migration behaviours in dendritic cells. Nat Cell Biol *18*, 43–53.

Vascotto, F., Lankar, D., Faure-André, G., Vargas, P., Diaz, J., Roux, D.L., Yuseff, M.-I., Sibarita, J.-B., Boes, M., Raposo, G., et al. (2007). The actin-based motor protein myosin II regulates MHC class II trafficking and BCR-driven antigen presentation. J Cell Biol *176*, 1007–1019.

Vermaelen, K.Y., Cataldo, D., Tournoy, K., Maes, T., Dhulst, A., Louis, R., Foidart, J.-M., Noël, A., and Pauwels, R. (2003). Matrix Metalloproteinase-9-Mediated Dendritic Cell Recruitment into the Airways Is a Critical Step in a Mouse Model of Asthma. The Journal of Immunology *171*, 1016–1022.

Viaud, S., Saccheri, F., Mignot, G., Yamazaki, T., Daillère, R., Hannani, D., Enot, D.P., Pfirschke, C., Engblom, C., Pittet, M.J., et al. (2013). The Intestinal Microbiota Modulates the Anticancer Immune Effects of Cyclophosphamide. Science *342*, 971–976.

Vicente-Manzanares, M., Ma, X., Adelstein, R.S., and Horwitz, A.R. (2009). Non-muscle myosin II takes centre stage in cell adhesion and migration. Nat Rev Mol Cell Biol *10*, 778–790.

Vicente-Manzanares, M., Newell-Litwa, K., Bachir, A.I., Whitmore, L.A., and Horwitz, A.R. (2011). Myosin IIA/IIB restrict adhesive and protrusive signaling to generate front–back polarity in migrating cells. The Journal of Cell Biology *193*, 381–396.

Vicente-Suarez, I., Larange, A., Reardon, C., Matho, M., Feau, S., Chodaczek, G., Park, Y., Obata, Y., Gold, R., Wang-Zhu, Y., et al. (2015). Unique lamina propria stromal cells imprint the functional phenotype of mucosal dendritic cells. Mucosal Immunol *8*, 141–151.

Villablanca, E.J., Wang, S., de Calisto, J., Gomes, D.C.O., Kane, M.A., Napoli, J.L., Blaner, W.S., Kagechika, H., Blomhoff, R., Rosemblatt, M., et al. (2011). MyD88 and Retinoic Acid Signaling Pathways Interact to Modulate Gastrointestinal Activities of Dendritic Cells. Gastroenterology *141*, 176–185.

Webb, R.A., Hoque, T., and Dimas, S. (2007). Expulsion of the gastrointestinal cestode, Hymenolepis diminuta by tolerant rats: evidence for mediation by a Th2 type immune enhanced goblet cell hyperplasia, increased mucin production and secretion. Parasite Immunology *29*, 11–21.

Welty, N.E., Staley, C., Ghilardi, N., Sadowsky, M.J., Igyártó, B.Z., and Kaplan, D.H. (2013). Intestinal lamina propria dendritic cells maintain T cell homeostasis but do not affect commensalism. Journal of Experimental Medicine *210*, 2011–2024.

Wines, B.D., and Hogarth, P.M. (2006). IgA receptors in health and disease. Tissue Antigens *68*, 103–114.

Worbs, T., Hammerschmidt, S.I., and Förster, R. (2017). Dendritic cell migration in health and disease. Nat Rev Immunol *17*, 30–48.

Yona, S., Kim, K.-W., Wolf, Y., Mildner, A., Varol, D., Breker, M., Strauss-Ayali, D., Viukov, S., Guilliams, M., Misharin, A., et al. (2013). Fate Mapping Reveals Origins and Dynamics of Monocytes and Tissue Macrophages under Homeostasis. Immunity *38*, 79–91.

Zhang, Z., Li, J., Zheng, W., Zhao, G., Zhang, H., Wang, X., Guo, Y., Qin, C., and Shi, Y. (2016). Peripheral Lymphoid Volume Expansion and Maintenance Are Controlled by Gut Microbiota via RALDH+ Dendritic Cells. Immunity *44*, 330–342.

Zheng, D., and Tian, B. (2017). Polyadenylation Site-Based Analysis of Transcript Expression by 3′READS+. SpringerLink 65–77.

APPENDICES

Appendix 1

List of genes whose RNA is enriched in the identified clusters

cluster	gene	p_val	avg_diff	pct.1	pct.2
0	Cd83	3.4214783809679e-44	1.06803514929375	0.87	0.495
0	Btg1	5.53438766695922e-43	0.759318974220706	0.991	0.918
0	Nr4a2	1.81725132867998e-34	0.849650019202987	0.637	0.27
0	Il1r2	3.69595557073977e-31	0.750997003381168	0.946	0.808
0	Hilpda	1.21361179831967e-30	0.881970008533808	0.598	0.255
0	Csrnp1	1.60171358649391e-27	0.570892483811813	0.571	0.18
0	Junb	2.04058104935961e-26	0.389591883450231	0.997	0.93
0	Nr4a1	1.21645965759405e-24	0.640250758586501	0.752	0.4
0	Bhlhe40	1.42882513435236e-23	0.588722361261669	0.888	0.69
0	Dusp5	7.00131712279243e-23	0.652317715446372	0.556	0.232
0	Atf3	2.78573791268491e-21	0.664775970941549	0.903	0.695
0	Nfkbia	6.57330340270661e-21	0.990682321700079	0.644	0.422
0	Etv3	2.63098276151891e-20	0.542491727486483	0.544	0.245
0	Ifrd1	4.71821877101901e-20	0.632234104216168	0.737	0.48
0	Fosl2	1.28485506659997e-18	0.542561345999413	0.483	0.21
0	Ptp4a1	8.53233079963552e-18	0.46845387677805	0.716	0.438
0	Herpud1	2.25351592994444e-17	0.427326387466716	0.888	0.665
0	Rel	3.22565158695342e-17	0.553837577296269	0.719	0.438
0	Il1b	1.30619176645348e-16	0.680362409325077	0.825	0.595
0	Fosb	1.44470722833693e-16	0.398839206141327	0.822	0.53
0	Tnip3	5.23517956168104e-16	0.611082669639645	0.287	0.068
0	Crem	6.90498906620707e-16	0.476776843298564	0.45	0.175
0	Pde4b	7.31599919631744e-16	0.390241522905174	0.725	0.425
0	Arf4	3.00633811216882e-15	0.408101720553184	0.834	0.64
0	Ier2	3.54524942294124e-15	0.503881846399471	0.918	0.752
0	Arid5a	4.26840505129224e-15	0.399195579956685	0.414	0.152
0	Slc3a2	1.11303090446209e-14	0.329051622972592	0.81	0.54
0	Btg2	2.62010837565973e-14	0.449029152417591	0.955	0.822
0	Ccrl2	2.78043790799758e-14	0.53381947180844	0.785	0.558
0	Tbc1d4	3.04741325494175e-14	0.443600352734025	0.338	0.1
0	Cytip	5.90678567952809e-14	0.434443190759015	0.891	0.735
0	Tnfaip3	1.20066660083477e-13	0.313606009507976	0.529	0.255
0	Nfil3	1.27871205724232e-13	0.318519612925112	0.387	0.135
0	Nr4a3	2.04584400506717e-13	0.448679088175349	0.299	0.1
0	Plek	4.52471567434117e-13	0.404752065959309	0.674	0.41
0	Serpinb9	4.6197635107852e-13	0.463665270827891	0.465	0.25
0	Pim3	5.22568440626365e-13	0.40508281841663	0.514	0.242
0	Gpr132	6.53193889267944e-13	0.355301977043628	0.532	0.26
0	Maff	7.88553766345653e-13	0.377477210916336	0.447	0.188
0	Bcl2a1d	8.91705663935882e-13	0.457862630513284	0.843	0.69
0	Pmaip1	1.12245199853671e-12	0.462736803664569	0.71	0.475
0	Pim1	1.32181871028244e-12	0.292655782842718	0.918	0.748
0	Grasp	1.95173778601918e-12	0.339110000940319	0.329	0.108
0	Slc25a20	2.21624097757339e-12	0.444708885324575	0.529	0.282

0	Klf4	3.03249238907046e-12	0.454329435467208	0.595	0.35
0	Stk17b	4.21713215973906e-12	0.394108895397865	0.807	0.6
0	Nfkbiz	1.29891727825414e-11	0.419927794270707	0.517	0.26
0	Traf1	1.69199967299508e-11	0.388339058142897	0.332	0.142
0	Nedd9	2.22532407747791e-11	0.360664305727229	0.447	0.285
0	Rell1	2.79018584831373e-11	0.285659490328415	0.296	0.112
0	Arl5c	3.13844307271842e-11	0.375544514672122	0.305	0.168
0	Ptgs2	1.00102767307887e-10	0.411743709688554	0.465	0.222
0	Map3k14	1.31328220012806e-10	0.347625559951983	0.405	0.185
0	Zfand5	1.47760033527043e-10	0.416587206870235	0.668	0.468
0	Socs3	3.59340326581246e-10	0.433035551989661	0.308	0.115
0	Plscr1	3.72277346816289e-10	0.32182196100087	0.375	0.172
0	Gsn	6.85932055909813e-10	0.263891714014072	0.967	0.842
0	Gadd45b	8.68884646655188e-10	0.520672534582233	0.474	0.262
0	March7	1.35924415604926e-09	0.318726388161362	0.459	0.232
0	Themis2	2.13656822846506e-09	0.328505335615436	0.523	0.33
0	Coq10b	2.43680186619073e-09	0.326440146362852	0.61	0.385
0	Bcl2a1b	2.45253770649103e-09	0.453017149211001	0.743	0.685
0	Ifitm2	2.47144254473196e-09	0.312033330147738	0.912	0.832
0	Ndel1	2.57831333273343e-09	0.355331290634525	0.55	0.345
0	Ppp1r15a	3.18788017523895e-09	0.286078489121042	0.662	0.425
0	Rab11fip1	6.23042785017406e-09	0.254738527211352	0.302	0.125
0	Mt1	1.2414096210988e-08	0.54495397992871	0.885	0.815
0	Slc16a6	1.3947542363218e-08	0.277139971215877	0.341	0.168
0	Jund	1.97285613156563e-08	0.339680565585364	0.888	0.745
0	Ifitm3	2.15946413644753e-08	0.270725465890822	0.949	0.86
0	Akap13	2.52573747323698e-08	0.322612757366531	0.755	0.555
0	Lmnb1	6.60790530177394e-08	0.308430989996703	0.592	0.415
0	Mmp12	1.15197284922514e-07	0.43326826229502	0.317	0.262
0	Icam1	1.25133974615753e-07	0.340516368631476	0.453	0.28
0	Spag9	1.35068533616267e-07	0.283992598674006	0.492	0.282
0	Eif5a	1.97578291444303e-07	0.261067080784725	0.909	0.85
0	Csf2rb	2.16802141440541e-07	0.363041942187261	0.707	0.59
0	Serpinb6b	2.50965861179387e-07	0.36909367175403	0.514	0.345
0	Fam177a	3.51845343151158e-07	0.272956112123711	0.32	0.205
0	Errfi1	4.2514799883906e-07	0.275840688542771	0.266	0.118
0	Ddx21	4.6388076759418e-07	0.267080997316104	0.571	0.388
0	Sqstm1	4.78298116057857e-07	0.265748369262412	0.565	0.358
0	Agpat4	6.20694249555036e-07	0.279996142164787	0.459	0.265
0	Ahr	6.33936645947385e-07	0.303189925571865	0.637	0.455
0	Cxcl2	6.43676489003613e-07	0.522757872112037	0.674	0.485
0	Dnajb6	6.71685282460313e-07	0.265465277871646	0.731	0.568
0	Klf6	9.45926268918221e-07	0.276949309260914	0.761	0.575
0	Tiparp	1.74778384380863e-06	0.28295081473629	0.595	0.402
0	Nabp1	2.66966519962617e-06	0.312362580891885	0.441	0.27

0	Cd7	2.94401321667227e-06	0.372385965293095	0.293	0.242
0	Chd7	3.46263391783673e-06	0.262619469787341	0.366	0.198
0	Bcl2a1a	6.09576310956909e-06	0.322634325126409	0.574	0.498
0	Ptger4	7.43108027468635e-06	0.282870339533406	0.269	0.125
0	Wnk1	1.5799083212103e-05	0.282885060268303	0.71	0.575
0	Ccnd2	2.07985792896412e-05	0.282881184603808	0.779	0.652
0	Tmem123	5.33544327095913e-05	0.250744820225312	0.631	0.49
0	Ass1	7.3726087655658e-05	0.303983370339017	0.251	0.14
0	Dapk1	8.82126869722072e-05	0.253551138365221	0.42	0.285
0	Ifitm1	0.00243534126375804	0.36475656723299	0.456	0.345

cluster	gene	p_val	avg_diff	pct.1	pct.2
1	Id2	2.81802868925332e-29	0.775721696543936	0.841	0.579
1	Gm10036	1.41786592152283e-26	0.571671281461505	0.97	0.89
1	Qpct	2.19697983809819e-25	0.72270968540263	0.875	0.645
1	S100a11	9.6463334240412e-25	0.341559058779008	0.974	0.88
1	Gm6133	4.81393258692455e-20	0.37039391727024	0.888	0.832
1	Gsg1	5.62455853523327e-19	0.530105906472252	0.672	0.481
1	Ear2	3.16109533412368e-18	0.548005549433047	0.703	0.455
1	Lsp1	1.04778558035716e-17	0.299492683711863	0.97	0.876
1	Rpl9-ps6	1.62102725822773e-17	0.365438907060788	0.918	0.86
1	Xlr	2.45367912926951e-17	0.528577617326017	0.836	0.629
1	Pilrb2	5.69482002622435e-16	0.417829787955177	0.879	0.715
1	Gm9844	5.9576061956671e-16	0.345966214754025	0.944	0.846
1	H2-Oa	1.84292021214508e-15	0.465196972249565	0.892	0.723
1	Ifitm6	2.60919058731912e-15	0.474668686978026	0.892	0.689
1	Cd209a	4.91457106578741e-15	0.45968239287602	0.944	0.784
1	AY036118	7.9436405789011e-15	0.420838719905719	0.724	0.557
1	Rpl29	1.46864475551622e-14	0.271893460436078	0.961	0.91
1	Pilra	3.25549897354386e-14	0.342557952269789	0.905	0.828
1	Pilrb1	6.92426082919336e-14	0.400438155453514	0.841	0.687
1	Rnase6	2.758994788003e-13	0.404597322686362	0.845	0.651
1	Rpl13-ps3	3.50748283218956e-13	0.320240474678466	0.944	0.874
1	Cd24a	6.46691302181278e-13	0.4488469853942	0.823	0.633
1	Napsa	1.13211109512621e-12	0.364723172498666	0.961	0.824
1	Cox7a2l	1.28773739584527e-12	0.340240299993587	0.948	0.886
1	Alox5ap	2.89475039570485e-12	0.428575850451485	0.858	0.661
1	Ifi30	4.16102305343643e-12	0.343039088658123	0.983	0.916
1	Fxyd5	2.16366174317738e-11	0.342079082951598	0.927	0.85
1	Tnni2	2.17556006614782e-11	0.451176824830072	0.828	0.665
1	Epcam	2.84711764874972e-11	0.428733372478166	0.806	0.641
1	Cxx1a	3.04112840552125e-11	0.385028859130625	0.603	0.437
1	Plet1	2.13291578094583e-10	0.424619251756721	0.871	0.655
1	Clec4a4	2.87658762406569e-10	0.322413628992891	0.491	0.351
1	Cxx1b	4.7909196776712e-10	0.363266160886731	0.522	0.317
1	Rsrp1	8.09641494493671e-10	0.351079936003507	0.858	0.747
1	Hepacam2	8.5210071527602e-10	0.397039066838248	0.569	0.361
1	Milr1	1.19046416705036e-09	0.364178741620649	0.668	0.493
1	Gabarapl2	1.35578844196785e-09	0.300479326557826	0.862	0.782
1	Cd209b	2.45033510937624e-09	0.511261519424746	0.543	0.307
1	Armc7	3.10992548595933e-09	0.275289730176942	0.28	0.144
1	Casp1	1.53003213105974e-08	0.29368146810109	0.552	0.437
1	Rps18-ps3	2.00533457557763e-08	0.273228966477578	0.879	0.826
1	Tnfaip8l2	2.12854497923495e-08	0.311445683227342	0.526	0.313
1	Rpl36-ps3	3.07565849712363e-08	0.265771807003147	0.892	0.83
1	Ptpn18	3.36919177732255e-08	0.283156062591525	0.918	0.85

1	Gm26740	3.97934557508783e-08	0.311412869367012	0.371	0.176
1	Slc36a3os	5.30615634570312e-08	0.353436875176286	0.655	0.479
1	1810058I24Rik	1.32463575306724e-07	0.28744722749381	0.629	0.477
1	Ypel3	1.39076089768037e-07	0.315218603292522	0.616	0.461
1	Hexb	1.67619215335788e-07	0.345870493581748	0.797	0.719
1	Ppp1r1a	1.80365560237055e-07	0.335155402407325	0.44	0.283
1	Anxa1	2.07232738825485e-07	0.294759009463733	0.741	0.539
1	Gm10020	2.1908758544628e-07	0.286026271411342	0.763	0.663
1	1810011H11Rik	3.12081936738853e-07	0.250708921434237	0.332	0.208
1	Dynlt1c	4.733294202713e-07	0.279109359322484	0.621	0.483
1	Eif3k	5.95323031912887e-07	0.250127925418148	0.892	0.836
1	H2-DMb2	5.97669110360551e-07	0.276089067768025	0.948	0.826
1	Ccdc12	7.08663500894016e-07	0.254083708507365	0.914	0.832
1	9530059O14Rik	1.13012323724943e-06	0.319684889964271	0.353	0.277
1	Sult1a1	1.5204857231067e-06	0.307105461799788	0.418	0.283
1	Fam105a	1.62548391733457e-06	0.26269102585389	0.927	0.862
1	Orai1	1.69768615699699e-06	0.264679331645641	0.392	0.279
1	Ap1s2	1.76533998635582e-06	0.279971074753402	0.556	0.441
1	Spint2	1.95742536719284e-06	0.258839065309243	0.565	0.469
1	Unc119	6.09046737738612e-06	0.284434249887235	0.759	0.633
1	Klk8	8.69661041096271e-06	0.27765122739859	0.603	0.425
1	Bloc1s2	8.77022608253536e-06	0.263131556031664	0.789	0.665
1	Clec2i	9.91360029629964e-06	0.276933115341049	0.263	0.124
1	Hhex	1.00590319048877e-05	0.285640777441071	0.474	0.337
1	Hfe	1.08142458000998e-05	0.267690046698664	0.746	0.637
1	Gng10	1.18580562722487e-05	0.272468825708965	0.565	0.429
1	Ppm1m	1.59245940278174e-05	0.259856909679828	0.642	0.515
1	Sh2d1b1	2.43921002655346e-05	0.256751978047949	0.453	0.301
1	Cd68	3.24128553170457e-05	0.253962105796187	0.858	0.78
1	Fndc5	4.87339828893285e-05	0.261139662298845	0.414	0.297
1	Slfn2	7.88606079943987e-05	0.271090843234461	0.517	0.383
1	Myh9	8.42288392165598e-05	0.289655070855742	0.379	0.24
1	Clec4b1	0.000105815927727037	0.278308389863065	0.47	0.345
1	Cd48	0.000114430841694585	0.254959459107925	0.793	0.711
1	Cd72	0.00023372979153728	0.280062948442262	0.608	0.465
1	Scimp	0.000460984398555502	0.256823047960469	0.487	0.357
1	Gdpd3	0.000480607527602544	0.254998413582993	0.323	0.22

cluster	gene	p_val	avg_diff	pct.1	pct.2
2	Hmgb2	1.51615177043178e-105	1.86927694583323	0.966	0.69
2	Tuba1b	3.83795316370447e-91	1.76859403675297	0.966	0.682
2	Stmn1	2.80634705197111e-90	2.12982261622233	0.888	0.114
2	Tubb5	3.85081437147452e-84	1.61844699331733	0.955	0.674
2	Top2a	1.15701141915782e-78	1.73101728532693	0.876	0.07
2	2810417H13Rik	9.19428883776509e-71	1.96778161044361	0.854	0.067
2	Birc5	2.9867577702597e-70	1.56353115228259	0.831	0.055
2	Hist1h2ap	1.39563645692896e-68	2.40072837212866	0.798	0.137
2	H2afz	5.81564099567624e-67	1.1866768551524	1	0.916
2	H2afx	5.07607511423793e-66	1.4567701619424	0.809	0.201
2	Hmgb1	2.84624022058376e-63	1.10885417849183	0.966	0.815
2	Cks1b	1.72589856585074e-58	1.28965858296258	0.91	0.296
2	Spc24	1.08188166373792e-54	1.08869424198313	0.809	0.076
2	Ube2c	1.98744767052096e-53	1.45530604775865	0.663	0.044
2	Ube2s	2.03676531018055e-51	1.04553215939376	0.888	0.509
2	Ccna2	2.31709059505186e-50	0.797488554275014	0.584	0.008
2	Nusap1	1.09469590761234e-47	0.927716155711067	0.573	0.011
2	Cdca3	5.58890318036927e-47	0.827238637134918	0.685	0.033
2	Mki67	1.120980627173e-45	0.819493540553587	0.674	0.045
2	Rrm2	1.4911062540058e-43	1.15961076604708	0.64	0.042
2	Spc25	1.90355573126845e-42	0.655498418993756	0.596	0.02
2	Cdca8	2.27612326787104e-42	0.963018709461324	0.629	0.065
2	Tmpo	1.09758453876408e-41	1.03090080429324	0.82	0.271
2	Cdk1	2.16274445597314e-41	0.833684728111564	0.663	0.047
2	Smc4	7.63638994413426e-41	1.00402353223976	0.798	0.21
2	Asf1b	9.81305531827258e-41	0.915885916018076	0.618	0.047
2	Racgap1	7.09464332684651e-40	0.716834923451698	0.652	0.047
2	Cks2	4.48695718484764e-38	1.07400589152447	0.831	0.221
2	Hmgn2	6.80513068897551e-38	1.02868184758169	0.809	0.269
2	Kifc1	8.92051335861756e-38	0.46879217024682	0.427	0.003
2	Tubb4b	1.05877421753913e-37	0.956508264056547	0.73	0.179
2	H2afv	3.63341740616568e-37	0.98837851085258	0.831	0.343
2	Hist1h2ae	6.40280300628566e-37	1.10928306720487	0.562	0.04
2	Tk1	4.22912790273986e-36	0.682250217828834	0.596	0.039
2	Mad2l1	5.16932781104035e-36	0.53029685037057	0.539	0.023
2	Ran	7.8758253143533e-36	0.857367347969637	0.955	0.785
2	Aurkb	2.08927104272007e-35	0.730911466811688	0.551	0.039
2	Ccnb2	5.52704725363302e-35	0.830333432661893	0.618	0.05
2	Dek	4.78072098836879e-34	0.917967561739409	0.899	0.522
2	Cep55	4.87921345140733e-34	0.509789173429552	0.438	0.006
2	Smc2	5.04334462077728e-34	0.812243013511975	0.674	0.101
2	Pbk	5.92807480952724e-34	0.51565093856888	0.449	0.008
2	Ndc80	7.61095311798274e-34	0.458158410971655	0.461	0.011
2	Ccnb1	5.3587895715063e-33	0.645063360255262	0.427	0.006

2	Cenpm	6.12868925750742e-33	0.585660556779691	0.483	0.02	
2	Sgol1	5.13248181545203e-32	0.358144274387327	0.371	0.003	
2	Casc5	5.44922972575464e-32	0.417281192018446	0.438	0.012	
2	Plk1	8.52020769720861e-32	0.434062957972992	0.382	0.005	
2	Kif11	1.85017849598372e-31	0.439600974838364	0.382	0.002	
2	Prc1	2.09514030730018e-31	0.577027400354454	0.449	0.012	
2	Lockd	2.99516114282424e-31	0.740658311517541	0.551	0.042	
2	Tyms	5.2779146506892e-31	0.877632446762622	0.618	0.101	
2	Tacc3	7.38480297762806e-31	0.614978506727852	0.506	0.05	
2	Rrm1	1.05485406928794e-30	0.725891512992256	0.584	0.072	
2	Kpna2	1.74058200329204e-30	0.742320361935833	0.607	0.093	
2	Anp32b	3.02388165621568e-30	0.801532607714525	0.91	0.603	
2	Neil3	3.40487390007494e-30	0.337751555863234	0.371	0.002	
2	Mxd3	2.06885768813872e-29	0.406253347267031	0.337		0
2	Kif22	5.82979810637424e-29	0.49291954245466	0.416	0.012	
2	Shcbp1	1.10782707164177e-28	0.479334284830312	0.461	0.022	
2	Rad51	3.7113740282042e-28	0.480862049215061	0.427	0.017	
2	Bub1b	4.27937530920298e-28	0.457135019871675	0.427	0.017	
2	Cbx3	6.09494316711537e-28	0.835626599084272	0.865	0.469	
2	Cenpw	6.64426289612797e-28	0.594180075807584	0.584	0.072	
2	Kif20a	8.46040740760391e-28	0.386245084626771	0.393	0.011	
2	Ankle1	3.74994984924628e-27	0.388613796718724	0.337	0.002	
2	Cdkn3	5.92309143687498e-27	0.426221433441644	0.382	0.009	
2	Pcna	6.25699078036631e-27	0.870385699529035	0.753	0.389	
2	Fam64a	1.79234689013383e-26	0.419978329811184	0.371	0.008	
2	Hsp90aa1	1.83342030547264e-26	0.814330912849103	0.933	0.727	
2	Cenpa	2.03522551152144e-26	0.860794210995642	0.539	0.059	
2	Hist1h1b	2.64376116043806e-26	0.561771581273766	0.393	0.016	
2	Hmmr	2.81022677372054e-26	0.444350667876969	0.36	0.006	
2	Dnajc9	3.90994993167546e-26	0.668271712743861	0.674	0.123	
2	Cdc20	7.38588338415992e-26	0.673317761515019	0.371	0.009	
2	2700094K13Rik	8.22319932430937e-26	0.761149965348102	0.831	0.45	
2	Incenp	8.64863621610918e-26	0.550951600875343	0.483	0.04	
2	Melk	1.42786916961289e-25	0.37955421609241	0.36	0.011	
2	Mns1	3.56220917653269e-25	0.405338091963253	0.36	0.014	
2	Cenpf	3.79187050100961e-25	0.466226547378261	0.393	0.017	
2	Ska1	1.22135096497772e-24	0.374449839137686	0.326	0.005	
2	Cbx5	1.22338244726287e-24	0.551452907412648	0.584	0.09	
2	Anp32e	2.02147723536514e-24	0.739097131853353	0.854	0.422	
2	Esco2	3.26187825242228e-24	0.284581132606939	0.315	0.005	
2	Cks1brt	7.65655096518196e-24	0.500986311336172	0.483	0.055	
2	Nek2	8.21658302269098e-24	0.284783326654438	0.303	0.006	
2	Ckap2l	1.08997831319829e-23	0.399935758641698	0.371	0.016	
2	Cit	1.31814577560686e-23	0.423340337910053	0.371	0.014	
2	Dut	1.67497848207393e-23	0.788851502386404	0.742	0.266	

2	Nuf2	1.7409349835565e-23	0.289822548624775	0.326	0.009
2	Fen1	3.58896547349287e-23	0.59316937332943	0.573	0.107
2	Tagln2	3.59630520965353e-23	0.868634996128203	0.888	0.514
2	Mcm5	7.11265530672089e-23	0.676288376521203	0.663	0.142
2	Cdca2	7.13430925966355e-23	0.333004278109561	0.36	0.014
2	Kif20b	8.10540488736966e-23	0.33447145043111	0.303	0.005
2	Ezh2	1.07419665967032e-22	0.596728054083821	0.618	0.136
2	Ncapd2	1.14291766171879e-22	0.432023054468091	0.404	0.026
2	Apitd1	1.16024084804802e-22	0.451711934892309	0.393	0.023
2	Kif15	1.34577007312488e-22	0.382475934845971	0.315	0.006
2	Ranbp1	2.50514998920625e-22	0.776095283701718	0.921	0.651
2	Rfc5	2.62515380864866e-22	0.580275636161534	0.539	0.093
2	Ccnf	3.35261739539476e-22	0.317317615362521	0.303	0.005
2	Ncaph	3.50184991492452e-22	0.404563409162319	0.326	0.02
2	Tpx2	3.86024863674607e-22	0.497097903377683	0.506	0.064
2	Hnrnpa2b1	4.72022872629416e-22	0.590579253390212	0.989	0.872
2	Ncapg	5.59891589901525e-22	0.303442945186892	0.337	0.011
2	Arl6ip1	5.60198147770511e-22	0.733751560614722	0.899	0.66
2	Ccdc34	7.32923010529702e-22	0.526415210468374	0.551	0.09
2	Bub1	1.09102390680799e-21	0.345125782383129	0.326	0.009
2	Cenpe	1.32702983097961e-21	0.418761676893023	0.371	0.02
2	Cdc45	1.47844275831994e-21	0.271982080400583	0.348	0.025
2	Nucks1	2.25156976142451e-21	0.654575943056702	0.73	0.277
2	Rangap1	2.90343475609394e-21	0.543876112415086	0.663	0.153
2	Knstrn	3.27518022521845e-21	0.467137247694599	0.427	0.037
2	Hn1	3.7679600640873e-21	0.664128964715906	0.91	0.654
2	Rad51ap1	5.79204545777973e-21	0.325740174424051	0.337	0.016
2	Cdca5	1.12114018570567e-20	0.353646537109788	0.382	0.028
2	Dlgap5	1.61780520692133e-20	0.322118223505763	0.303	0.009
2	Hnrnpa3	3.55869447145031e-20	0.593909889067771	0.955	0.849
2	Dbf4	3.88537043442464e-20	0.38501450692364	0.416	0.039
2	Dtl	6.87583142484354e-20	0.449884652424419	0.382	0.03
2	Plk4	6.94290924866997e-20	0.445649498592	0.438	0.048
2	Nsl1	1.49119111219633e-19	0.331989824461152	0.36	0.023
2	Mcm7	1.80422867560868e-19	0.70316863405553	0.573	0.139
2	Kif23	2.24672688846445e-19	0.486811861682919	0.416	0.042
2	Lsm5	2.72607349156561e-19	0.626212543848642	0.899	0.536
2	Mis18bp1	2.75200215914138e-19	0.293768313474631	0.27	0.012
2	Trip13	3.40560350665056e-19	0.259869982638871	0.292	0.017
2	Uhrf1	4.30496790660403e-19	0.482416252567006	0.416	0.055
2	4930579G24Rik	9.65944685590407e-19	0.309409852319676	0.371	0.03
2	Nasp	1.70034876232304e-18	0.517806168489689	0.584	0.139
2	Aurka	1.7012101965851e-18	0.463616395862907	0.382	0.037
2	Rad21	1.77677120388849e-18	0.481533831720724	0.607	0.15
2	Prdx4	3.54278045056143e-18	0.263965056561181	0.404	0.053

2	Pkmyt1	3.92774911514555e-18	0.398238974779526	0.438	0.056
2	Tcf19	8.52657919363651e-18	0.453681108402367	0.382	0.039
2	Slbp	1.3264189005359e-17	0.678353013367173	0.719	0.321
2	Cmc2	1.61748442133947e-17	0.417847196517135	0.618	0.164
2	Rfwd3	2.07831527719346e-17	0.374387766194158	0.382	0.039
2	Gmnn	2.20660066186285e-17	0.553722072785378	0.652	0.193
2	Sae1	2.37267187727041e-17	0.531314313093783	0.697	0.234
2	Atad2	3.34762669575763e-17	0.46535169591106	0.438	0.065
2	Smc6	3.77122060819265e-17	0.608887362092524	0.663	0.234
2	Haus4	4.49889279686571e-17	0.44835124293893	0.416	0.058
2	Ube2t	5.71745976939574e-17	0.428248487145122	0.404	0.05
2	Cenpk	6.81166998167119e-17	0.271825547246674	0.292	0.017
2	Lig1	7.55803033774058e-17	0.56028682521646	0.494	0.093
2	Cenpq	1.27306040997036e-16	0.296631482301762	0.393	0.053
2	Lsm2	1.31017395720866e-16	0.558990583121432	0.663	0.221
2	Chaf1a	2.07802035285964e-16	0.363108248671672	0.348	0.036
2	E2f8	2.76977613624757e-16	0.360289518494481	0.348	0.044
2	Cenph	3.72668943483211e-16	0.31038181988505	0.292	0.017
2	Set	3.8335911435881e-16	0.611201776658178	0.921	0.659
2	Hirip3	3.9744452664396e-16	0.364107551458196	0.438	0.07
2	Mcm6	5.40098232279682e-16	0.571692536509102	0.573	0.153
2	Tuba1c	8.56795688146504e-16	0.645348840695228	0.764	0.474
2	Srsf3	1.09239484553941e-15	0.513723162644486	0.944	0.749
2	Mis18a	1.76418035036105e-15	0.450419953738913	0.472	0.092
2	Alyref	2.01052740341114e-15	0.543859108583682	0.787	0.361
2	Ncaph2	3.09277954702154e-15	0.455246683431573	0.64	0.202
2	Psip1	4.75662652934834e-15	0.482348067735954	0.584	0.182
2	Rbm3	6.10554364449818e-15	0.4171129147203	0.978	0.889
2	Mcm3	1.3038346917414e-14	0.582020766976163	0.562	0.176
2	Ppil1	1.82047885572604e-14	0.360927193705771	0.517	0.125
2	Topbp1	2.0857237458628e-14	0.252363578796966	0.393	0.073
2	Tipin	2.10960755153264e-14	0.525176797089816	0.596	0.181
2	Fam111a	3.14871638919806e-14	0.418020754286	0.674	0.245
2	Diaph3	9.42698899885619e-14	0.268559923118757	0.371	0.058
2	Syce2	9.5526032760839e-14	0.420124197422232	0.427	0.109
2	Ckap2	1.35698857928337e-13	0.264707032217781	0.258	0.017
2	Hnrnpab	1.74731170372608e-13	0.508841090134428	0.899	0.576
2	Arhgef39	2.25924790352395e-13	0.316907927412617	0.315	0.036
2	Nudc	2.47756492211784e-13	0.52154905635775	0.798	0.466
2	Psmc3ip	2.50229909082898e-13	0.258758370513723	0.303	0.033
2	Rfc4	2.52284147875667e-13	0.366266682846223	0.461	0.103
2	Bub3	2.57573369434364e-13	0.523625541271764	0.73	0.447
2	Nrm	2.87761292444964e-13	0.440069115207291	0.562	0.174
2	Hdgf	3.19859384075003e-13	0.454373988144198	0.809	0.391
2	Tubg1	3.60304337686859e-13	0.328819059863471	0.416	0.083

2	Trim28	3.65519258613787e-13	0.449073235082802	0.708	0.287
2	Maz	3.72239932359598e-13	0.372399267768386	0.618	0.21
2	Erh	3.93129691774511e-13	0.503523582675881	0.933	0.735
2	Dnmt1	4.00099443510708e-13	0.38979259085792	0.348	0.05
2	Kpnb1	5.44477466764332e-13	0.272252525771097	0.607	0.224
2	Usp1	5.89070447271724e-13	0.367644766243148	0.517	0.139
2	Lsm8	8.20458389253676e-13	0.396818813833338	0.685	0.276
2	Exosc8	8.22625600004153e-13	0.454835899992967	0.629	0.224
2	Pcna-ps2	1.28819485609102e-12	0.315395181706393	0.348	0.053
2	Rdm1	1.29771430934711e-12	0.31464938225484	0.382	0.072
2	Impdh2	1.32244961117959e-12	0.498643345895224	0.798	0.436
2	Mrpl18	1.43977285544762e-12	0.509437582309982	0.775	0.445
2	Rpa2	2.34205749021073e-12	0.417512813514148	0.393	0.09
2	Snrpe	2.74625144981559e-12	0.461834402228184	0.91	0.727
2	Wbp5	2.84253712620721e-12	0.458335477021747	0.708	0.302
2	Pmf1	2.92040545548683e-12	0.368057961386947	0.618	0.22
2	Rpa3	3.3378739630398e-12	0.472952568805118	0.685	0.294
2	Hjurp	3.56596412988252e-12	0.318986655409223	0.539	0.179
2	Snrpd1	3.8147654838105e-12	0.480871243648198	0.798	0.542
2	Nsmce4a	4.40091560821769e-12	0.414586820289625	0.607	0.231
2	Hmgn1	4.71399169839447e-12	0.519539870392385	0.764	0.433
2	Pold1	4.78725184387502e-12	0.278800447424386	0.348	0.058
2	Txn1	7.45159091334002e-12	0.518674313264472	0.888	0.601
2	Fkbp4	9.39366803824416e-12	0.505968317721781	0.719	0.347
2	Ncapd3	9.75666821328939e-12	0.265057983556007	0.337	0.056
2	Ppih	1.20631344768724e-11	0.284971916741015	0.472	0.132
2	Dctpp1	1.35962711178956e-11	0.490578582030351	0.674	0.332
2	Raly	1.39623470741607e-11	0.458142610469379	0.82	0.597
2	Hn1l	1.68013213565806e-11	0.361457537598607	0.472	0.132
2	Nt5dc2	1.73732267959561e-11	0.275838719644139	0.303	0.047
2	Haus5	1.88134463530027e-11	0.257870139372904	0.315	0.047
2	Sumo2	2.67842275169289e-11	0.433106894220774	0.888	0.76
2	Ska2	3.53496528669836e-11	0.306073008892421	0.292	0.039
2	Cnot6	3.705484799178e-11	0.279581143586602	0.494	0.154
2	Anapc11	4.35725187884844e-11	0.454851762975666	0.843	0.54
2	Magoh	4.78203968817168e-11	0.323414187034596	0.775	0.385
2	Fignl1	5.63003330913506e-11	0.250177729396326	0.27	0.031
2	Rbbp4	5.88740150277695e-11	0.466461303697238	0.73	0.391
2	Aars	7.02737751074107e-11	0.289730577682026	0.618	0.245
2	Arpp19	7.2545373051401e-11	0.318293766704083	0.955	0.804
2	Haus8	8.9812233972297e-11	0.471324457547684	0.663	0.293
2	Anapc5	9.8936445307294e-11	0.426776452527531	0.697	0.315
2	Cdk4	1.20450748421845e-10	0.474346301154895	0.697	0.338
2	Whsc1	1.36750547892606e-10	0.291144870809348	0.404	0.098
2	Rnaseh2c	1.53952799509421e-10	0.369334561009255	0.674	0.302

2	Mrpl13	1.74367510693849e-10	0.275425879539202	0.517	0.179
2	Cdkn2c	1.81919405831384e-10	0.265988384417003	0.315	0.053
2	Psme3	2.12076060397144e-10	0.354770192446469	0.64	0.271
2	Orc6	2.14437781536421e-10	0.256846373344287	0.371	0.087
2	Hspa14	2.21879718151306e-10	0.380002487955643	0.64	0.263
2	Dtymk	2.36339022310143e-10	0.396372210419989	0.618	0.254
2	Mthfd2	2.53594126729963e-10	0.367291521304636	0.618	0.268
2	2700029M09Rik	2.57237298335988e-10	0.45161630928585	0.607	0.259
2	Snrpf	2.67296559455084e-10	0.416027515099406	0.955	0.771
2	Cacybp	3.03441733176414e-10	0.357199120410628	0.753	0.374
2	Smc1a	3.28140307311312e-10	0.392929150907707	0.618	0.249
2	Suz12	3.72788462467935e-10	0.270016258898997	0.404	0.112
2	Rnaseh2b	3.87008313396639e-10	0.267268571695657	0.449	0.134
2	Ptbp1	4.04838351170869e-10	0.303112104512863	0.64	0.274
2	Psat1	4.6533212656949e-10	0.263345095998212	0.36	0.078
2	Hnrnpd	4.72560833100299e-10	0.415391519142248	0.764	0.403
2	Odf2	5.33846229355408e-10	0.264134032846024	0.371	0.089
2	Hspa1a	5.61389540834738e-10	0.728880938918586	0.652	0.285
2	Hells	5.8909142356601e-10	0.305892277763247	0.258	0.033
2	Hnrnpf	7.28868733430002e-10	0.301281993748711	0.955	0.863
2	G3bp1	7.61359825757406e-10	0.433507538849986	0.899	0.626
2	Lsm3	8.18984854414959e-10	0.414647956301597	0.685	0.319
2	Hnrnpa1	8.7756784738536e-10	0.428361022855863	0.933	0.692
2	Actn4	1.14899135207124e-09	0.370272189288672	0.573	0.22
2	Snrpd3	1.18171930584018e-09	0.409177724974261	0.865	0.603
2	Snrnp25	1.30670361947759e-09	0.310017669097225	0.506	0.173
2	Crip1	1.5069863737367e-09	0.384567627916951	0.989	0.899
2	Strbp	1.56219366977112e-09	0.276021263696445	0.506	0.179
2	Dcps	1.71612856046234e-09	0.26394538131425	0.596	0.251
2	Prim1	1.8183437213975e-09	0.335711729860513	0.348	0.078
2	Hsph1	1.94120007384356e-09	0.381997155787884	0.416	0.128
2	Fzr1	2.00601390426971e-09	0.337058578867178	0.393	0.117
2	Lbr	2.27593160908061e-09	0.44125827558757	0.663	0.322
2	Banf1	2.28354757309769e-09	0.441698284462359	0.742	0.425
2	Rbbp7	2.34526810079211e-09	0.426044012271989	0.809	0.497
2	Cpsf2	2.40772153523334e-09	0.298451883992172	0.472	0.154
2	Cenpc1	2.7647704443701e-09	0.277915311328655	0.292	0.055
2	Rfc2	2.85680621436878e-09	0.493301358549814	0.663	0.35
2	Srsf10	3.66619354099774e-09	0.269922885491618	0.742	0.396
2	Nudcd2	4.16125533227218e-09	0.302724579479989	0.562	0.227
2	Tardbp	4.86116359813941e-09	0.354011858743375	0.674	0.316
2	Ngfrap1	5.45536457168651e-09	0.378223570321274	0.652	0.298
2	Mcm2	5.73903905774909e-09	0.309981447465058	0.404	0.114
2	Cycs	7.26082243664209e-09	0.423547672719421	0.921	0.768
2	Ywhae	7.34454781502892e-09	0.353795155065078	0.899	0.762

2	Nans	7.98252797162477e-09	0.354663703496779	0.618	0.274
2	Serbp1	8.04456600990136e-09	0.397077281098286	0.944	0.768
2	Npm1	8.13495154905672e-09	0.386515789344783	0.944	0.843
2	Ssrp1	8.30190960456328e-09	0.424925135722621	0.674	0.358
2	Srsf2	8.77856233340598e-09	0.341653323185976	0.888	0.721
2	Eri1	8.85118708753901e-09	0.289386362006527	0.438	0.14
2	Sap30	1.17219215655747e-08	0.26839714920373	0.708	0.363
2	Ssb	1.17782642571837e-08	0.401576759345722	0.843	0.575
2	Ppp2r4	1.23385195859722e-08	0.388659466731883	0.708	0.379
2	Tpi1	1.58958281948593e-08	0.297817098922547	0.685	0.341
2	Hat1	1.66373473013151e-08	0.345085555867297	0.64	0.308
2	Lta4h	1.7363553007505e-08	0.358365516698153	0.775	0.436
2	Ybx1	1.84696357430834e-08	0.343990000512409	0.989	0.925
2	Tpm2	1.99764511336562e-08	0.376221492586574	0.539	0.246
2	Snrpg	2.02047174839491e-08	0.376999634298056	0.966	0.855
2	Eif3b	2.23007251235312e-08	0.31995324421275	0.697	0.372
2	Hdac2	2.37909690637647e-08	0.268176667969747	0.562	0.238
2	Nde1	2.70963368221721e-08	0.294456426397797	0.393	0.143
2	Hprt	3.0116224783465e-08	0.392791918600711	0.798	0.593
2	Hspa9	3.29181478824274e-08	0.31424491899409	0.674	0.377
2	Ctcf	3.3368119857624e-08	0.269187183377341	0.461	0.171
2	Nudt21	3.41125851927928e-08	0.372165130475791	0.685	0.377
2	Vdac1	3.59613189640373e-08	0.295210325516161	0.775	0.442
2	Mrpl51	3.72840956272162e-08	0.368748870690004	0.674	0.346
2	H3f3a	3.77358739399271e-08	0.270905070112148	1	0.947
2	Hmgn5	4.24967891435612e-08	0.283692390979996	0.404	0.128
2	Nono	4.27773870678304e-08	0.411549234690559	0.787	0.519
2	Ncl	4.60282880567775e-08	0.385132280637796	0.899	0.662
2	Hspa1b	4.71930107237178e-08	0.403422024283251	0.404	0.128
2	Lsm4	4.79797448163324e-08	0.374747141043271	0.888	0.678
2	Hnrnpm	5.01131324874226e-08	0.370410229949812	0.91	0.648
2	Ddx39	6.38040884154999e-08	0.319578833463543	0.685	0.358
2	Nsmce1	7.73528438923988e-08	0.415865245281262	0.562	0.269
2	Rpp30	8.58782144211808e-08	0.292959821463332	0.416	0.136
2	Anapc15	8.66056764175986e-08	0.255738786819685	0.449	0.162
2	Ndufa5	9.85438032221985e-08	0.27189078110435	0.787	0.492
2	Nap1l1	1.01707601298674e-07	0.396697732174117	0.933	0.813
2	Srsf1	1.07524803786282e-07	0.31749521775954	0.685	0.357
2	Atp5h	1.16104790801067e-07	0.318672466401116	0.989	0.869
2	Tuba1a	1.2299588055338e-07	0.405860191431294	0.753	0.46
2	Hnrnpul1	1.32480827383198e-07	0.274153207512738	0.618	0.299
2	Gapdh	1.32667023662814e-07	0.306725103008721	0.989	0.903
2	Mrps18c	1.36337711188922e-07	0.336005248323841	0.775	0.456
2	Srsf7	1.48040858357851e-07	0.367411709468558	0.876	0.69
2	Ywhaq	1.48534883283727e-07	0.287676443133949	0.888	0.615

2	AI662270	1.6086116530634e-07	0.360253086681077	0.787	0.54
2	Vars	1.67354334210432e-07	0.292214282043099	0.528	0.221
2	Cct3	1.84997164298568e-07	0.353180657094133	0.787	0.488
2	Ppp1cc	2.02011831629546e-07	0.372449104749847	0.775	0.502
2	Fh1	2.04072791551309e-07	0.320056941133707	0.697	0.374
2	Hint1	2.09817205325009e-07	0.33527092316367	0.933	0.857
2	Dnaja1	2.308459283384e-07	0.437858476052029	0.82	0.629
2	Pih1d1	2.64448539729299e-07	0.280065911322488	0.494	0.199
2	Hspd1	2.88793733440823e-07	0.399787269898244	0.775	0.5
2	Rps27l	2.97774941020738e-07	0.328804488274354	0.966	0.826
2	Snrpd2	3.28008027769928e-07	0.339690175705483	0.876	0.625
2	Larp7	3.28338755034596e-07	0.297408782120277	0.528	0.243
2	Parvg	4.01839043600079e-07	0.270847063793787	0.506	0.212
2	Med30	4.50793858199463e-07	0.301457063382782	0.584	0.296
2	Xist	4.65940491828629e-07	0.355102053354954	0.82	0.544
2	Vrk1	4.84468087884239e-07	0.326565630221059	0.798	0.491
2	Ppm1g	5.69871831548544e-07	0.367009438214803	0.719	0.427
2	Mcm4	6.14136925423318e-07	0.368575743951189	0.472	0.193
2	Tmem109	6.81323629861964e-07	0.32121810992671	0.562	0.274
2	Mdh2	6.93121716250404e-07	0.267629839953997	1	0.941
2	Trappc5	8.57792578502608e-07	0.371124953782039	0.708	0.439
2	Rbm8a	9.34591738078095e-07	0.33115388172298	0.854	0.601
2	Lsm6	1.09197217279781e-06	0.343988751673422	0.888	0.651
2	Rtn3	1.19215119956956e-06	0.312325041150284	0.753	0.467
2	Sms	1.20431954335589e-06	0.257168780870362	0.517	0.232
2	Eif4g2	1.22458471793332e-06	0.303068168411384	0.865	0.643
2	Suds3	1.22612923917385e-06	0.303249893320576	0.562	0.266
2	Mrpl12	1.24099285383964e-06	0.33008040470665	0.674	0.402
2	Lmnb1	1.47203505391573e-06	0.334392987363319	0.753	0.46
2	Eed	1.70403376832499e-06	0.317185912934786	0.562	0.285
2	Snrpb	1.78570488209745e-06	0.281650960364035	0.876	0.76
2	Mif	1.99806428988644e-06	0.36155739655802	0.899	0.754
2	Ctbp1	2.03253949973488e-06	0.250582772710481	0.685	0.397
2	Rpa1	2.24078037548405e-06	0.273741738361265	0.584	0.293
2	Sarnp	2.3187980057315e-06	0.303811470740458	0.854	0.589
2	U2af2	2.31973624225701e-06	0.313145876153228	0.663	0.383
2	Paics	2.44336111840277e-06	0.30059079529206	0.584	0.307
2	Gm8186	2.52804299450255e-06	0.34514826348415	0.91	0.755
2	Ipo5	2.65856124581326e-06	0.2504434221521	0.36	0.136
2	Mrpl28	3.05175933074042e-06	0.301005986491879	0.607	0.34
2	Fkbp2	3.05318629090121e-06	0.286362680916601	0.685	0.389
2	Cox5a	3.09757027924851e-06	0.319646184944711	0.955	0.879
2	Nfkb1	3.10267160277292e-06	0.319845059207167	0.719	0.445
2	Parp2	3.6015580969202e-06	0.271698666629229	0.438	0.184
2	Csrp1	3.86110766713129e-06	0.259911990379835	0.775	0.522

2	Ndufb7	4.23410745926656e-06	0.304486486176564	0.933	0.743
2	Hnrnpu	5.04299171042549e-06	0.315726477305189	0.798	0.573
2	U2af1	5.29883516701555e-06	0.303886172087298	0.82	0.623
2	Map4k1	5.69206752409486e-06	0.259584055804529	0.629	0.343
2	Ube2i	6.02250078350022e-06	0.27586779710685	0.843	0.583
2	Stra13	6.26125882968647e-06	0.307841118808283	0.674	0.386
2	Atp5o	6.45283145679863e-06	0.288046684808408	0.899	0.673
2	Gcat	6.5581786745158e-06	0.277167591369748	0.438	0.188
2	Pbdc1	6.62679801891493e-06	0.312247965200577	0.483	0.299
2	Rbmxl1	6.75127669930128e-06	0.257283650640291	0.596	0.312
2	Nutf2	7.40303852910448e-06	0.319797010420349	0.618	0.344
2	Fkbp3	7.48063703485289e-06	0.308019468197684	0.697	0.417
2	Srrt	7.93759926228846e-06	0.258128369218785	0.449	0.198
2	Serinc3	8.44458598776165e-06	0.327509853518819	0.798	0.564
2	Nop58	8.47681936505498e-06	0.326941382987388	0.573	0.322
2	Stip1	8.76201028892077e-06	0.277020993054923	0.584	0.324
2	Ddx39b	1.1083806266924e-05	0.318154477778718	0.775	0.516
2	Calm3	1.15921295841472e-05	0.308104382203584	0.865	0.667
2	Psmc3	1.20581299464481e-05	0.267139121157585	0.775	0.5
2	Lyar	1.30921696176933e-05	0.272456334513485	0.562	0.299
2	Gltp	1.31176615137708e-05	0.329892661059587	0.764	0.525
2	Cox5b	1.34146245501546e-05	0.26024738926432	0.966	0.855
2	Eif4a1	1.39157978043411e-05	0.279680264416145	0.989	0.903
2	Mphosph8	1.54462815728705e-05	0.280898477477554	0.393	0.162
2	Wdfy4	1.54970678918972e-05	0.295496330917465	0.798	0.542
2	Siva1	2.39517704357297e-05	0.324827751816558	0.539	0.307
2	Fus	2.44990823186779e-05	0.269578312142638	0.91	0.695
2	Nubp1	2.7083837030875e-05	0.259528394138064	0.629	0.36
2	Sptssa	2.74053854211076e-05	0.26629161546689	0.82	0.586
2	Mndal	3.36644795768212e-05	0.290536735594269	0.483	0.234
2	Dbi	3.52011846311424e-05	0.261258269984226	0.955	0.79
2	Nhp2l1	3.56558397854908e-05	0.27395261742804	0.843	0.603
2	Sf3b5	3.80495206174419e-05	0.264547106887445	0.831	0.59
2	Tpm4	4.03560375090347e-05	0.293214100741343	0.854	0.715
2	Snrpa	4.88136969179124e-05	0.264525412725213	0.584	0.346
2	Ndufb6	4.903254475138e-05	0.250616683116139	0.753	0.497
2	Hdac1	6.54834904691592e-05	0.279880415934012	0.64	0.411
2	Lsm7	6.86544932306774e-05	0.253670460522149	0.629	0.369
2	Nme1	6.99587494143015e-05	0.272493626112648	0.91	0.715
2	Ilf2	7.22216296383812e-05	0.25302368246115	0.494	0.249
2	Pa2g4	7.46148317111034e-05	0.339337687144241	0.685	0.486
2	E2f1	7.93496915832122e-05	0.251213687163036	0.315	0.114
2	1810037I17Rik	9.32071281016275e-05	0.253189451577048	0.989	0.882
2	Elavl1	0.000120314732806514	0.259255396369813	0.685	0.439
2	Psmc1	0.000127650448129946	0.255098091485034	0.573	0.322

2	Nop10	0.000146536765593527	0.261563181387532	0.944	0.813
2	Ppp4c	0.000151430374357062	0.250203229230973	0.831	0.632
2	Atp5g2	0.000153013030548327	0.284436900219602	0.944	0.843
2	Eif4h	0.00017762692254267	0.274046422075056	0.787	0.583
2	Myadm	0.000209177228380776	0.277655605600971	0.809	0.584
2	Ddit3	0.000233626073808302	0.300930546076973	0.348	0.15
2	Rpn2	0.000258269150257981	0.257731590395744	0.82	0.598
2	Trp53	0.000259674095685538	0.277480523056265	0.584	0.35
2	Psmb6	0.000261812353522324	0.250597139461076	0.831	0.673
2	Cct8	0.000266366215353771	0.263827415402984	0.798	0.676
2	Cox7a2	0.000284615997875301	0.250653134340248	0.933	0.866
2	Mrpl23	0.000288862047748499	0.279200475614943	0.708	0.477
2	H1f0	0.00030695501672898	0.358836502516402	0.551	0.329
2	Tra2b	0.000317762664585279	0.255088348730909	0.933	0.782
2	Cbfb	0.000322228825408137	0.271980054163408	0.719	0.502
2	Gm10053	0.000356147697632055	0.261609207686551	0.652	0.475
2	Vim	0.000432711577991479	0.325050964257021	0.91	0.771
2	Psmd13	0.000437119565327055	0.25218676407693	0.685	0.452
2	Atf4	0.000464510327691378	0.26086335291471	0.708	0.512
2	Hspe1	0.000490187714614415	0.264233257166483	0.944	0.81
2	Prelid1	0.00050608857048232	0.300785327048062	0.798	0.646
2	Mrpl33	0.000590839084285693	0.268645817678151	0.899	0.787
2	Cct7	0.000921741071572082	0.273421648898094	0.764	0.581
2	Dynlt1f	0.00104128803769577	0.270592970051777	0.629	0.45
2	Fos	0.00130319167859732	0.359579487069813	0.888	0.796
2	Eif4e	0.00157031783255195	0.274711791025697	0.652	0.455
2	Pkm	0.00165514224670244	0.266574052352646	0.91	0.832
2	Acin1	0.00172799075850012	0.258010241605806	0.551	0.352
2	Neat1	0.00401207793825111	0.331265468895241	0.663	0.483

cluster	gene	p_val	avg_diff	pct.1	pct.2
3	Apoe	2.94710153959369e-244	4.64527098109668	1	0.583
3	Lgmn	4.67119229568647e-148	2.55538675041811	0.987	0.54
3	C1qa	1.68229624890979e-147	3.734931170237	1	0.152
3	C1qc	8.98704163195461e-146	3.59727809153153	0.987	0.14
3	Ctsb	5.40966271054137e-131	2.03864169596281	1	0.814
3	C1qb	7.41743717286051e-129	3.60365968093955	0.987	0.138
3	Csf1r	4.38344547398107e-127	2.65761522815208	1	0.17
3	Sepp1	4.73975354610601e-116	2.63971933167796	0.975	0.126
3	Npc2	9.8056900325358e-105	1.72534603648941	0.987	0.587
3	Sat1	3.1629795157163e-103	1.87085189845158	0.975	0.83
3	Ms4a7	3.99442145240937e-101	2.56020241674045	0.937	0.161
3	Cd81	8.26376159134388e-101	2.78120858895641	0.962	0.075
3	Mpeg1	1.78699335777618e-100	1.9659040520417	0.962	0.391
3	Pla2g7	5.38471867932294e-85	2.09076121848422	0.987	0.317
3	Cd63	1.8026887653896e-83	2.47588449049448	0.937	0.144
3	Fcer1g	4.64652325195004e-82	1.52898363718413	1	0.919
3	Mafb	2.05139824971674e-78	2.29739535680396	0.886	0.051
3	Ctsc	2.81505200396879e-78	1.46018858803415	0.975	0.785
3	Dnase1l3	8.54854382604923e-78	1.69860414824405	0.987	0.515
3	Tgfbi	5.95478064303414e-77	2.11349763962683	0.899	0.055
3	Adamdec1	8.92258051988222e-76	2.54654871820089	0.823	0.054
3	Ptgs1	1.34730584040123e-71	1.85110201603078	0.823	0.031
3	Irf8	1.45299521607391e-69	1.84731738742189	0.911	0.084
3	Npl	5.89203710590913e-66	1.69788000616219	0.785	0.026
3	Acp5	1.20538491911496e-65	1.45887740065891	0.975	0.698
3	Svbp	3.1780713034704e-65	1.57161721787788	0.709	0.327
3	Aif1	4.10521271204214e-64	1.34085700266345	0.949	0.77
3	Mmp13	3.91823446037649e-63	2.29322179849005	0.785	0.057
3	Cebpb	5.46610179715574e-62	1.87464649709508	0.848	0.362
3	Hes1	1.41870690472107e-60	2.17679972197722	0.785	0.031
3	Pf4	1.62794738583431e-59	1.9838283785373	0.747	0.034
3	Wfdc17	4.05644464203114e-59	1.96897079608946	0.759	0.25
3	Cx3cr1	9.79752615625471e-59	1.70776692847668	0.684	0.008
3	Lair1	1.57202072905118e-57	1.44071533385002	0.835	0.241
3	Ecm1	1.16570219056641e-56	1.89105189498124	0.684	0.046
3	Lst1	2.87930158025185e-56	1.20634215398935	0.962	0.612
3	Atp2b1	3.39565285907473e-56	1.39117538691832	0.797	0.258
3	Msr1	3.93831546875392e-56	1.48888579913098	0.709	0.026
3	Fcgr4	2.60548807858419e-54	1.62830092162617	0.709	0.032
3	Mmp14	2.67394039043163e-53	1.36746739412656	0.633	0.011
3	Ctsl	2.05785402836308e-52	1.44900213045639	0.797	0.204
3	Blvrb	2.78411867730939e-52	1.28637843560097	0.671	0.117
3	Tmem176b	1.5165968823252e-51	1.89728734984668	0.81	0.107
3	Stab1	4.43592426229238e-50	1.60997345798083	0.722	0.063

3	Clec4n	6.89022352373598e-50	1.24440434848161	0.861	0.646
3	Wnt4	2.17687989454721e-48	1.48565868757621	0.582	0.023
3	Tlr12	2.49224574203769e-48	1.46111402780333	0.633	0.032
3	Mmp9	1.12001427766804e-47	2.10790972784098	0.557	0.025
3	Itgb5	8.78144981947401e-47	1.28831072454314	0.608	0.014
3	Cxcl16	8.92712806816003e-47	1.30413371311634	0.949	0.595
3	Gbp2b	1.02852064852447e-46	1.5603911661169	0.696	0.078
3	Pxdc1	1.34256555499413e-46	1.48321402534434	0.658	0.094
3	Vsir	1.28652292004891e-45	1.2310764600785	0.684	0.242
3	C3ar1	1.80747595295268e-45	1.31128020555251	0.57	0.02
3	Cybb	1.77495545263462e-44	1.22659230206765	0.911	0.663
3	Itm2c	4.51791027639652e-44	1.0721969836927	0.899	0.64
3	Clec1b	6.36264312271984e-44	1.39013088550385	0.595	0.025
3	Fcgr3	3.72158603536524e-43	1.31326147792785	0.759	0.383
3	Slc11a1	6.55959503063283e-43	1.04547083538616	0.57	0.012
3	Lamp1	3.38798469845086e-42	1.0017905070039	0.937	0.776
3	Ctsh	1.05291791242646e-41	0.889289291781179	0.949	0.883
3	Axl	2.01296258071853e-41	1.28716619741153	0.557	0.012
3	Grn	1.16715196289775e-39	0.978206296494624	0.924	0.692
3	Hpgds	1.61543081321035e-39	1.20730591694302	0.671	0.113
3	Cadm1	3.8320103787703e-39	1.21990756699892	0.519	0.018
3	Gm10116	2.33114427252925e-38	0.961015448345452	0.848	0.752
3	Lyz2	2.61557042364358e-38	1.40018094919976	0.975	0.923
3	H2-M2	2.67727360713022e-38	1.42344595740239	0.418	0.003
3	Lpcat2	9.51770195660397e-38	1.04350580456766	0.81	0.443
3	Plaur	2.12659253813606e-37	1.34488185645506	0.722	0.164
3	Klra2	2.42200285458034e-37	1.13135835040077	0.608	0.044
3	C5ar1	2.46112034892835e-37	1.13856257205558	0.494	0.008
3	Tmem37	2.99247942658319e-37	1.12369249699913	0.456	0.003
3	Marcks	5.09326400985863e-36	1.12694940560009	0.823	0.554
3	Atp6v0b	6.54864035018806e-36	0.840943733409011	0.899	0.736
3	Rcbtb2	8.88169062368132e-36	1.02622860229279	0.582	0.209
3	Maf	2.06413234698074e-35	1.04362850213071	0.443	0.002
3	Slc15a3	2.8302823633184e-35	1.00262752319562	0.785	0.508
3	Pla2g2d	3.21270796531179e-35	1.60002401867275	0.443	0.011
3	P2ry6	6.00749970826642e-35	0.970201999827257	0.519	0.06
3	Sdc4	9.67734200024202e-35	1.24162428300793	0.456	0.008
3	Zeb2	1.10258458994154e-34	1.26823418065175	0.684	0.167
3	Fcgr1	2.26415922142906e-34	0.970111919299823	0.43	0.005
3	Rnf149	3.13938626325098e-34	1.04713092342987	0.886	0.606
3	Tmem176a	7.97689910983719e-34	1.39957647852675	0.595	0.071
3	Thbs1	1.77106565228021e-33	1.59760190717933	0.468	0.035
3	Serinc3	2.08781303147857e-33	0.957040313339118	0.823	0.564
3	Laptm4a	2.58254311788485e-33	0.916410473927776	0.684	0.388
3	Ctsz	4.8639015706676e-33	0.847680011684325	0.987	0.928

3	Ms4a6d	1.2852937515326e-32	1.03348051761608	0.696	0.322
3	Fcgr2b	1.64822400212679e-32	1.1495526563774	0.582	0.061
3	Sema6d	1.7071355848308e-32	0.995034390719512	0.443	0.015
3	Gm5150	1.88605265856823e-32	0.999333283399282	0.494	0.034
3	Cd4	2.30106024235828e-32	1.14191789223852	0.506	0.032
3	Sdcbp	4.24146531114188e-32	0.894438868177948	0.924	0.672
3	Dusp6	8.55560812723849e-32	1.10511918894753	0.608	0.198
3	AF251705	1.27686525662701e-31	0.821579652719952	0.861	0.667
3	Gpr65	1.3406506266322e-31	1.1659086161488	0.62	0.104
3	Ppt1	2.56343078523258e-31	0.962286056144648	0.696	0.391
3	Ifi204	5.2074956783052e-31	0.96085502122749	0.456	0.015
3	Mrc1	1.53306336939352e-30	1.01156845448953	0.443	0.014
3	Selm	4.34067502655862e-30	1.03845136766125	0.519	0.081
3	P2rx4	4.77707763355288e-30	1.05388190931417	0.633	0.213
3	Olfml3	1.03977453316013e-29	0.823461463052822	0.405	0.009
3	Kctd12	5.2620742960256e-29	1.07942717050544	0.747	0.261
3	Lilra5	1.04933356212116e-28	0.85176417883084	0.456	0.025
3	Zmynd15	6.3958522189863e-28	0.97753443352343	0.367	0.034
3	AI607873	7.33112551010942e-28	0.9218574879122	0.468	0.052
3	Irf2bp2	7.94534402706381e-28	1.07009602163606	0.785	0.491
3	Lyn	7.94881037067785e-28	0.795807856271327	0.759	0.558
3	C6	5.47290628013186e-27	0.779024930247502	0.354	0.018
3	Tspan13	5.89723606832739e-27	0.874985750198783	0.937	0.773
3	Nfe2l2	7.16978672865295e-27	0.931334755671436	0.671	0.371
3	Cd93	8.11262871475991e-27	0.725728365407671	0.342	0.005
3	Ms4a6b	9.06742926007476e-27	0.843529200125324	0.722	0.52
3	Rab7b	1.18775013112343e-26	0.909224333109798	0.405	0.014
3	Cmklr1	1.1954925122359e-26	0.817825429929526	0.342	0.002
3	Lamp2	1.32800397412802e-26	0.798775619528654	0.671	0.377
3	Pld3	1.76353410136188e-26	0.910207894576372	0.405	0.026
3	Adgre1	4.21136893877779e-26	0.908967027819321	0.658	0.288
3	Hsp90b1	5.8399594586591e-26	0.92930644943915	0.899	0.793
3	Rab3il1	1.64296373346435e-25	0.737349275908145	0.367	0.014
3	Acp2	2.31712667201018e-25	0.943657134261892	0.443	0.071
3	Rrbp1	2.35087976995218e-25	0.773935516572186	0.759	0.609
3	Lgals3bp	2.68326611489679e-25	0.875997061175371	0.481	0.158
3	Gns	3.0992195341886e-25	0.982051881262301	0.62	0.287
3	Sec14l1	4.58239352943897e-25	0.889915971752081	0.506	0.08
3	Cndp2	4.91843277865451e-25	0.698143792501641	0.532	0.242
3	Isg15	8.19660522507961e-25	1.08982878896566	0.506	0.351
3	Ctsd	8.46820484981377e-25	1.01258358271378	0.405	0.084
3	Prdm1	1.22007851053475e-24	1.09600774879665	0.557	0.121
3	Ubl3	1.5052236039329e-24	0.742426502239419	0.734	0.56
3	Gnl2	1.89923431043366e-23	0.805345343999642	0.506	0.192
3	AW112010	1.91147332261399e-23	0.886275089127414	0.962	0.885

3	Ccl24	2.45514722143648e-23	1.35605648783058	0.342	0.006
3	Itga9	2.76031776383523e-23	0.78746860555776	0.316	0.006
3	Plin2	4.59197168097667e-23	0.841177804606647	0.696	0.4
3	Tpst2	5.17993968156302e-23	0.813110776074683	0.418	0.034
3	Gatm	5.73596351612808e-23	0.779862573847353	0.557	0.287
3	Sgk1	8.2107483632079e-23	1.18681370885881	0.544	0.146
3	Ninj1	2.20737980788764e-22	0.725154239982885	0.418	0.256
3	Ccl3	2.68023119441676e-22	1.27570319721158	0.468	0.097
3	Cxcl9	2.84321045524353e-22	1.37854189248621	0.456	0.054
3	Gbp8	3.08517718777573e-22	0.732602802278573	0.443	0.259
3	Hebp1	3.97461820023165e-22	0.90963892444151	0.38	0.041
3	Rhob	4.55901335400709e-22	0.983987391921803	0.494	0.143
3	Nampt	4.89499740683329e-22	0.764105959054271	0.494	0.264
3	Cela1	5.9829256604366e-22	0.594998676553725	0.291	0.005
3	BC005537	6.06811027073785e-22	0.953379230322882	0.544	0.244
3	Camk2d	1.16514988208275e-21	0.876321977630822	0.494	0.118
3	Pmepa1	1.34178637756869e-21	0.868285723770961	0.532	0.156
3	Dok3	1.39326102412072e-21	0.591016643596187	0.354	0.041
3	Cd14	2.10032092343055e-21	1.0805369686066	0.468	0.12
3	Mfsd1	2.11404651744802e-21	0.724495989941603	0.405	0.141
3	Snx18	2.43389850409783e-21	0.942824113324157	0.443	0.146
3	Sirpa	3.26626950588585e-21	0.698702364613745	0.595	0.448
3	Slc40a1	4.09550992345035e-21	0.73100817584193	0.304	0.009
3	Cyp4f18	4.64181818351772e-21	0.841567238997779	0.684	0.379
3	Creg1	7.03687988209778e-21	0.649761852665426	0.734	0.661
3	Kcnj10	9.26289828678416e-21	0.745877691778082	0.342	0.028
3	Notch1	1.01021573968104e-20	0.767687265650248	0.291	0.046
3	Hjurp	1.21542067135888e-20	0.844237473516221	0.494	0.19
3	Fam26f	1.72485788360713e-20	0.821756804342178	0.392	0.034
3	Basp1	1.9413686701086e-20	1.00107596650143	0.646	0.262
3	Ucp2	2.11673747538053e-20	0.654829328778574	0.962	0.882
3	Vps37b	2.58680186621646e-20	0.949067387846269	0.658	0.279
3	Lbh	3.43056149685724e-20	0.739260667902497	0.557	0.419
3	Ccr5	3.77255050411225e-20	0.667690321084059	0.342	0.04
3	Ctsa	4.83694147772476e-20	0.648753804062533	0.873	0.773
3	Atp6v1b2	7.03437608108419e-20	0.650366730887279	0.494	0.319
3	Fam234b	8.06056301745584e-20	0.826679900185698	0.519	0.221
3	Man2a1	9.2536345904812e-20	0.759381585815547	0.443	0.127
3	Adgre4	1.02869297113324e-19	0.726784976231583	0.342	0.018
3	Tgfbr1	1.70904295744208e-19	0.920118642920926	0.481	0.161
3	Gpx3	2.25128612943432e-19	0.705799045008721	0.253	0.003
3	Spty2d1	5.23865782077247e-19	0.693876745939146	0.481	0.313
3	Camk1	5.48233687186671e-19	0.567832719728705	0.342	0.15
3	Ehd1	5.73201498007626e-19	0.737217607202316	0.595	0.363
3	Tpp1	6.65061983353595e-19	0.649255114173202	0.405	0.221

3	Frmd4b	6.98026631699901e-19	0.813299017640582	0.456	0.101
3	Sema4b	8.14922885685335e-19	0.772827473724911	0.304	0.015
3	Ms4a6c	9.89549483830437e-19	0.660095997097459	0.949	0.842
3	Gna12	1.078527859018e-18	0.712683728703981	0.38	0.071
3	Agpat3	1.68136690428477e-18	0.630964793965303	0.291	0.029
3	Cd200r4	1.94077356096853e-18	0.538066126824701	0.253	0.02
3	Gm43603	2.46699600393646e-18	0.671607542056681	0.266	0.011
3	Gbp7	2.5462735542117e-18	0.789608359909735	0.595	0.327
3	Clec4a3	3.68849347254379e-18	0.658626141436061	0.278	0.008
3	Atp13a2	3.9142319400381e-18	0.608120944253641	0.291	0.011
3	Ccl4	4.9332241832158e-18	1.51153230778475	0.519	0.121
3	Sgpl1	6.59487896063135e-18	0.806415583069699	0.418	0.135
3	P2ry13	7.56352083558037e-18	0.577884100744092	0.253	0.008
3	Ptprj	7.59669035381066e-18	0.716784139360529	0.43	0.11
3	Fyb	8.12675291755847e-18	0.633586476081462	0.671	0.546
3	Litaf	8.20553133310146e-18	0.589660794208456	0.709	0.632
3	Tmem51	8.94689389269416e-18	0.719203215100911	0.367	0.038
3	Trf	1.38077559006859e-17	0.738132872220972	0.684	0.462
3	Abr	1.51135634378098e-17	0.83085344502481	0.481	0.202
3	Sepw1	1.68296335876241e-17	0.622930972839453	0.646	0.541
3	Fxyd2	2.24479594120222e-17	0.843302173922498	0.266	0.018
3	Clec4a1	2.28903721377966e-17	0.787048585770869	0.456	0.106
3	Tnfaip2	4.55750985975342e-17	0.96961488216195	0.747	0.567
3	Dmxl2	6.13574919631546e-17	0.575418512709242	0.253	0.005
3	Rnf19b	6.45532037398015e-17	0.754520451532431	0.443	0.123
3	Rab20	6.62888047326146e-17	0.738505459405566	0.468	0.198
3	Ptms	7.9329969805041e-17	0.620971109305438	0.835	0.745
3	Loxl3	1.25114804468498e-16	0.500404832456149	0.291	0.014
3	Arap1	1.5034362075546e-16	0.631009419834914	0.278	0.061
3	Mxd1	2.82628480617759e-16	0.666572896701048	0.354	0.201
3	Abi1	2.89205223959068e-16	0.54453349585615	0.544	0.379
3	Pla2g15	3.08272241531389e-16	0.489459507211211	0.253	0.008
3	Qk	3.09390225431409e-16	0.593410140324049	0.38	0.253
3	Vps41	4.04124328706566e-16	0.56723397355971	0.342	0.166
3	Cln8	4.37257973069644e-16	0.630571302960328	0.481	0.233
3	Prkcd	4.62792567202274e-16	0.725325902021331	0.468	0.299
3	Gsr	5.72534043944605e-16	0.822545420618574	0.506	0.183
3	Ntpcr	6.36712155254601e-16	0.551778257633857	0.544	0.468
3	Atp8a1	7.33257013120518e-16	0.695762987907133	0.38	0.17
3	Apobec1	8.21116163790811e-16	0.614688652286208	0.304	0.029
3	Clic4	9.6431651334733e-16	0.712761246754289	0.532	0.327
3	Adipor1	1.05508310180542e-15	0.525220920801239	0.582	0.434
3	Mgat4a	2.08233797069529e-15	0.659601463679715	0.468	0.207
3	Cebpa	4.33003122167058e-15	0.598160307658674	0.456	0.227
3	Laptm5	4.50014884514389e-15	0.575616106091093	0.911	0.831

3	Il18bp	7.2728633196011e-15	0.621629352248005	0.304	0.051
3	Cdkn1a	1.3265158583947e-14	0.996095856238292	0.57	0.38
3	Lrrc25	1.55477073173996e-14	0.547560421452517	0.519	0.37
3	Lag3	1.61383219873126e-14	0.61059948668492	0.278	0.021
3	Skil	1.64211699512645e-14	0.63575025226598	0.468	0.374
3	P2ry14	1.71034484759659e-14	0.533418508808234	0.253	0.012
3	Slc43a2	2.05740152384682e-14	0.641396739224949	0.354	0.13
3	Derl1	2.14554751099205e-14	0.545186968278475	0.532	0.405
3	Glul	2.25398170699795e-14	0.495988099142171	0.354	0.13
3	Txnip	2.4360923669244e-14	0.740944857815932	0.506	0.39
3	Arhgap17	3.51551798171845e-14	0.585016002740414	0.418	0.225
3	Entpd1	3.74742594588708e-14	0.542893586826458	0.38	0.252
3	PISD	4.88861423427387e-14	0.692650245733737	0.608	0.408
3	Mcfd2	4.91962009508895e-14	0.643579200237246	0.418	0.206
3	Pgf	7.0140873219808e-14	0.832930795229497	0.468	0.144
3	Abcf1	1.00129878064851e-13	0.333863445842476	0.316	0.376
3	Gna13	1.09370687158596e-13	0.496264310858526	0.532	0.48
3	Snx5	1.20683554409602e-13	0.496020968103105	0.671	0.584
3	Slc7a7	1.33784335203426e-13	0.552972944633137	0.304	0.097
3	AW011738	2.1557253148343e-13	0.492851418598665	0.266	0.061
3	Tmem86a	2.35871591982474e-13	0.573908901019315	0.342	0.064
3	Epb41l2	2.78862682189213e-13	0.675556377196891	0.304	0.169
3	Nckap1l	3.14977903093345e-13	0.485818980906906	0.544	0.459
3	Tcf7l2	3.15363406829695e-13	0.483151069067206	0.266	0.066
3	Epsti1	4.38462584149031e-13	0.615262834407209	0.468	0.149
3	Gbp3	4.89604089609097e-13	0.511906662502245	0.43	0.301
3	Lamtor4	5.04279110217932e-13	0.517053231290152	0.481	0.38
3	Anxa3	6.76789962292607e-13	0.597111157232578	0.291	0.04
3	Ptprc	7.10789513938441e-13	0.571086530203447	0.987	0.902
3	Neu1	7.17942828127576e-13	0.540517058515212	0.405	0.201
3	Uap1l1	7.65201150512006e-13	0.529371687508083	0.278	0.1
3	Ifnar1	7.98396313022229e-13	0.543441129927561	0.443	0.236
3	Cd72	8.02858845827456e-13	0.651894649091146	0.633	0.495
3	Pik3cd	8.40870010953523e-13	0.566784612226995	0.38	0.265
3	Tssc4	9.19041199870037e-13	0.588417613968355	0.291	0.117
3	Ocstamp	9.44777379193955e-13	0.621786386460961	0.494	0.294
3	Csnk1e	9.74596065346934e-13	0.499086979410832	0.43	0.299
3	Tmem189	9.77301116168599e-13	0.491386753965958	0.291	0.183
3	Prdx5	9.82796892143719e-13	0.40415652796458	0.823	0.899
3	Cd38	1.2014769235473e-12	0.504749976071718	0.266	0.02
3	Ppt2	1.24212122245189e-12	0.567384065976702	0.253	0.017
3	Tcirg1	1.26814939111611e-12	0.520883065538939	0.443	0.362
3	Rasgef1b	1.31742556766603e-12	0.556129209760408	0.342	0.147
3	Gng2	1.49024374640028e-12	0.339080267029169	0.443	0.502
3	Tpd52	1.57394038456087e-12	0.559931888061824	0.696	0.549

3	Atp6v1a	1.66409930324474e-12	0.415400345086941	0.405	0.337
3	AU020206	1.86656049446513e-12	0.57139501844375	0.367	0.176
3	Man1c1	1.87690473102264e-12	0.506415491737925	0.253	0.044
3	Hacd4	1.99866033346119e-12	0.542467783854888	0.342	0.094
3	Cxcr4	2.17651060079373e-12	0.843382115611106	0.329	0.11
3	Tubb2a	2.86889409151865e-12	0.523261463748502	0.316	0.118
3	Lgals9	3.00366142165881e-12	0.459666787233091	0.443	0.371
3	Cbl	3.29793857863532e-12	0.61582263747552	0.506	0.408
3	Usp8	3.52850528355784e-12	0.37123752279854	0.291	0.222
3	Cebpzos	3.72909619289643e-12	0.39800700878731	0.329	0.25
3	Nmt1	4.08645559097804e-12	0.393892143791957	0.671	0.735
3	Tgfbr2	4.73154333698633e-12	0.525283128942959	0.278	0.081
3	Sash1	4.83324684028686e-12	0.647135746345531	0.532	0.294
3	Slc9a3r2	4.92741120670473e-12	0.574499996553987	0.354	0.14
3	Fip1l1	5.83961119217238e-12	0.455979400043479	0.354	0.278
3	Scarb2	6.09046792860421e-12	0.579308085021885	0.392	0.221
3	Arl4c	6.66524306382734e-12	0.56762182272845	0.658	0.604
3	Klra17	6.88522898967333e-12	0.516252013829414	0.304	0.051
3	Slc29a3	7.23651251835766e-12	0.517091708371674	0.278	0.046
3	Pirb	7.50570731453672e-12	0.543164537205533	0.544	0.442
3	Sh3glb1	8.08326766602565e-12	0.312126882645761	0.57	0.666
3	Rbms1	9.78117282233512e-12	0.468999027206515	0.494	0.422
3	Mcl1	1.00528521162693e-11	0.613422308603461	0.81	0.735
3	Ppp1r9b	1.33710147887585e-11	0.459701984987383	0.304	0.137
3	C130050O18Rik	1.49033332516127e-11	0.647201947674551	0.443	0.198
3	Lilr4b	1.54217332798167e-11	0.618534403021766	0.43	0.121
3	Rap1b	2.13235515077628e-11	0.376481470313892	0.734	0.793
3	Fuca2	2.15818370910757e-11	0.470994999390714	0.456	0.339
3	Il1rn	2.49130328594984e-11	0.56420395350294	0.316	0.055
3	Slco3a1	2.51982971941076e-11	0.511875793535019	0.443	0.383
3	Ptbp3	3.38349437951829e-11	0.498280887006504	0.557	0.5
3	Csde1	3.72282002519321e-11	0.486567027468279	0.62	0.558
3	Trafd1	3.8286973524854e-11	0.521094552232291	0.494	0.35
3	Cttnbp2nl	3.9507822929627e-11	0.515275773869333	0.253	0.044
3	Lcp2	3.95575356464472e-11	0.434683045859962	0.43	0.373
3	Mapkapk2	3.98883156725904e-11	0.529358938936548	0.481	0.291
3	Il10rb	4.0459872830606e-11	0.439168759121841	0.38	0.311
3	Runx2	4.85708854561851e-11	0.540316443075359	0.253	0.11
3	Amdhd2	5.2192866725586e-11	0.475332180802464	0.304	0.149
3	Lmna	6.20361170626891e-11	0.538230556824339	0.304	0.054
3	Acvrl1	6.23865264179965e-11	0.580308391423192	0.43	0.146
3	March1	6.33641607725261e-11	0.372291585170605	0.342	0.291
3	Canx	6.62267628321688e-11	0.479851147185028	0.684	0.626
3	Nceh1	6.82192750017885e-11	0.647667490957495	0.468	0.204
3	Gbp4	7.23083092835855e-11	0.550932951242985	0.367	0.155

3	Msrb1	9.22906351664169e-11	0.497341060598359	0.519	0.368
3	Cd274	9.50065747726439e-11	0.680877133566935	0.532	0.35
3	Renbp	1.00195708170655e-10	0.447131524607764	0.354	0.144
3	Slc29a1	1.05387774237236e-10	0.499259287580029	0.43	0.324
3	Mapk1ip1l	1.08670395011463e-10	0.397098405194875	0.278	0.127
3	Asph	1.19825728555303e-10	0.439189824801035	0.316	0.155
3	Tcn2	1.54781631284018e-10	0.569497461398718	0.506	0.258
3	Ttyh3	1.56867268665333e-10	0.462441797094049	0.304	0.141
3	Ap1b1	1.61524342881548e-10	0.432876197370258	0.316	0.192
3	Atp2a2	1.66211871708958e-10	0.556385454548079	0.329	0.152
3	Trim30a	1.78879975126997e-10	0.535061640688031	0.43	0.198
3	Tnfrsf21	1.81599188430341e-10	0.484455993346115	0.278	0.061
3	Grina	2.19709987579858e-10	0.421879514633992	0.392	0.267
3	Atp6v0d1	2.58736499818698e-10	0.423897032473151	0.532	0.442
3	Cd9	2.63863602990695e-10	0.39482093380132	0.81	0.902
3	Tmed10	2.64347088451501e-10	0.27284166270681	0.57	0.649
3	Rbfa	2.8736510963393e-10	0.425397751770449	0.329	0.216
3	Agpat5	3.36087744307867e-10	0.457603444351187	0.329	0.201
3	Leprot	3.46272977293767e-10	0.47320189006896	0.582	0.502
3	Usf2	3.46976219432801e-10	0.264978511024668	0.304	0.362
3	Pdxk	3.55049502599834e-10	0.326886029352082	0.266	0.202
3	Tnfaip3	3.89608512850854e-10	0.79630649844511	0.595	0.353
3	Rbpj	3.97196485301429e-10	0.287064056081054	0.38	0.488
3	Ets2	4.5457593509922e-10	0.586268023644467	0.291	0.061
3	Tmem106a	6.05336634231435e-10	0.446631815727221	0.354	0.233
3	Stra6l	6.0821264514343e-10	0.438841963626029	0.354	0.218
3	Zmynd8	6.1213371446297e-10	0.40880541340392	0.291	0.196
3	Ubald1	6.62237174751178e-10	0.394054697399136	0.367	0.253
3	Abcg3	7.19233182295028e-10	0.492582419695184	0.43	0.301
3	Coa5	7.26706477087911e-10	0.485299261471882	0.329	0.15
3	Snx2	8.84607831862295e-10	0.37296725428718	0.392	0.322
3	Ifnar2	9.17448377594079e-10	0.446624191134362	0.392	0.253
3	Cxcl2	1.13258817114818e-09	0.879633838154696	0.759	0.548
3	Cox14	1.15503542837267e-09	0.292643978057282	0.646	0.715
3	Ppfibp2	1.41499249232101e-09	0.405094049304595	0.253	0.058
3	Surf4	1.45118038057355e-09	0.390674261677145	0.392	0.337
3	Pgs1	1.47690798680758e-09	0.456527179499062	0.418	0.316
3	Specc1l	1.49836346267335e-09	0.441437317589097	0.266	0.083
3	Tbc1d10a	1.62294605495786e-09	0.356886287708758	0.316	0.193
3	Atp1b3	2.04035641068024e-09	0.432470308653438	0.418	0.287
3	Ehf	2.16705809233077e-09	0.456603521979536	0.266	0.08
3	Inpp5d	2.26128600069942e-09	0.472082147528614	0.519	0.428
3	Ganc	2.53673719950656e-09	0.376074645795056	0.266	0.103
3	Peli1	2.64033670119294e-09	0.502087236473775	0.354	0.207
3	Il1b	3.0554821393417e-09	0.728615555910817	0.848	0.681

3	Mob1a	3.10213330620494e-09	0.418614993588371	0.506	0.44
3	Nisch	3.23138847824935e-09	0.431095980028016	0.405	0.333
3	Lilrb4a	3.53752513437318e-09	0.590347238861569	0.43	0.19
3	Cltc	4.43033641561443e-09	0.508399693680902	0.443	0.35
3	Itgax	6.89849877137817e-09	0.263376359614052	0.671	0.808
3	H2-T23	7.93158230204712e-09	0.253846604496624	0.759	0.865
3	Nktr	8.43227070634474e-09	0.521190523918349	0.57	0.416
3	A930007I19Rik	8.67483959249231e-09	0.407132768575907	0.253	0.06
3	Dtnbp1	9.86624994953888e-09	0.356608235153402	0.291	0.121
3	Prex1	1.11319673411123e-08	0.474960436039554	0.38	0.275
3	Tnfrsf1a	1.13701037741364e-08	0.28437485965921	0.392	0.445
3	Sorl1	1.21597994400822e-08	0.432473937305304	0.342	0.233
3	Ifngr2	1.24977834955871e-08	0.41850412025787	0.57	0.477
3	Sod1	1.34045543964261e-08	0.471782797493892	0.506	0.413
3	Lrrc8d	1.50051535195565e-08	0.377010000020194	0.253	0.166
3	mt-Atp8	1.79634794112051e-08	0.3237009949695	0.633	0.735
3	Ppp2ca	1.80333267027596e-08	0.300072903959081	0.544	0.6
3	Gpr137b-ps	1.85751819779588e-08	0.4555501695938	0.291	0.141
3	Rin2	2.42865234245862e-08	0.544039220282022	0.304	0.104
3	Ndufc2	2.8229841130626e-08	0.276087178315342	0.62	0.672
3	Susd6	2.84578358039977e-08	0.547093617756858	0.38	0.166
3	Akirin2	2.84778766434261e-08	0.340468911679211	0.291	0.201
3	Man1a	2.88394266565907e-08	0.525153534659015	0.316	0.198
3	Per1	3.82404452820504e-08	0.482680351763094	0.367	0.244
3	Nrip1	3.98552155281021e-08	0.440196273060553	0.38	0.304
3	Rhog	4.38751513357919e-08	0.300094122421878	0.557	0.613
3	Metrnl	4.70376722155173e-08	0.530873986005562	0.278	0.086
3	Rabep1	6.94126338918054e-08	0.33947309445613	0.253	0.161
3	Lmo4	7.7478292561626e-08	0.498270326833774	0.392	0.218
3	Irak2	8.65096509733436e-08	0.459091411206635	0.418	0.241
3	S100a13	9.36655086918999e-08	0.277193983608687	0.481	0.532
3	mt-Nd2	9.90737821713813e-08	0.459065861599576	0.987	0.913
3	Lipa	1.09193098974977e-07	0.364444522408505	0.532	0.475
3	Pnrc1	1.29175743669736e-07	0.404093404427184	0.633	0.564
3	Slc39a7	1.39725983841065e-07	0.3570391675301	0.291	0.213
3	Gm19434	1.42965865864334e-07	0.364720126664178	0.405	0.353
3	Ddi2	1.45021618086962e-07	0.411481841939789	0.316	0.198
3	Fos	1.47136568699799e-07	0.650249827953258	0.886	0.798
3	Comt	1.94821265108745e-07	0.479483462704232	0.671	0.604
3	Cmtm3	1.96882510053618e-07	0.340250761489868	0.354	0.255
3	Manf	2.04413960154512e-07	0.387831988952739	0.658	0.581
3	Tbxas1	2.59834472480978e-07	0.427695850491552	0.418	0.236
3	Rgs10	2.64700706840963e-07	0.274654251524531	0.772	0.851
3	Adam19	2.73048372681861e-07	0.399961208573927	0.544	0.475
3	Lacc1	3.07724823082376e-07	0.355976424015137	0.342	0.252

3	Mkln1	3.1605917063251e-07	0.423673313117377	0.43	0.345
3	Adrbk2	3.26669549793675e-07	0.400938079797239	0.329	0.23
3	Neurl3	3.52575100231162e-07	0.26476527968752	0.519	0.62
3	Tiparp	4.60314891482786e-07	0.300772889899252	0.443	0.495
3	Cux1	5.50649353118087e-07	0.342414826129797	0.304	0.224
3	St8sia4	5.9868325988679e-07	0.478532568073261	0.544	0.452
3	Tab2	1.29954023747171e-06	0.418424637959598	0.367	0.294
3	Ptpre	1.48866957550788e-06	0.334985506152037	0.418	0.357
3	Asb2	1.75770018958298e-06	0.281419337112524	0.646	0.742
3	Ifi203	1.76882049292928e-06	0.336414228276467	0.304	0.247
3	Tnfrsf1b	2.09976612438259e-06	0.406977349358829	0.291	0.193
3	Hcst	2.24475337349281e-06	0.358404270805823	0.266	0.172
3	Itpripl2	2.2860374378038e-06	0.46660609943714	0.316	0.201
3	Fam46c	2.41862666202058e-06	0.364798655308531	0.253	0.179
3	Cd40	2.45846599939099e-06	0.423481946301132	0.354	0.21
3	Eif2b2	2.4666899284793e-06	0.403982428735567	0.519	0.428
3	Zfp36l1	3.48889519310971e-06	0.503966422221595	0.494	0.321
3	Lyz1	3.89180355463735e-06	0.999381618375455	0.342	0.187
3	Ppp1r21	3.91891588239995e-06	0.310086244149519	0.291	0.227
3	Tet2	4.1105119479242e-06	0.39419470775825	0.266	0.158
3	Nucb2	4.53585931040615e-06	0.360793862732219	0.456	0.367
3	Clec2d	4.80379108765777e-06	0.516888133581772	0.367	0.19
3	Tapbp	4.93488794226158e-06	0.272778073020273	0.646	0.704
3	Dnase2a	4.95922763469491e-06	0.416153777987164	0.38	0.235
3	Ptgs2	5.24499993609363e-06	0.649921298575137	0.506	0.311
3	Antxr2	5.75632208796965e-06	0.417919184822844	0.342	0.167
3	Tmcc3	6.04284395980431e-06	0.426476616249246	0.316	0.147
3	Nt5c	6.25010369114445e-06	0.294533002411042	0.354	0.284
3	Abhd12	6.86878494738731e-06	0.320815846211271	0.392	0.29
3	Adam17	7.38330202766282e-06	0.368355390126543	0.253	0.146
3	Tmem261	7.84206581017283e-06	0.274509999360422	0.367	0.305
3	Sirt2	8.5778140006605e-06	0.323125444572502	0.367	0.222
3	Cep170	9.33724213392292e-06	0.329381676746757	0.266	0.179
3	Apol10b	9.62321023156295e-06	0.359558084692265	0.456	0.34
3	Lat2	1.01280046875178e-05	0.295341762998932	0.291	0.202
3	Gpr137b	1.4964967507167e-05	0.355934756266378	0.367	0.236
3	Il13ra1	1.66439638360694e-05	0.34611878133431	0.266	0.166
3	Bcl2a1b	1.69072135269446e-05	0.343327992955542	0.848	0.695
3	Fcgrt	1.96881404008108e-05	0.315433637449138	0.266	0.121
3	Il10ra	2.02769879549615e-05	0.329532937401662	0.354	0.23
3	Sppl2a	2.06090711723611e-05	0.42130512732762	0.354	0.196
3	Apol7c	2.22896289554259e-05	0.417050219588082	0.848	0.778
3	Ncstn	2.24651740128183e-05	0.289617552549369	0.253	0.198
3	Tomm34	2.5776596029468e-05	0.311628877197949	0.38	0.304
3	Impact	2.72462219057101e-05	0.317299483337528	0.316	0.227

3	Slc31a2	3.37275967034511e-05	0.320736404262808	0.278	0.155
3	Synj1	3.53010776593557e-05	0.324435537633448	0.329	0.245
3	Il6ra	3.53959336118516e-05	0.36289411900651	0.266	0.158
3	Slc39a1	3.9193062901968e-05	0.332099055577387	0.329	0.241
3	Pdlim4	4.04418546023968e-05	0.318311011259116	0.253	0.106
3	Cd1d1	4.24417845822223e-05	0.295479835679213	0.266	0.166
3	Smap2	4.77605811321922e-05	0.261513093506386	0.304	0.242
3	Cept1	8.46848778058633e-05	0.311986838010932	0.291	0.219
3	Scimp	9.01030541435347e-05	0.356113808223477	0.532	0.382
3	Adgrl3	9.21112814555369e-05	0.319827246514019	0.253	0.164
3	Hpgd	0.000104381708806961	0.400245463194752	0.418	0.336
3	Dnajc3	0.00010656544484553	0.315693356060459	0.506	0.431
3	Igsf6	0.000111062359951718	0.293602528678731	0.456	0.376
3	Strn3	0.000134238295506403	0.330964965394487	0.304	0.17
3	Kansl1	0.000141331572867399	0.308767529985481	0.266	0.167
3	Zfhx3	0.000166945416787815	0.364615450229779	0.38	0.232
3	Snx10	0.000171388902901828	0.272853361175802	0.354	0.302
3	Gadd45b	0.000174224450578715	0.449179083731098	0.519	0.339
3	Ppm1h	0.000218663469218339	0.252174257478209	0.253	0.176
3	Gpr171	0.000219721076228584	0.340703900289477	0.266	0.173
3	Lpar6	0.000221495112675058	0.33467710707524	0.392	0.311
3	Lmbrd1	0.000225569146520232	0.304730907560821	0.253	0.132
3	Pik3r1	0.000230624228496486	0.305792945236542	0.329	0.253
3	Hlx	0.000235849632337359	0.344594590789947	0.278	0.17
3	Irs2	0.000251931536411875	0.404603274318113	0.266	0.163
3	Arih1	0.00029426008366983	0.30210330532092	0.367	0.258
3	Dtx3	0.00053039553491639	0.315481035711026	0.278	0.15
3	Hist1h2bc	0.000722520652987092	0.381449822823968	0.367	0.287
3	Rassf2	0.000730807574961371	0.32414128468748	0.291	0.204
3	Ypel5	0.00101975080359755	0.260019835268311	0.253	0.153
3	Cwc25	0.00109704851778666	0.371684876577303	0.304	0.204
3	Samhd1	0.00110520788726004	0.289497263444653	0.658	0.598
3	Nfil3	0.0012001401066856	0.262824723115324	0.304	0.242
3	Ehmt2	0.00139054219903932	0.295838256616945	0.291	0.17
3	mt-Nd3	0.0017576846630858	0.269096297082905	0.658	0.712
3	Tnks2	0.00257158349498463	0.291839937805272	0.266	0.172
3	Ddit3	0.0043532717675757	0.285013013226282	0.253	0.164

Appendix 2

Collaborative Review Article

Dynamics of the membrane-cytoskeleton interface in
MHC class II-restricted antigen presentation

Marine Bretou[1]*, Anita Kumari[1]*, Odile Malbec[1]*, Hélène D. Moreau[1]*, Dorian Obino[1]*, Paolo Pierobon[1]*, Violaine Randrian[1]*, Pablo J. Sáez[1]* and Ana-Maria Lennon-Duménil[1]*

Immunological Reviews 2016 Vol. 272: 39–51

[1] Inserm U932, Institut Curie, ANR-10-IDEX-0001-02 PSL* and ANR-11-LABX-0043,
12 rue Lhomond, 75005, Paris, France.

*All the authors equally contributed to this review.